

HYDRO-MECHANICAL ANALYSIS OF LOW ENRICHED URANIUM FUEL PLATES FOR
UNIVERSITY OF MISSOURI RESEARCH REACTOR

A Thesis presented to the Faculty of the Graduate School

University of Missouri

In Partial Fulfillment

Of the Requirements for the Degree

Master of Science

by

JOHN C. KENNEDY

Dr. Gary L. Solbrekken, Thesis Supervisor

MAY 2012

The undersigned, appointed by the Dean of the Graduate School, have examined the thesis entitled

HYDRO-MECHANICAL ANALYSIS OF LOW ENRICHED URANIUM FUEL PLATES FOR
UNIVERSITY OF MISSOURI RESEARCH REACTOR

Presented by John C. Kennedy

A candidate for the degree Master of Science

And hereby certify that in their opinion it is worthy of acceptance

Dr. Gary L. Solbrekken

Dr. Douglas E. Smith

Dr. Stephen Montgomery-Smith

ACKNOWLEDGEMENTS

I would first like to thank my advisor, Dr. Gary Solbrekken, for his support during this research project. His continued encouragement, patience, and input have been invaluable in the completion of this project. Next, I must thank my parents, John and Lisa, my brother Josh, and my grandmothers Donna and Marita. Their encouragement from an early point in my life to pursue science and engineering has led me to where I am today. Without their immense support, none of this would have been possible. Finally, my colleagues throughout this project have been incredibly supportive, even during the most trying moments. In particular I would like to thank Kyler Turner, Srisharan G. Govindarajan, Philip Makarewicz, Bobby Slater, and Logan Compton for their help throughout this project.

TABLE OF CONTENTS

ACKNOWLEDGEMENTS.....	ii
LIST OF FIGURES.....	vi
LIST OF TABLES.....	viii
NOMENCLATURE.....	ix
Abstract.....	xi
Chapter 1: INTRODUCTION AND PURPOSE	1
Forward.....	1
History and Background.....	1
Global Threat Reduction Initiative (GTRI).....	3
Engineering Analysis Techniques.....	5
Purpose of Study.....	8
Chapter 2: University of Missouri Research Reactor	11
MURR Conversion	11
Current MURR HEU design	11
Proposed LEU design.....	13
Design Concerns.....	14
Chapter 3: Numeric Modeling	16
Code Coupling Process.....	16

CFD Solution Process	17
FEM Solution Process.....	21
Stability	22
Efficiency.....	24
Chapter 4: Analytic Modeling.....	26
Flow Model Development	26
Deflection Model Development	29
Chapter 5: Flat Plate Modeling.....	31
Computational Models	31
Experimental Setup.....	35
Chapter 6: Flat Plate Results and Discussion	41
Experimental Results	41
Computational Results.....	46
Chapter 7: Conclusion and Future Work	57
APPENDIX 1: Numeric Procedure (Tutorial)	59
Introduction	59
Preparing for Coupled Simulations.....	59
Required Software	59
System Configuration.....	60

Preparing the Abaqus Solid Model	61
Building the Model in Abaqus CAE	61
Editing the Abaqus INput File	85
Preparing the Star-CCM+ Fluid Model	87
Building the Fluid Model	88
APPENDIX 2: Experimental Data	123
APPENDIX 3: Numeric Data	126
REFERENCES	129

LIST OF FIGURES

1. Current HEU dispersion fuel cross-section	11
2. Current MURR HEU Fuel Element (MURR, 2011).	12
3. MURR fuel element arrangement (MURR, 2011).....	13
4. Plate 23 cross section. 0.4572 mm (18 mil) thick U-10Mo foil clad with 0.025 MM (1 Mil) Zirconium and 0.229 mm (9 mil) aluminum.	14
5. FSI Co-Simulation Process.....	16
6. Basic Geometry from CFD model. Note the gap in the middle of the flow channel for the plate.	17
7. Examples of Mesh, pressure, and velocity at the leading edge of a plate.	18
8. Abaqus node and element surface definitions (Simulia, 2011).....	21
9. FEA model mesh, stress, and deflection plots.....	22
10. Assembly Geometry. Fluid flow is from the top down	26
11. Flow Channel Contraction (left) and expansion (right).	28
12. Plate model setup.....	31
13. Simulated geometry. Note b is the plate width.....	32
14. Abaqus mesh independence deflection results.....	33
15. Percent Change in plate pressure drop as mesh density increases	34
16. Missouri Flow Loop.....	36
17. Flat Plate Test Section.....	37
18. Channel gap profiles.	38
19. Channel gap at midpoint during intial test phase.	41

20. Flow rate during the initial test phase.....	42
21. Flow Channel Velocity during initial testing phase.....	43
22. Maximum plate deflection Vs. Flow Velocity.	44
23. Channel pressure profiles at max flow rate.....	45
24. Plate pressure differential.	46
25. FSI Model velocity ramping schemes.	49
26. Deflection profile caused by numeric instability in Model 1.....	50
27. Comparison of the mesh from model 1 (left) and model 2 (right).....	51
28. Deflection profile caused by numeric instability in Model 1.....	52
29. Pressure differential through plate	53
30. Model 2 static pressure distributions.....	53
31. Leading Edge Deflection Profile at Various Velocities.....	54
32. Average Deflection Comparison between Numeric and Analytic Models	55
A1. Flow rate data from phase 2 of flow test.	123
A2. Channel gap data from Phase 2 of Flow Test.	123
A3. Flow rate data from phase 3 of flow test.	124
A4. Channel gaps during phase 3 of flow test.	125

LIST OF TABLES

1. Summary Of Assembly Dimensions.....	39
2. Thickness measurements at center, leading edge of plate.....	39
3. FSI Model Properties.....	48

NOMENCLATURE

a	Plate thickness	<u>Greek</u>	
A_1	Upstream flow area	α_R	Mass proportional Rayleigh damping factor
A_2	Downstream flow area		
b	Plate width	β_R	Stiffness proportional Rayleigh damping factor
D_h	Hydraulic diameter	Γ	Diffusion coefficient
E	Young's modulus of elasticity	δ	Deflection
f	Friction factor	δ_{AVE}	Average deflection
G	Grid flux	δ_{MAX}	Maximum deflection
g_1	Channel 1 outer wall to plate mid-plane thickness	ϵ	Surface roughness
g_2	Channel 2 outer wall to plate mid-plane thickness	μ	Dynamic viscosity
h_1	Channel 1 thickness	ν	Poisson's Ratio
h_2	Channel 2 thickness	ξ	Fraction of critical damping
I	Moment of inertia	ρ	Density
L	Plate length	ϕ	General CFD transport quantity
\dot{m}	Mass flow rate	ω	Natural frequency
Re	Reynold's number	<u>Vectors</u>	
S	Source term	\vec{a}	Area vector
t	Time	\vec{v}	Velocity vector
V	Volume		

<u>Subscripts</u>		MU	University of Missouri
f	Cell face identifier	MURR	University of Missouri Research Reactor
i	Iteration		
n	Time level	NBSR	National Bureau of Standards Reactor
<u>Abbreviations</u>		NIST	National Institutes of Standards and Technology
ANL	Argonne National Laboratory		
ATR	Advanced Test Reactor	NNSA	National Nuclear Security Administration
CFD	Computational Fluid Dynamics	ORNL	Oak Ridge National Laboratory
DOE	Department of Energy		
FEM/FEA	Finite Element Method/Analysis	RERTR	Reduced Enrichment for Research and Test Reactors
FSI	Fluid Structure Interaction	RDD	Radiological Dispersion Device
GTRI	Global Threat Reduction Initiative	U-235	Uranium 235 (fissionable)
		U-238	Uranium 238 (common)
HEU	Highly Enriched Uranium		
HFIR	High Flux Isotope Reactor	USHPRR	United States High Performance Research Reactors
INL	Idaho National Laboratory		
		WMD	Weapons of Mass Destruction
LEU	Low Enriched Uranium		
MITR	Massachusetts Institute of Technology Reactor		

Abstract

As part of the Global Threat Reduction Initiative (GTRI) Reactor Conversion program, work is underway to analyze and validate a new fuel assembly for the University of Missouri Research Reactor (MURR). The Low Enriched Uranium (LEU) design currently under investigation is a significant departure from the current High Enriched Uranium (HEU) design. This includes a change in the fuel meat from U-Al dispersion to a monolithic U-10Mo composition. Additionally, the proposed LEU plates are 25% thinner than the current HEU plates. These design changes increase the potential for coolant flow induced deflection of the fuel plates which could lead to a local loss of coolant, and therefore a hot spot on a plate. If the temperature on a fuel plate rises too high, there is a risk of fuel plate rupture and fission gas release into the coolant system.

Previous methods for assessing fuel plate deflection have relied heavily on analytic and experimental techniques. With the continued advancement of computational codes, new options are emerging to assess structural stability. This research explores the potential of explicitly coupled fluid-structure interaction (FSI) numeric modeling. Work was completed to evaluate a method for coupling a computational fluid dynamics (CFD) code with a finite element analysis (FEA) code. After coupling the codes and understanding the deficiencies in the coupling technique, additional research was completed on methods to improve the stability and efficiency of coupled simulations. Pressure ramping, material damping, and mesh refinement were successfully used on simulations of high aspect ratio geometries to increase simulation stability and decrease

total runtime. This research has successfully provided a way to analyze the complex interactions of fluid and structural systems. These techniques will be invaluable in evaluating the proposed LEU fuel plate structure for MURR. Additionally, proposals for future and ongoing work to validate results against fresh experimental and analytic models are provided.

Chapter 1: INTRODUCTION AND PURPOSE

Forward

After World War II, nuclear technology began to play an ever expanding role in the modernization of science and technology. At the core of much of this scientific progress has been the work of research and test reactors throughout the world. This research has led to breakthroughs in fields ranging from medical radiopharmaceuticals to advanced polymer designs and next generation battery technology. In order to accomplish this research, many of these reactors have relied upon highly enriched uranium (HEU) fuel. The use of this fuel at civilian sites presents a significant security concern, as HEU material can be used as a weapon. Therefore, under the guidance of the Global Threat Reduction Initiative (GTRI), work is currently underway to develop and qualify new low enriched uranium (LEU) based fuels for five domestic research and test reactors. One of these reactors, the University of Missouri Research Reactor (MURR), is considering dramatic changes to their fuel structure. These changes have led to concerns of the hydro-mechanical stability of the new fuel plates. As a result, work is underway to validate the use of coupled computational fluid-structure interaction (FSI) modeling for analysis of nuclear reactor fuel plates.

History and Background

In August of 1945, the world got its first glimpse of the nuclear age with the dropping of two atomic bombs on the Japanese cities of Hiroshima and Nagasaki. With these acts, nuclear technology was largely perceived only as a massive destructive force. As a result, in the decades since the first use of nuclear weapons, countries around the

world have worked to develop their own nuclear arsenal. Today, these efforts have expanded to include terrorist organizations, who are working to develop devices capable of spreading hazardous radiological material over a large area. These radiological dispersion devices (RDDs) provide a simple, yet effective means of attack against western powers. Perhaps recognizing the future threat of nuclear proliferation, President Eisenhower announced his Atoms for Peace initiative to the United Nations in 1953 (Eisenhower, 1953). The Atoms for Peace initiative was developed to encourage peaceful uses of nuclear technology to help solve a range of problems. In the decades since this initial speech, nuclear research has expanded to areas including power production, radiopharmaceuticals, medical imaging, spacecraft propulsion, and advanced materials development. These peaceful uses for nuclear technology have proven invaluable to the advancement of scientific research.

This research, however, has also increased the proliferation of potentially dangerous nuclear material. Highly Enriched Uranium (HEU), defined as uranium with a concentration greater than 20% of U-235, was the primary fuel source for these reactors. In the early 1960s, the first of these reactors were constructed in Iran and Pakistan. These reactors and many that would follow were initially designed to utilize HEU, with U-235 enrichment sometimes reaching levels greater than 90%, in order to achieve U-235 densities that were high enough for the targeted performance of the reactors. At the time, there were limited known options for research reactor fuels, thereby limiting fuel design to HEU rather than LEU (Moses, 2005). In the years to

follow most of the new research reactors constructed both as a part of the Atoms for Peace program and other programs utilized HEU fuel.

One of these early research reactors was the University of Missouri Research Reactor. Beginning operation in 1966 as a 5 MW facility, MURR has gone on to support nearly 50 years of cutting edge research. Upgraded in 1974 to 10 MW, MURR has operated with an HEU core throughout its entire existence (MURR, 2011). Until recently, there were no technically or economically feasible alternatives to the current HEU core at MURR and several other reactors. Under research conducted initially through the Reduced Enrichment for Research and Test Reactors (RERTR) program, and now through the Global Threat Reduction Initiative (GTRI), a new, high density LEU foil is being investigated as a possible alternative to the current HEU fuels in use at many reactors.

Global Threat Reduction Initiative (GTRI)

With the threats posed by nuclear terrorism and the advent of new methods for developing high density LEU foils, there is an effort currently underway to convert many US and international research reactors from their current HEU fuel to a new, foil based LEU fuel. As part of the National Nuclear Security Administration (NNSA), the office of Global Threat Reduction is working to, “reduce and protect vulnerable nuclear and radiological materials located at civilian sites worldwide” (NNSA, 2011). To date, the Global Threat Reduction Initiative has succeeded in removing more than 120 nuclear bombs worth of highly enriched uranium and plutonium from both fresh and waste fuel sites around the globe. Additionally, the program has secured a large amount of

vulnerable nuclear and radiological material at sites around the world. This material may be considered useful to a terrorist organization for the construction of nuclear weapons or dirty bombs. As part of ongoing GTRI efforts in the US, work is underway to complete conversion of five domestic research and test reactors. These reactors include MURR, the Advanced Test Reactor at Idaho National Laboratory, the High Flux Isotope Reactor at Oak Ridge National Laboratory, the MIT Reactor, and the National Bureau of Standards Reactor at the National Institute of Standards and Technology (Wachs, 2008).

Since the start of the RERTR program, more than 40 reactors worldwide have been converted from HEU to LEU fuel (ANL, 2010). Today, conversion efforts continue for only a handful of remaining HEU reactors in the United States as part of the Global Threat Reduction Initiative. Additionally, the NNSA is working to expand HEU reduction efforts in other countries such as Russia (NNSA, 2011). Aside from reactor fuel conversion, GTRI is also focused on securing sites that still use HEU but are unable to convert, as well as disposing of unnecessary nuclear material which is no longer used. These efforts have resulted in the removal and securing of enough nuclear material for thousands of dirty and nuclear bombs.

Engineering Analysis Techniques

When many of the reactors now targeted for conversion, including MURR, were first designed, computational power had not yet reached a level that allowed for detailed analysis of complete reactor systems. When the initial design work for these reactors was completed in the 1950s and 1960s, the majority of the analysis was based on conservative analytic modeling and experiments. These efforts were sufficient at the time for producing quality reactor systems with high margins of safety. However, due to the conservative nature of these engineering analyses, there was limited understanding of the true limits of the reactor systems. With the expense required for complex experiments, it was impractical to experimentally simulate every possible scenario. Therefore, favoring analytic solutions, the work of D.R. Miller (Miller, 1958) was especially useful in determining an approximate critical coolant flow velocity at which reactor fuel plates may potentially fail. MURR, like many reactors of the time, utilizes fuel assemblies based on a series of parallel fuel plates, with coolant flow channels between the plates. In order to dissipate the heat produced in the fuel plates, water is pushed through these flow channels at high velocities. Miller sought to determine the velocity at which the hydraulic force would become high enough to cause a plate to deform, thereby closing off a coolant channel. This critical velocity is determined using simple Bernoulli flow and wide beam theory. Miller's formulation does not take into account the relationship between flow redistribution and plate deflection. As a result, the critical velocity determined using the Miller formulation is highly conservative, and can be significantly improved.

Seeking to build upon the work of Miller, several experimental studies were conducted in the 1960s. In 1963, Groninger and Kane conducted tests on arrays of five parallel, flat plates. In these tests, the plates were instrumented with strain gages in the side walls in order to measure the plate deflection at high flow rates. The strain gages were calibrated for deflection measurements by pressurizing each flow channel with air and measuring the resulting strain and deflection. The strain gages were then used to determine deflection at lower flow rates, until a violent flutter was encountered at approximately 1.9 times the Miller critical velocity. When flow was decreased below the point of the onset of the flutter, the flutter stopped (Groninger & Kane, 1963). Similarly, in 1964, a study completed by Scavuzzo analyzed a geometry with a single flat plate with channels of differing thickness. This work looked at the effect of non-uniform channel thicknesses on plate deflection. It was observed that the plate will deflect at velocities below the Miller critical velocity if the flow channels are of different thicknesses. Additionally, a non-dimensional analytic model was developed for comparison to Miller (Scavuzzo, 1965).

In 1968, Smitsaert continued this analysis by looking at arrays of five parallel, flat plates. In these tests, one of the goals was to duplicate the flutter effect seen by Groninger and Kane. In order to achieve flutter at lower flow rates, PVC plates with a lower elastic modulus than aluminum were used. This allowed for the flutter effect to be observed at lower flow rates than what was necessary previously. In these tests, the flutter effect was seen at approximately 2.2 times the Miller velocity. Additionally, the frequency of vibration and the speed of the wave down the length of the plate were

recorded. These tests expanded significantly on the initial work at the beginning of the decade, while also demonstrating the need for additional investigation (Smitsaert, 1968).

More recently, experimental work has been done to investigate the potential for flow induced deflection in the Australian Replacement Research Reactor (ARR). This work showed plate collapse occurring at 78% of the predicted Miller critical velocity, a lower velocity than previous studies. Additionally, plastic deformation was observed at higher flow rates and the frequency of vibration was monitored using strain gages (Ho, Hong, & Mack, 2004).

As numeric modeling gains popularity, much work has been done in recent years to evaluate the feasibility of numerically coupled fluid structure interaction (FSI) simulations. Typically, structural problems are solved using a Lagrangian algorithm which involves having the nodes of a mesh follow the motion of the continuum. This differs from the Eulerian technique used in fluid dynamics where a fixed mesh is used to solve for a continuum moving relative to a grid. A hybrid approach, known as Arbitrary Lagrangian-Eulerian (ALE) permits the flexing of a mesh similar to a Lagrangian solution, but also monitors motion relative to the grid like an Eulerian method (Donea, Huerta, Ponthot, & Rodriguez-Ferran, 2004). This method requires a compromise of both the fluid and solid domain solutions by forcing them to use a hybrid solution method rather than a typical Lagrangian or Eulerian approach. Additionally, this technique provides for meshing of both domains with a single grid rather than independent grids. Research using this method has focused on the difficulty in maintaining reasonable meshes,

establishing computational efficiency, and determining ways to analyze transient problems (Dowell & Hall, 2001). When it comes to applying the ALE method, some previous work has focused on laminar flow with small deformations (Razzaq, Turek, Hron, & Acker, 2010).

Other studies of numeric FSI modeling have examined issues of stability associated with separately defined grids for the fluid and solid domains. It has been shown that simulations which maintain the original finite volume definition of the fluid domain and the finite element definition of the solid domain are highly sensitive to the velocity of the interface. If the coupled interface moves at too high a speed, or experiences a relatively large deformation at a specified time interval, instabilities can arise in the solution (Roe, Haselbacher, & Geubelle, 2007).

Purpose of Study

Today, as computer systems continue to see gains in speed and capability, most engineering analysis is done numerically. The two dominant methods of analysis are divided by the type of system that is being analyzed. For fluid systems, computational fluid dynamics (CFD) is commonly used. CFD solvers discretize the fluid region into a set of finite volume cells, and then solve for the flow properties in these cells. For solid systems, finite element method (FEM) is commonly used. FEM solvers discretize the structure of a solid into a set of solid elements composed of nodes. The code solves the solid mechanics equations at these nodal locations, providing the user with data on the deflection, stress, and strain in the model.

While many codes offer the ability to solve FSI problems using only CFD or FEM methods, they are limited in their ability since they are being used to solve for domains for which they are not optimized. Therefore, there is a growing interest in combining the power of CFD and FEM solvers for problems involving Fluid Structure Interaction (FSI). Such an approach would allow for a CFD code to solve for the fluid domain and an FEM code to solve for the solid domain, thereby giving the user the best of both worlds by ensuring that each domain is solved by the optimal code. Until recently, computational FSI solutions were limited by the type of problem that they could be applied to, as well as the availability of computational power. Additionally, FSI codes up to this point have generally been self-written. The research presented here explores a not only a new application for FSI modeling of flow between reactor fuel plates, but also a new technique that is dependent on commercially available codes. The primary focus of this research is to validate FSI solutions using Star-CCM+, a commercial CFD code, and Abaqus, a commercial FEM code.

Given the previous work done in this field, particular emphasis is placed on developing techniques for stabilizing the numeric solution. As was noted by Roe, particular emphasis must be placed on controlling the velocity of the interface between the fluid and solid domains. This becomes particularly important when the high aspect ratio of the geometry is considered. A high aspect ratio, such as that seen in the cross section of reactor coolant channels means that even small deflections of a plate can result in large changes to the fluid solution. Controlling and maintaining stability as the FSI interface moves through the fluid domain is the prime concern of this research.

Additionally, since previous experiments dating back to the 1960s show inconsistent results, a flow loop and test section have been constructed to aid in determining the accuracy of the numeric solutions.

Chapter 2: University of Missouri Research Reactor

MURR Conversion

Along with four other US High Performance Research Reactors (USHPRR), MURR is currently working to validate the safety and performance characteristics of a new LEU fuel. As the primary design constraints for the new MURR fuel, particular emphasis has been placed on maintaining the current neutron flux and neutron energy distribution within the irradiation spaces of the reactor. This will ensure that after conversion MURR will be able to continue its current research and production missions. Additionally, as multiple designs have been identified for new LEU fuel plates, the costs of the new fuel assembly options has been an important factor. These criteria have led to selection of a new, thin plate fuel design. Once the review process is complete and the MURR core is converted to an LEU fuel, the research reactor will be able to continue operation well into the future without using an HEU fuel core.

Current MURR HEU design

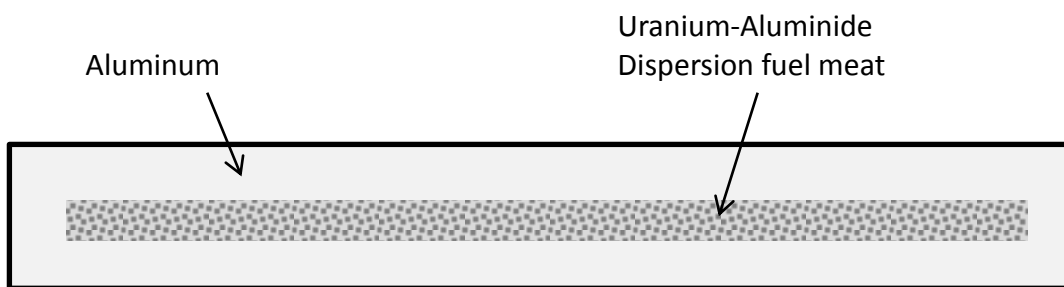


FIGURE 1. CURRENT HEU DISPERSION FUEL CROSS-SECTION

Currently, MURR operates as the nation's most powerful university research reactor at 10 MW. In 1971, MURR converted from its initial uranium-aluminum alloy fuel to the uranium-aluminide dispersion fuel shown in Figure 1. This conversion

allowed for an increase in ^{235}U loading from 650 grams per element to 775 grams. The fuel meat portion of the plate is 0.508 mm (20 mils) thick, with 0.381 mm (15 mils) of aluminum cladding on either side. With a total plate thickness of 1.27 mm (50 mils), the channel gap for coolant flow is 2.032 mm (80 mils). Each fuel assembly, as shown in Figure 2, contains 24 fuel plates arranged in a concentric orientation, and the fuel is enriched to 93% ^{235}U .

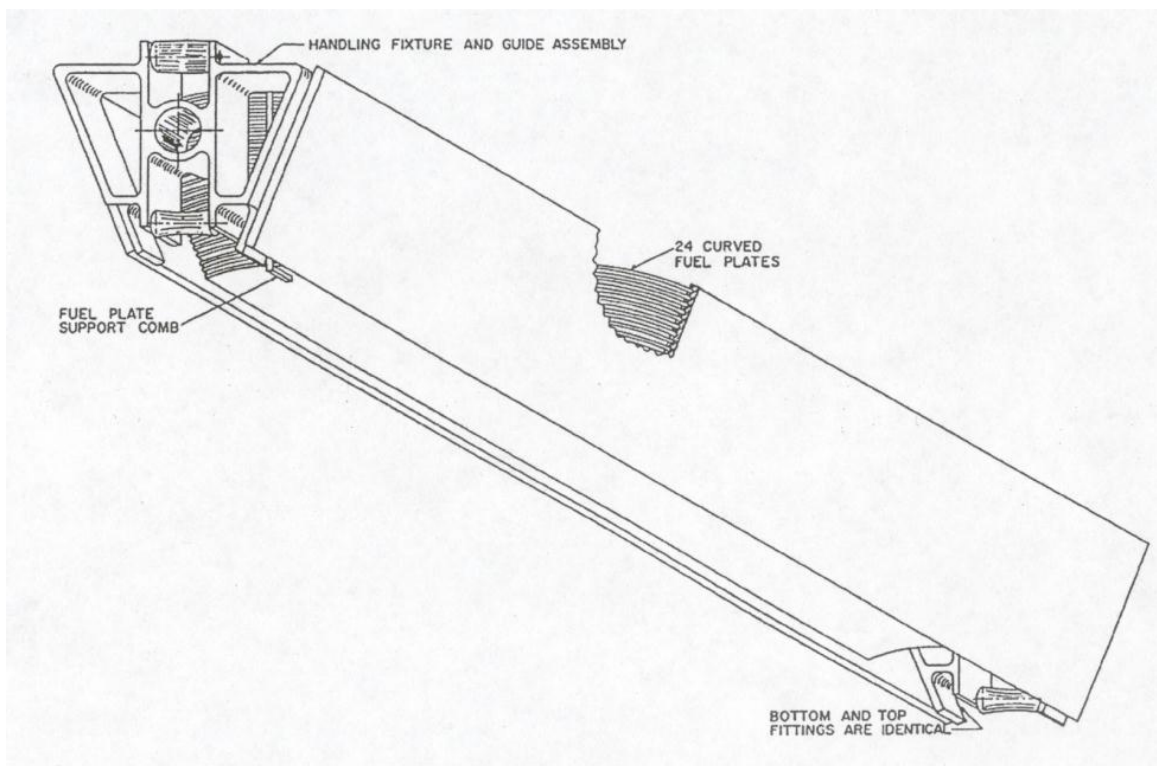


FIGURE 2. CURRENT MURR HEU FUEL ELEMENT (MURR, 2011).

The MURR core is composed of eight fuel assemblies, placed in a ‘pie’ arrangement, as shown in Figure 3. The core is highly compact, with outer and inner pressure vessel diameters of 29.97 cm (11.80 inches) and 13.51 cm (5.32 inches), respectively. The length of the fuel plates is 64.77 cm (25.5 inches), leading to core volume of $1.46 \times 10^{-1} \text{ m}^3$ (5.14 ft.³). In order to remove the 10 MW of heat produced in

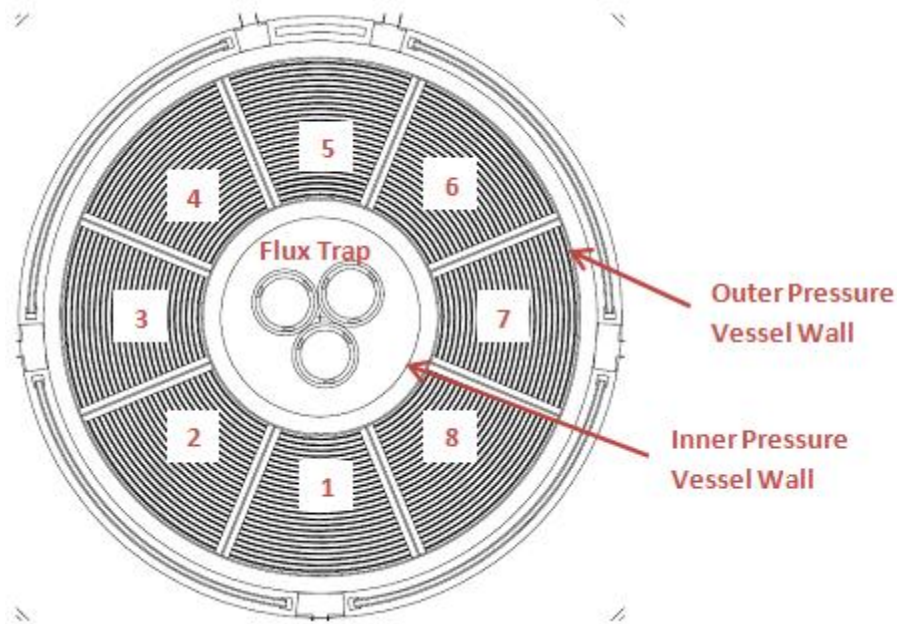


FIGURE 3. MURR FUEL ELEMENT ARRANGEMENT (MURR, 2011).

this volume, water is pushed through the core at high velocity, carrying heat away to external cooling towers. The current HEU design is resistant to flow induced deflections of the fuel plates for several reasons. The thickness and curvature of the plates provide sufficient rigidity to minimize deflection. Additionally, each fuel assembly is equipped with combs on the leading and trailing edges, which hold the fuel plates in place at those locations. These factors all provide for a stable design in the current HEU core.

Proposed LEU design

With the need to reduce ^{235}U enrichment from the current 93% to 19.75%, a new fuel foil composed of uranium and 10% molybdenum has been developed. In order to make up for the reduced fraction of ^{235}U present in the new fuel, the fuel density has increased from 1.53 grams/cm³ to 3.03 grams/cm³. In the majority of the plates, the uranium foil itself is only 0.457 mm (18 mils) thick, and is clad on either side by aluminum with a thickness of 0.229 mm (9 mils), as shown in Figure 4. Between the uranium foil and the aluminum cladding, a 0.025 mm (1 mil) thick zirconium layer is present to prevent interactions between the two materials during irradiation. These

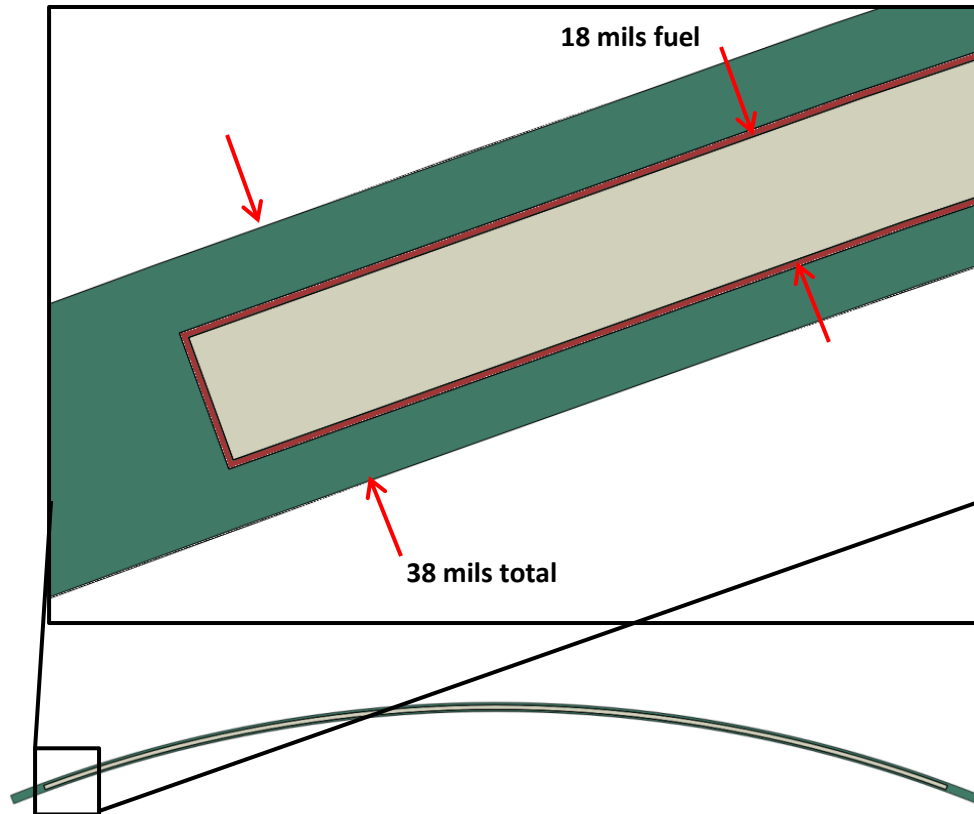


FIGURE 4. PLATE 23 CROSS SECTION. 0.4572 MM (18 MIL) THICK U-10MO FOIL CLAD WITH 0.025 MM (1 MIL) ZIRCONIUM AND 0.229 MM (9 MIL) ALUMINUM.

thickness values result in a total plate thickness of 0.965 mm (38 mils) for plates 2 through 23. Plates 1 and 24, the inner and outermost plates, are each 1.245 mm (49 mils) thick (MURR, 2011). With the thinning of the plates, the volume of water in the LEU core is higher than the present HEU core. This higher water volume provides greater neutron moderation, resulting in longer life and lower cost for the fuel elements.

Design Concerns

With the new LEU fuel plates being 24% thinner than the current HEU fuel plates, there is some concern about the loss in stiffness associated with the thinning of the plates. Additionally, with the layered composite structure, there is a potential slip

plane present at the interface between the clad and the fuel. These changes could potentially allow the coolant flow between the fuel plates to cause the plates to deflect into the coolant channel. This deflection would lead to a reduction in local coolant flow, and produce a hot spot on the plate. If the hot spot were to get hot enough, the plate could fail, leading to a release of fission products into the reactor coolant loop.

Two factors helping to prevent flow induced deflection of the plates are the curvature of the plates and the presence of a comb at the leading and trailing edges. In order to determine the actual benefit provided by both the comb and curvature, the research process focused on first identifying the deflection potential of a flat plate without a comb. This design was used experimentally to provide an upper bound for plate deflection. Additionally, the data from these experiments is useful in validating coupled fluid-structure interaction numeric simulations.

Validation of this novel FSI technique is critical, especially when considering the application of this analysis to a nuclear reactor system. Presently, only a handful of codes are available to solve FSI problems. The major disadvantage of these codes is that they generally rely only on CFD or FEA solution methods. These single method solution techniques lead to potentially significant disadvantages when adapting FEA to fluid problems, or CFD to solid mechanics problems. The dual method solution technique presented here avoids these concerns by ensuring a CFD code solves only for the fluid domain, and an FEA code solves only for the solid domain.

Chapter 3: Numeric Modeling

Code Coupling Process

In order to numerically solve for the effect of coolant flow on plate deflection, a computational fluid dynamics code, Star-CCM+, has been explicitly coupled with a finite element method code, Abaqus. Initially, this process was executed manually using a combination of Java and Fortran scripts to write data to external files. However, within the past year, the numeric codes have advanced and now include an integrated method for exchanging data between the programs. While this new technique does not afford the user the same level of control found in the scripting approach, it is significantly advantageous due to the data exchange process being completely automated, and not requiring that pressure and deflection data be written to external files before being read into the appropriate program.

After first running the fluid and solid models independently, the FSI co-simulation, based on a cyclic four step process, is executed. After building and meshing the independent solid and fluid domains in Abaqus and Star-CCM+, the co-simulation process described in Figure 5 is executed until a converged, steady state solution is obtained. While the overall steady state FSI solution process is time independent, the

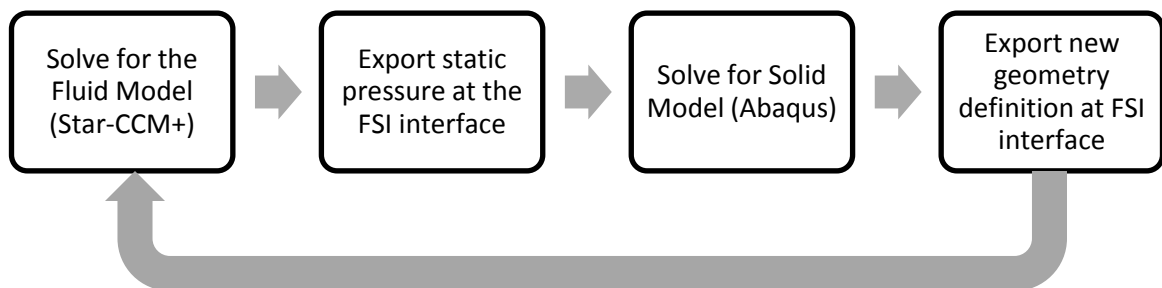


FIGURE 5. FSI CO-SIMULATION PROCESS

final FSI solution is found through the use of time dependent solutions from the CFD and FEM codes. The use of transient solvers in the CFD and FEM codes is necessary due to the use of differing solution techniques in the two codes. The CFD code utilizes an Eulerian solution process that solves for fluid motion through discrete control volumes, and the FEM code utilizes a Lagrangian solution process that solves for the deformation of discrete volumes of material in the body. To allow for simultaneous solution of both the fluid and solid domains, the physical values at the interface between the domains are utilized as boundary conditions for both codes. To facilitate updating of the boundary condition values, a 'pseudo-time' step is used to provide intervals at which data can be exchanged between the programs.

CFD Solution Process

To model the fluid domain, a computational fluid dynamics (CFD) code Star-

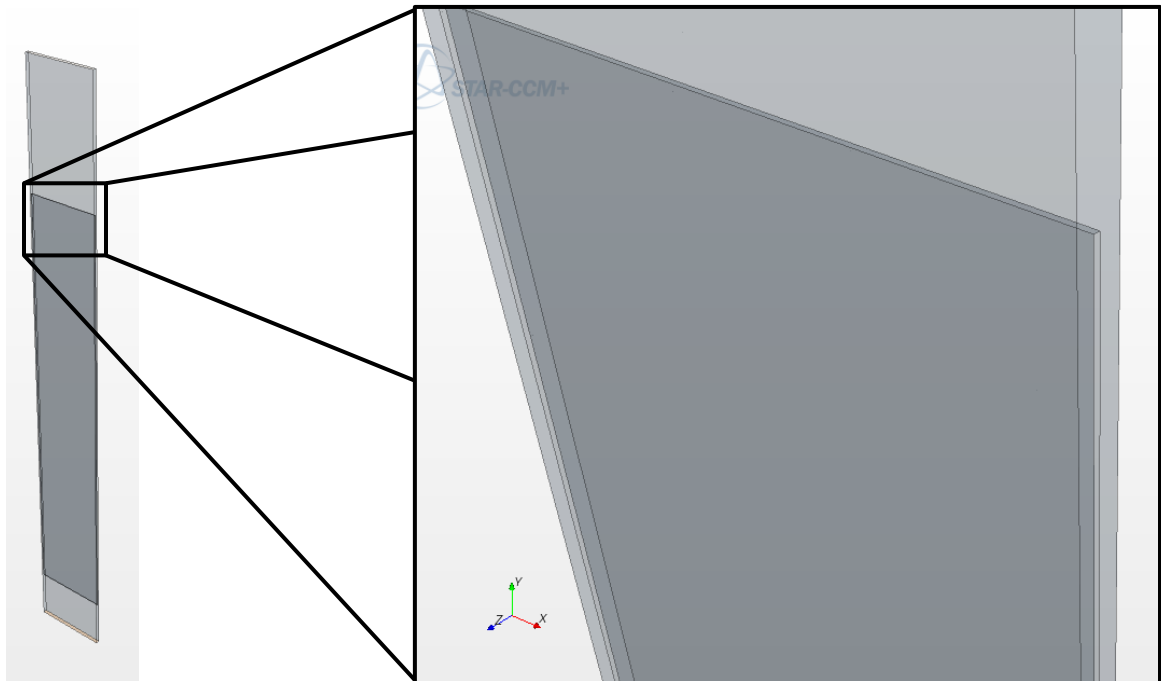


FIGURE 6. BASIC GEOMETRY FROM CFD MODEL. NOTE THE GAP IN THE MIDDLE OF THE FLOW CHANNEL FOR THE PLATE.

CCM+ was utilized (CD-Adapco, 2011). The basic geometry, shown in Figure 6, consists of a long, rectangular flow channel with a void where the plate is located. With flow being from the top down, the model includes an entrance plenum to allow for flow development, and an exit plenum to allow for pressure equalization at the end of the plate. In the case of a free leading edge boundary for the plate, much of the analysis is focused on the flow around the leading edge of the plate at the midpoint of the span. Figure 7 shows examples of the mesh, pressure, and velocity data available at this location. This data is useful for validating analytic and experimental results.

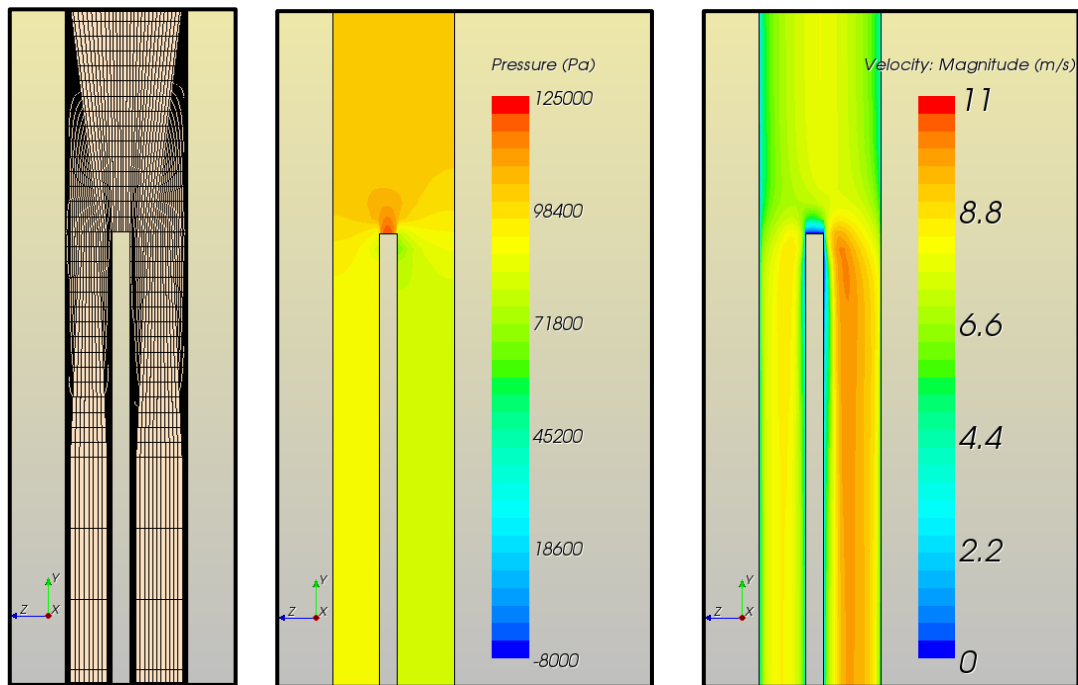


FIGURE 7. EXAMPLES OF MESH, PRESSURE, AND VELOCITY AT THE LEADING EDGE OF A PLATE.

As shown in Figure 7, the CFD code works by discretizing the fluid domain into small control volumes. In a transient solution process, the domain is updated at discrete time intervals. To solve for the updated fluid domain, a general CFD transport equation

methodology is used. The transport quantity ϕ is described by the general differential equation,

$$\frac{\partial}{\partial t}(\rho\phi) + \nabla(\rho\vec{v}\phi) = \nabla(\Gamma\nabla\phi) + S \quad (1)$$

where ρ is the density, \vec{v} is the velocity, Γ is the diffusion coefficient, and S is the source term. The terms in Eq. 1 are, from left to right, the unsteady (transient) term, the convection term, the diffusion term, and the source term. The variable ϕ represents any of a number of quantities, including enthalpy, velocity, or turbulent kinetic energy (Patankar, 1980). In order to be utilized by a numeric code such as Star-CCM+, Eq. 1 must be discretized so it can be applied to a control volume. In Star-CCM+, Eq. 2 is used as the discretized form of Eq. 1 (CD-Adapco, 2011).

$$\frac{d}{dt}(\rho\phi V)_i + \sum_f [\rho\phi(\vec{v} \cdot \vec{a} - G)]_f = \sum_f (\Gamma\nabla\phi \cdot \vec{a})_f + (S_\phi V)_i \quad (2)$$

where V is the volume, \vec{a} is the face area vector, and the subscripts f and i denote the cell face and solver iteration, respectively. From Eq. 2, the unsteady term can be discretized through a first or second order scheme. When running CFD simulations alone without code coupling, it is adequate to discretize the unsteady term through the first order Euler implicit scheme, as described in Eq. 3. This scheme is used to ascertain the initial flow field condition prior to running an FSI simulation.

$$\frac{d}{dt}(\rho\phi V)_i = \frac{(\rho_i\phi_i)^{n+1} - (\rho_i\phi_i)^n}{\Delta t} V_i \quad (3)$$

where n denotes the time step and Δt is the length of a time step. For FSI simulations, to help promote stability as the simulation progresses, it is advantageous to use the

previous two time steps when discretizing the unsteady term. Therefore, the second order temporal discretization scheme shown in Eq. 4 is utilized.

$$\frac{d}{dt}(\rho\phi V)_i = \frac{3(\rho_i\phi_i)^{n+1} - 4(\rho_i\phi_i)^n + (\rho_i\phi_i)^{n-1}}{2\Delta t} V_i \quad (4)$$

Additionally, because the FSI process is used to find the steady state solution, the transient solution is not of particular interest. Therefore, ‘time’ as considered in the context of the FSI problems presented here is actually a ‘pseudo-time’, in that the time variable is used solely as a means to provide an interval for data exchange between the two codes. The time steps used in the CFD code, combined with the inertial motion of the plate boundary make transient fidelity difficult to obtain with current modeling techniques.

The convection term, as shown in Eq. 5, is discretized based not only on the mass flow through a cell, but also on the flux through the cell due to the morphing of the fluid mesh to accommodate the new solid geometry.

$$[\phi\rho(\vec{v} \cdot \vec{\alpha} - G)]_f = (\dot{m}\phi)_f = \dot{m}_f\phi_f \quad (5)$$

The grid flux term, G , is a volumetric flux which is calculated at each cell face when the fluid mesh is morphed due to the deflection calculated in the FEM model. To provide stability to the FSI solution, the grid flux term can be relaxed at each time step. While this has the effect of limiting the change in the fluid solution due to the motion of the interface and leads to a longer overall run time, it can also be useful in ensuring simulation stability.

The third term in Eq. 5 provides the diffusion gradient of the variable ϕ between cells in the mesh. The source term is neglected as no mass or heat generation is present in the model.

FEM Solution Process

To find a solution to the plate deflection problem, a finite element code, Abaqus was utilized. The plate modeling process involved building a three dimensional solid model of the plate in Abaqus, and then meshing the model with 8 node or 20 node solid, deformable elements, as defined in Figure 8. This element type was chosen for its ease of use when coupling with an FSI simulation. Another option for modeling thin plates is to use shell elements. However, given the relatively large deflections expected with these models, shell elements would yield less accurate results.

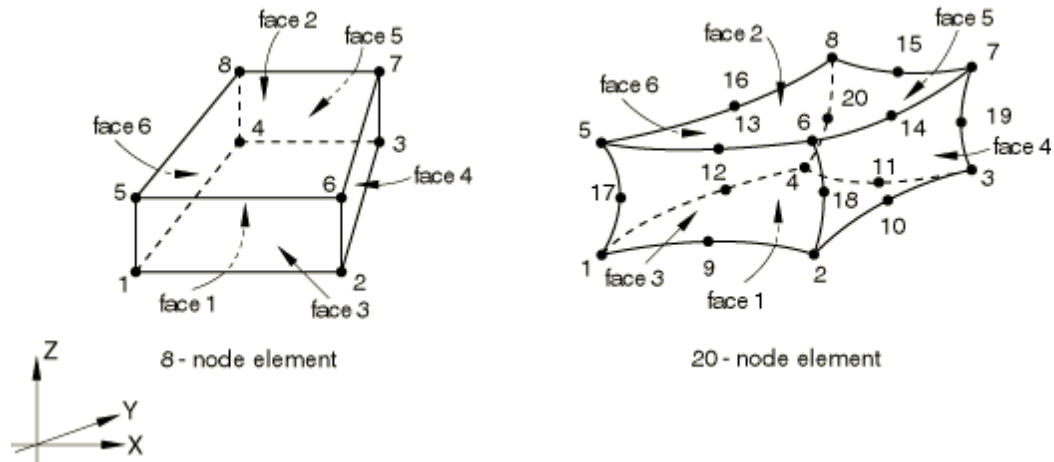


FIGURE 8. ABAQUS NODE AND ELEMENT SURFACE DEFINITIONS (SIMULIA, 2011).

To mesh the model, the edges were seeded to provide the spacing for the nodes. Then, a mesh was generated as shown in Figure 9. On the outside edges of the plate, a clamped boundary condition was applied, and the mesh is coarser at these locations

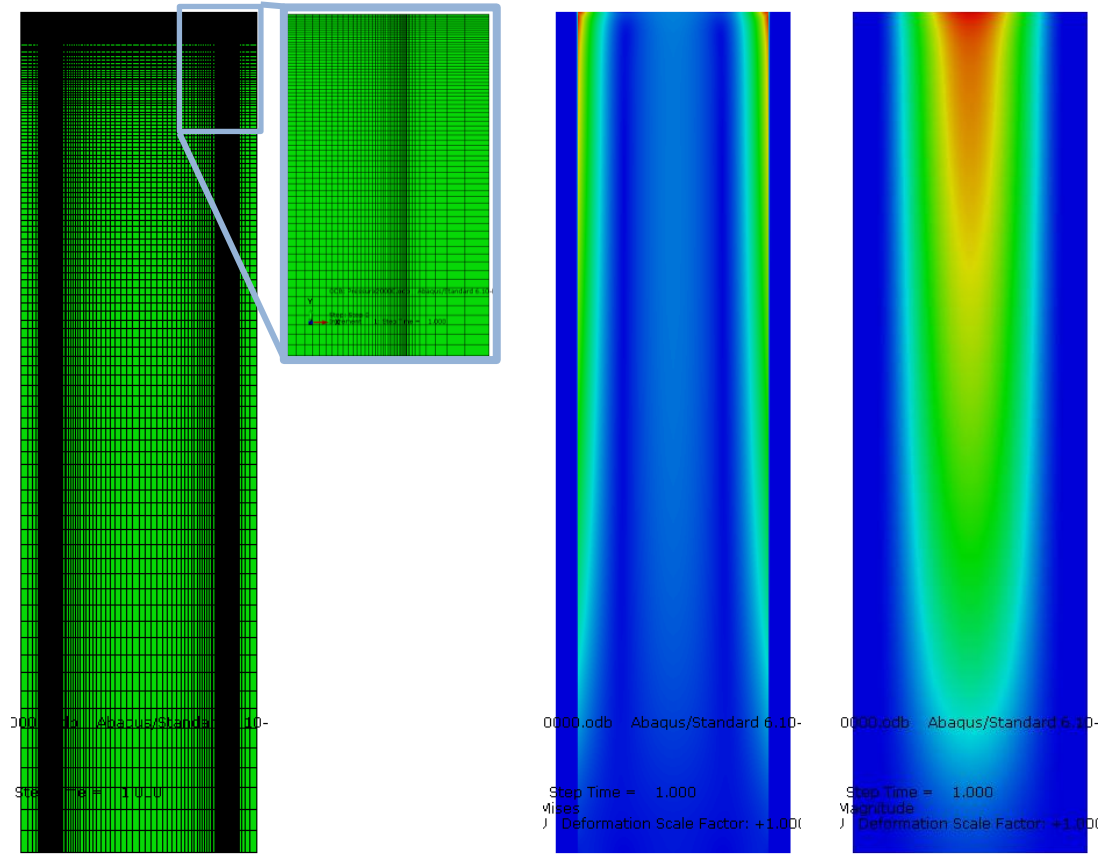


FIGURE 9. FEA MODEL MESH, STRESS, AND DEFLECTION PLOTS

due to the absence of any deflection. Additionally, the mesh was made significantly more dense through the thickness of the plate to help provide a more accurate profile of the plate deflection and stresses. These deflection and stress values, as shown in Figure 9, are visualized at the completion of a simulation. Additionally, plots are created of the out of plane deflection across the leading edge of the plate for comparison to analytic models.

Stability

The nature of FSI modeling lends itself to instabilities in the solution process. For instance, it is critical to ensure that the CFD model reaches a converged solution at each time step before exporting the pressure field to the FEM model. Failure to export a

converged pressure field at a time step will result in an inaccurate solution to the solid model. This inaccuracy propagates through subsequent steps, yielding an unstable, divergent solution. Because much of the difficulty in ensuring a converged solution comes from the CFD solution, criteria for solution convergence have been established. Within the CFD model, the static wall pressure and wall shear stress are monitored as the solution iterates. The solution is not considered converged until both of these criteria have reached a steady solution for a given time step.

In addition to ensuring a converged solution at each time step, other controls are used to prevent dramatic changes in the solution between time steps. Due to the high aspect ratio of the geometry under consideration, any large deflection of the plate or large change in the pressure field between time steps could make it difficult for the solvers to find a converged solution in subsequent time steps. In the CFD model, pressure under-relaxation factors are used to dampen the response of the pressure field between time steps. In the FEM model, mass proportional damping is applied as a material property to the model.

To determine the damping factors for the FEM model, Abaqus is used to complete a modal analysis prior to running the FSI simulation. From this modal analysis, the first vibration mode is extracted, and 10% critical damping is applied. In the Abaqus model, the fraction of critical damping, ξ , is defined through application of mass proportional and stiffness proportional damping factors α and β to the natural frequency ω .

$$\xi = \frac{\alpha_R}{2\omega_i} + \frac{\beta_R\omega_i}{2} \quad (6)$$

To critically damp the model, ξ should be equal to 1. However, given the uncertainty associated with determining the natural frequency of the plate through purely numeric means, ξ is targeted for approximately 10% of the estimated critical damping.

A final stability control is to gradually ramp the pressure load on the plate at the start of the simulation. This prevents ‘shocking’ the FEM model with a large pressure load in the initial step. The pressure ramping is controlled through Star-CCM+, and involves ramping the pressure on the entire surface of the plate to approximately 1/3 of the maximum expected pressure, and then gradually ramping from that point to the actual pressures experienced by the plate. Because the pressure is dependent upon the inlet velocity, pressure ramping can alternatively be applied by ramping the velocity of the flow at the inlet of the fluid model. Both techniques work well, but the direct method tends to be more efficient as it maintains a converged fluid solution throughout the course of a simulation. This reduces the number of iterations necessary in the fluid solution at each time step, and therefore reduces the overall run time.

Efficiency

To assist with these FSI simulations, a mini cluster of high performance workstations has been constructed. This cluster consists of three workstations, a desktop, and a server/controller. For most simulations, two workstations are typically used, providing 8 Intel Xeon cores at 2.4 GHz, and 12 Intel Xeon cores at 3.33 GHz. Additionally, post processing is completed on a desktop with 4 Intel Core i7 cores at 3.33

GHz. Even with these machines, simulation runtimes are still a concern. Depending on the model being investigated, and the density of the fluid mesh, a single FSI simulation can take anywhere from a couple of days to a month to complete.

The primary factor in determining the run time of an FSI simulation is the density of the CFD mesh. Higher density meshes which are on the order of 22 million + cells will take almost a month to complete. For this reason, much focus has been on ways to maintain simulation accuracy and stability through the use of meshes with densities on the order of 5 million cells or less. These simulations tend to complete in only a few days. Conversely, meshes which have very low density tend to yield unstable and inaccurate results.

Chapter 4: Analytic Modeling

Flow Model Development

To model the flow around a single plate, a basic geometry was designed which contains a flat, rectangular plate with channel gaps of differing thicknesses on either side. The geometry considered is shown in Figure 10, and includes regions for flow development at the inlet and exit of the plate region.

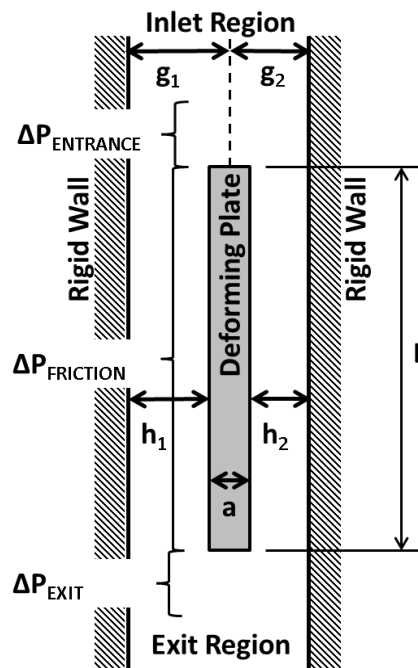


FIGURE 10. ASSEMBLY GEOMETRY. FLUID FLOW IS FROM THE TOP DOWN

To determine the pressure drop through the assembly without considering plate deflection, a simple equation was developed to account for pressure drop from friction, flow contraction at the leading edge of the plate, and flow expansion at the trailing edge of the plate. The frictional pressure drop is defined by Eq. 7, where the hydraulic diameter, D_h is shown in Eq. 8.

$$\Delta p_{friction} = f \frac{L}{D_h} \frac{\rho V^2}{2} \quad (7)$$

$$D_h = \frac{4bh}{2(b+h)} = \frac{2bh}{(b+h)} \quad (8)$$

The friction factor is defined by the Colebrook equation, Eq. 11, and is dependent on Eq. 12, the Reynolds number and surface roughness of the channel. It is important to note that only cases in the turbulent regime are being considered here, where the Colebrook equation is known to be valid (White, 2003).

$$\frac{1}{\sqrt{f}} = -2.0 \text{Log}_{10} \left(\frac{\varepsilon}{3.7} + \frac{2.51}{Re\sqrt{f}} \right) \quad (9)$$

$$Re = \frac{\rho V D_h}{\mu} \quad (10)$$

To account for the pressure contribution from the contraction at the leading edge of the plate, Eq. 11 is utilized, and expansion at the trailing edge of the plate is found using Eq. 12. These equations apply to the geometries outlined in Figure 11 (White, 2003).

$$\Delta p_{contraction} = \frac{\rho V_1^2}{2} * 0.42 * \left[1 - \left(\frac{A_2}{A_1} \right)^2 \right] \quad (11)$$

$$\Delta p_{expansion} = \frac{\rho V_1^2}{2} * \left[1 - \left(\frac{A_1}{A_2} \right)^2 \right]^2 \quad (12)$$

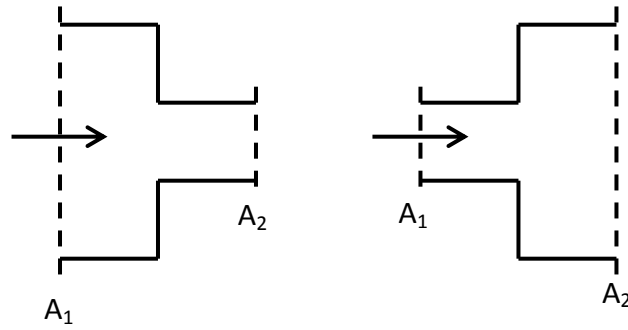


FIGURE 11. FLOW CHANNEL CONTRACTION (LEFT) AND EXPANSION (RIGHT).

Because much of the other analysis revolves around mass flow rates, Eq. 13 was used to modify Eqns. 7,10,11 and 12.

$$\dot{m} = \rho VA \quad (13)$$

This yields Eqns. 14-17:

$$\Delta p_{friction} = f \frac{L}{D_h} \frac{\dot{m}^2}{2\rho A^2} \quad (14)$$

$$Re = \frac{\dot{m} D_h}{\mu A} \quad (15)$$

$$\Delta p_{contraction} = \frac{\dot{m}^2}{2\rho A_1^2} * 0.42 * \left[1 - \left(\frac{A_2}{A_1} \right)^2 \right] \quad (16)$$

$$\Delta p_{expansion} = \frac{\dot{m}^2}{2\rho A_1^2} * \left[1 - \left(\frac{A_1}{A_2} \right)^2 \right] \quad (17)$$

To determine the flow rate in each channel, an iterative approach is used. Initial guesses of the flow rates in each channel are taken in order calculate approximate Reynolds numbers and friction factors. Then, by factoring out the \dot{m}^2 term from equations 14, 16, and 17, and summing them, coefficients for pressure drop in each channel are found.

$$c_{\Delta p,channel} = \frac{\Delta p_{contraction}}{\dot{m}_{channel}^2} + \frac{\Delta p_{friction}}{\dot{m}_{channel}^2} + \frac{\Delta p_{expansion}}{\dot{m}_{channel}^2} \quad (18)$$

By knowing the total flow rate into the assembly, a system of equations is solved to find the flow rate in each channel that produces an equal pressure drop in each channel.

This system yields Eqns. 19 and 20.

$$\dot{m}_{channel\ 1} = \dot{m}_{total} \frac{\sqrt{c_{\Delta p,channel\ 1}}}{\sqrt{c_{\Delta p,channel\ 1}} + \sqrt{c_{\Delta p,channel\ 2}}} \quad (19)$$

$$\dot{m}_{channel\ 2} = \dot{m}_{total} - \dot{m}_{channel\ 1} \quad (20)$$

If these values differ from the guessed values, then the Reynolds number and friction factor are recalculated, and the process is repeated until a converged solution is found.

A converged solution is typically found in less than five iterations. Once a converged solution for the flow rates is found, these values are substituted back into Eqns. 14, 16, and 17 and summed together to get the total pressure drop over the plate region. To find the pressure drop contribution from the inlet and exit regions, Eq. 14 is solved using the total flow rate into the assembly.

Deflection Model Development

The frictional pressure drop through the channels on either side of the plate produces a linear net pressure force along the length of the plate. The maximum pressure force occurs at the leading edge of the plate, and reduces to no net pressure at the trailing edge of the plate. The plate displays maximum deflection at the leading edge with no deflection at the trailing edge. Because the maximum deflection is of

greatest concern, initial modeling utilized a simple 1-D beam equation to estimate the deflection of the leading edge.

$$\delta = \frac{px^2}{24EI} (b - x)^2 (1 - \nu^2) \quad (21)$$

Equation 21 can be integrated over the plate width and divided by b to find the average deflection.

$$\delta_{AVE} = \frac{\int_0^b \delta dx}{b} = \frac{pb^4}{60Ea^3} (1 - \nu^2) \quad (22)$$

Knowing that the maximum deflection will be at the midpoint of the plate, Eq. 21 can be solved for $x=b/2$ to yield a model for the maximum plate deflection.

$$\delta_{max} = \frac{pb^4}{32Ea^3} (1 - \nu^2) \quad (23)$$

By examining Eq. 23, it can be seen that deflection is a cubic function of plate thickness and a quartic function of width. Given that the new fuel plates are being thinned down by 24%, and that the plates are significantly wider than they are thick, it is easy to understand why deflection is a potential concern in the new fuel design.

A simple wide beam model is useful for describing the qualitative deflection of the plate, and matches closely to numeric models where flow redistribution isn't considered. This provides a metric that can be used to validate the independent CFD and FEA models before the FSI problem is considered.

Chapter 5: Flat Plate Modeling

Computational Models

In the new MURR fuel assembly, the fuel plates are curved, adding to their rigidity. Additionally, there is a comb at the leading and trailing edges of the plates, pinning them in place at the midpoint of those edges. Bearing in mind that a curved plate will present greater resistance to flow induced deflection than a flat plate, the present analysis has instead focused on modeling a flat plate, as shown in Figure 12, in order to determine a bounding case for plate deflection. Additionally, the dimensions selected for the plate are roughly based on the dimensions of plate 23 from the new MURR assembly, as this is the most extreme case in the design. In order to correlate well with experimental results, the focus has been on monolithic aluminum plates,

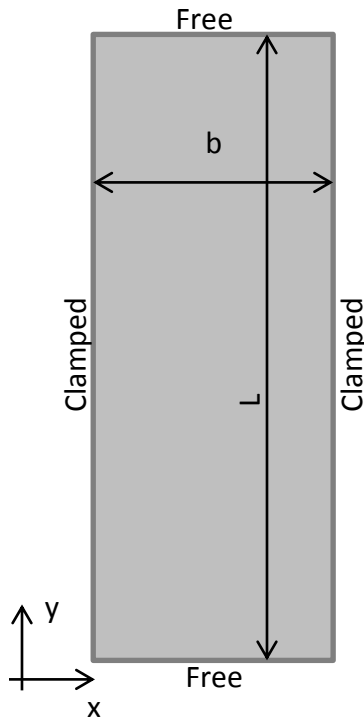


FIGURE 12. PLATE MODEL SETUP

foregoing the composite structure for the time being. While it is helpful from a modeling perspective to start with a simplified geometry, there is also cause from a fuel qualification perspective to start with this type of model. If it can be shown that this worst case scenario is capable of withstanding the hydraulic forces present in the reactor, then future work on more prototypic models will serve to illustrate the margin available in the design. However, if the worst case scenario shows significant deflection, then additional work will be necessary to verify that the real fuel plates are actually rigid enough to withstand the hydraulic forces in the flow loop.

To analyze this flat plate model, a worst case scenario was simulated. This involved using a 0.8128 mm (32 mil) thick flat plate with channels of 2.032 mm (80 mil) and 2.540 mm (100 mil) on either side.

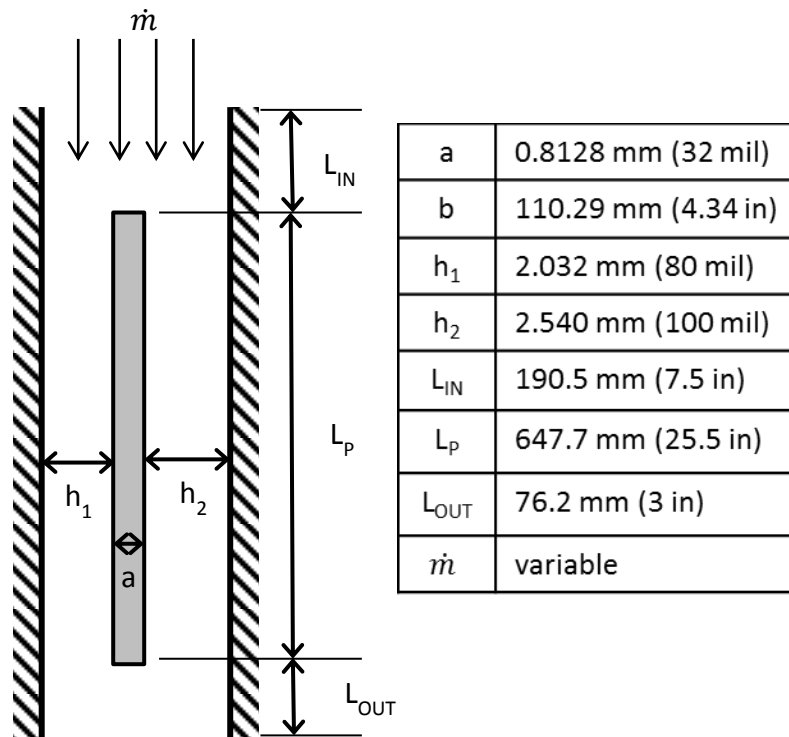


FIGURE 13. SIMULATED GEOMETRY. NOTE b IS THE PLATE WIDTH.

The plate model shown in Figure 13 was first modeled in Abaqus. Mesh density, and particularly the density of the mesh through the thickness of the plate, was gradually increased to ensure that the solution was not dependent on the mesh. From Figure 14, it can be seen that for a given pressure load, the maximum deflection seen on a plate changed very little with variation in the number of solid elements through the thickness.

Using the mesh of the solid plate model, a fluid model was built in Star-CCM+ around the solid model. This fluid model contains the outer surface of the plate, the fluid channel walls, and the inlet and exit boundaries. The solid model itself is not present in the fluid model, and the fluid boundary at the location of fluid structure interaction is co-located with the surface of the plate, providing the same geometric definition for the FSI boundary. Like the solid model, the fluid mesh was modified to gradually higher densities until an acceptable mesh was obtained. From Figure 15, the results from this mesh independence study show that as the mesh density neared 2

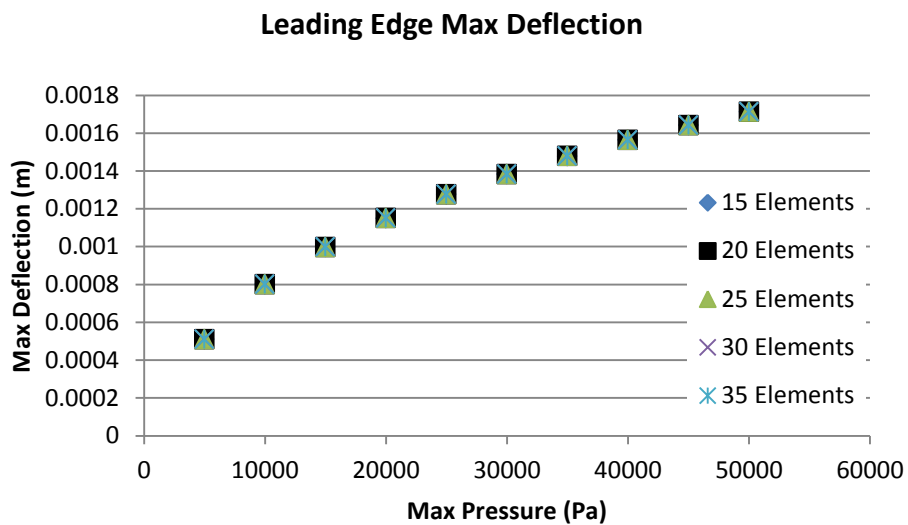


FIGURE 14. ABAQUS MESH INDEPENDENCE DEFLECTION RESULTS.

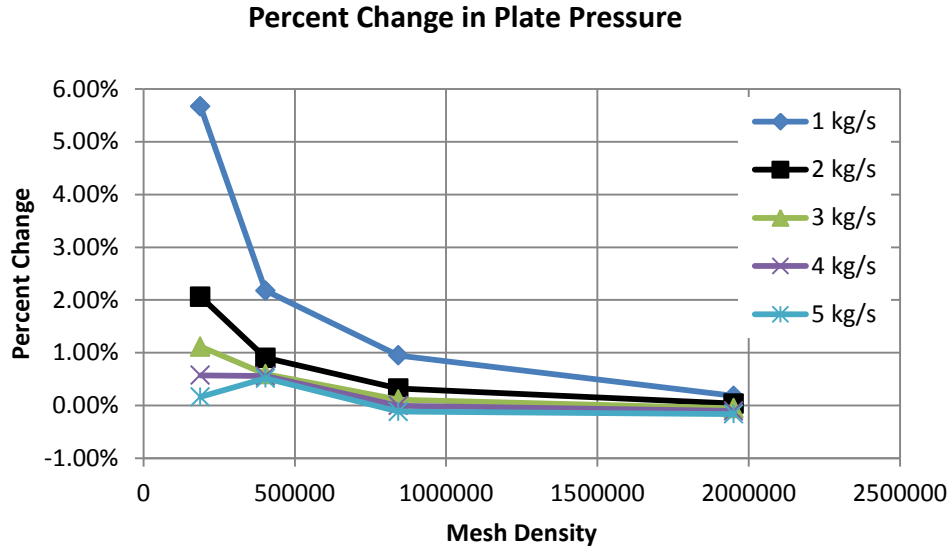


FIGURE 15. PERCENT CHANGE IN PLATE PRESSURE DROP AS MESH DENSITY INCREASES

million cells, the discrepancy in the solutions for numerous flow rates dropped to near zero. As the mesh density was incrementally increased, the percent change in the pressure solution was found by comparing the pressure drop of the current, higher density mesh with that of the previous mesh, as described in Eq. 24.

$$\% \text{ Change} = \frac{P_{\text{current}} - P_{\text{previous}}}{P_{\text{previous}}} * 100 \quad (24)$$

Once the solid and fluid models were constructed and the meshes validated, each code was run independently to verify that the independent models were valid prior to coupling through an FSI simulation. The coupled FSI simulation was set up by modifying the Abaqus input file to contain the commands for co-simulation. Additionally, the Star-CCM+ model was modified with the co-simulation parameters. These co-simulation parameters can be found in Appendix 1.

To ensure the CFD solution reaches convergence prior to exchanging data with the FEM solution, the approximate fluid transit time from inlet to outlet is utilized as the CFD time step. The FEM model is allowed to use time steps smaller than the CFD model, but cannot use a step size larger than the CFD model. This typically results in the FEM model taking multiple steps for each CFD step early on in the coupled simulation. In later increments, as the simulation approaches a steady state solution, the programs step at the same, constant CFD step size. To help determine the influence of flow rate on deflection, the same model was run at multiple flow rates. Additionally, the pressure profile in the fluid channels was extracted from the models for comparison to analytic and experimental results.

Experimental Setup

The flow loop shown in Figure 16 was constructed at the University of Missouri to analyze different plate and channel configurations. The primary purpose of the flow loop is to provide validation of the numeric models. The loop is instrumented with numerous tools to assist in analysis, including a pressure transducer, laser displacement measurement heads, a flow meter, and a pneumatic valve for flow control. These systems are controlled by an automated LabView system to complete flow tests.

To complete testing, a test section was designed for use in the flow loop. The test section shown in Figure 17, was constructed to simulate the same geometry from Figure 13. For the purposes of this analysis, only a single assembly was analyzed, as outlined previously. However, the test section is easily reconfigurable to accommodate a wide range of plate and channel sizes. Additionally, the section can hold an array of

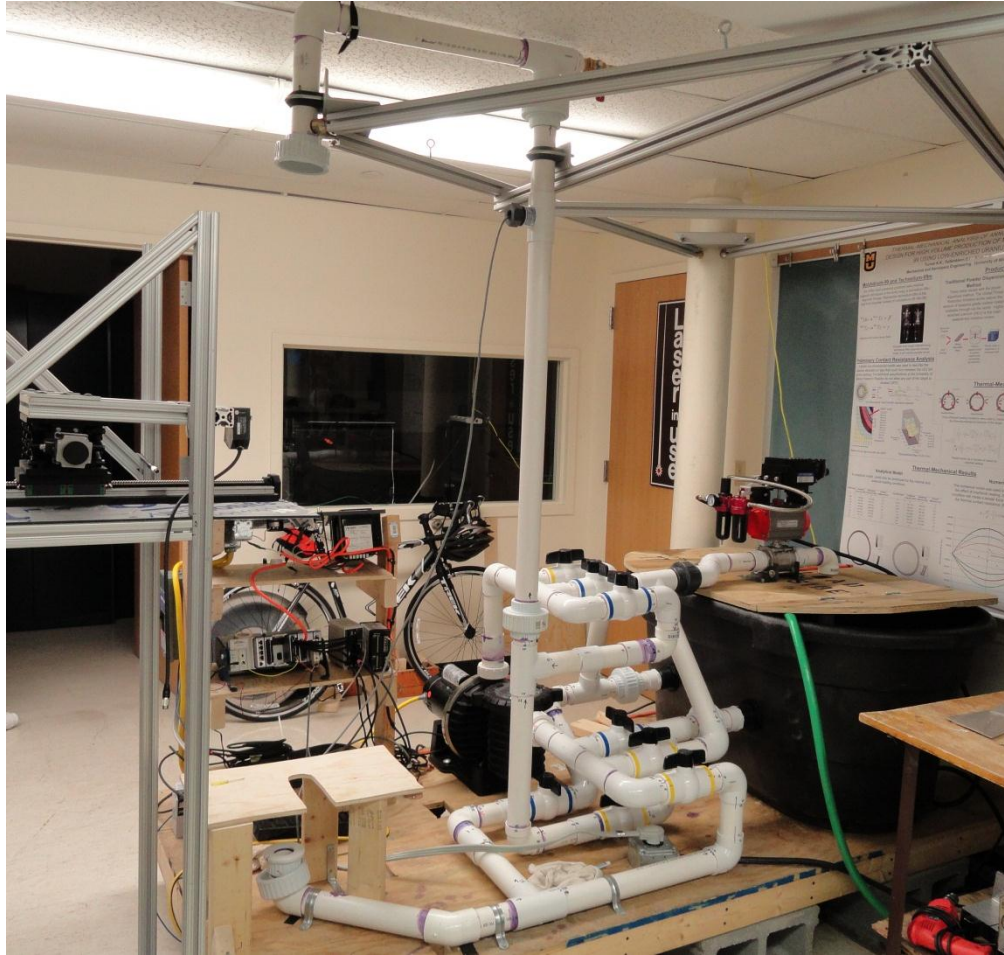


FIGURE 16. MISSOURI FLOW LOOP

up to five plates to assist in analyzing the effects of larger plate arrays. These tests are outside the scope of the current study, but may happen in later tests.

Prior to testing the assembly shown in Figure 13, measurements were taken using the optical laser heads to determine the initial channel gaps and any preexisting curvature to the plate. The lasers were first used to sweep across the width of the test section just above the leading edge of the plate. This measurement gives the profile of the gap between the two plexi glass panels ($h_1 + h_2 + a$ as a function of b). Next, the lasers were lowered down to the leading edge of the plate and used to map the profile of the flow channels on either side of the plate (h_1 and h_2). From the channel profiles

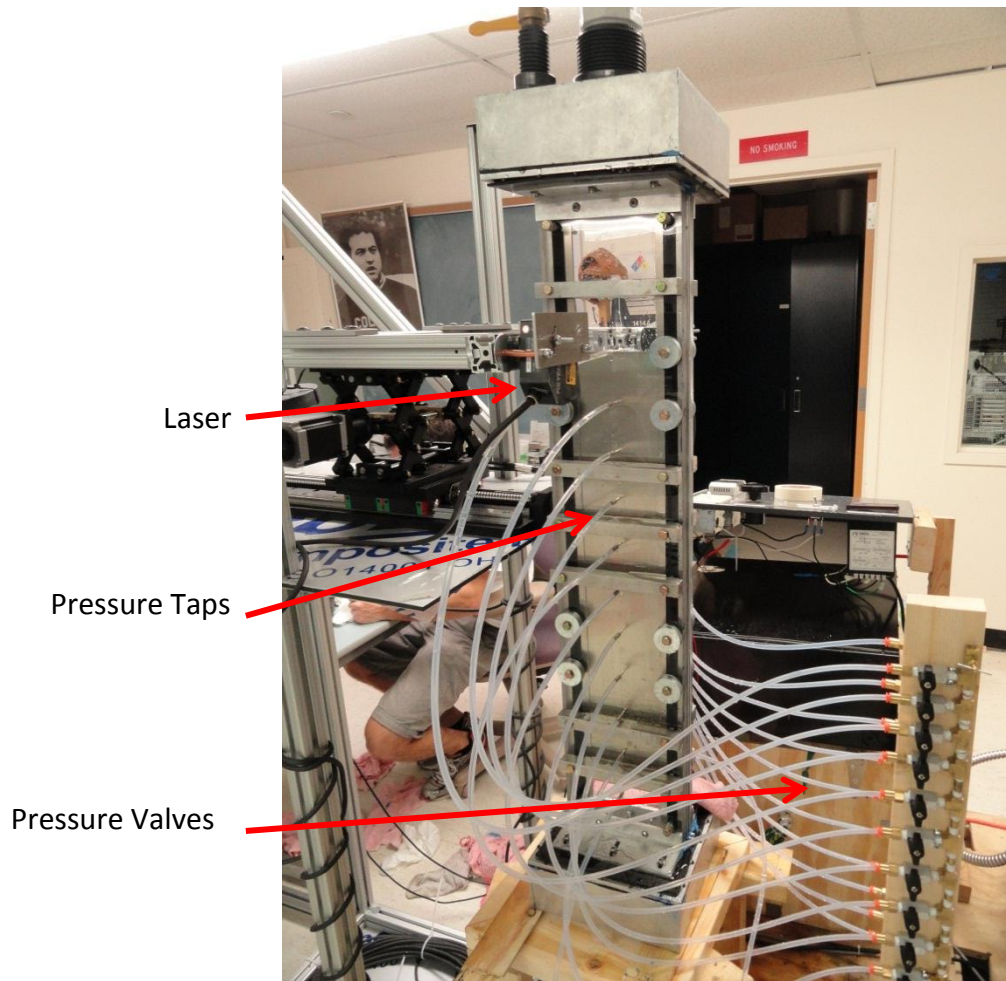


FIGURE 17. FLAT PLATE TEST SECTION.

shown in Figure 18, there appears to be a slight curvature of the plate into the larger channel, as indicated by the narrowing of the larger channel near the middle of the plate. Additionally, the overall channel gap narrows at the center indicating a slight curvature to the plexi glass outer panels. shows the average channel gap thicknesses from Figure 18. In addition to using the laser heads to measure the channel gap at the leading edge, manual measurements of the channel spacer and plate thicknesses were taken prior to assembly of the test section. These measurements were taken along the full length of the spacers and plates, not just the leading edge.

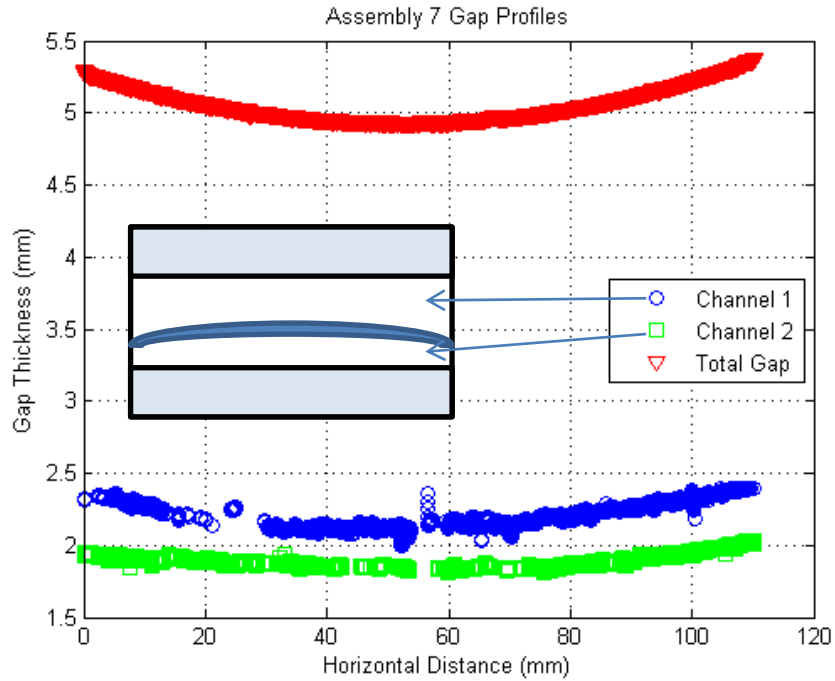


FIGURE 18. CHANNEL GAP PROFILES.

Finally, because the lasers will be located at the center ($b/2$), leading edge position of the plate during flow tests, it is important to have a good understanding of the dimensions at this location. The lasers were used to measure the thickness of the plexi glass, the channel gaps with air, and the distance from the outside of the plexi glass to the surface of the plate with water in the channels, as shown in Table 2. Due to the differing indices of refraction for air, plexi glass, and water, these values are necessary for determining correction factors for the laser heads so the data obtained during the flow tests can be properly interpreted.

TABLE 1. SUMMARY OF ASSEMBLY DIMENSIONS.

	Design	Assembly 7 Sweep	Micrometer
Gap h_1	2.540 mm	2.258 mm	2.432 mm
	100.000 mils	88.913 mils	95.767 mils
Gap h_2	2.032 mm	1.899 mm	1.952 mm
	80.000 mils	74.744 mils	76.869 mils
Plate a_1	0.813 mm	0.9037 mm	0.815 mm
	32.000 mils	35.579 mils	32.105 mils
$h_1+h_2+a_1$	5.385 mm	5.061 mm	5.200 mm
	212.000 mils	199.236 mils	204.705 mils

TABLE 2. THICKNESS MEASUREMENTS AT CENTER, LEADING EDGE OF PLATE.

	Design	Gap _{Air} (Actual)	Plexi (Measured)	Plexi + Gap _{Water} (Measured)	Correction Factor
Gap h_1	2.540 mm 100.000 mils	1.936 mm 76.232 mils	15.828 mm 623.130 mils	17.339 mm 682.622 mils	1.281
Gap h_2	2.032 mm 80.000 mils	1.796 mm 70.713 mils	15.698 mm 618.035 mils	17.002 mm 669.374 mils	1.377

While the test section was designed around the values outlined in Figure 13, it is obvious that the channels in the actual assembly are slightly thinner than the designed values. This variation, although small, will be important when comparing to results from the numeric simulations, which were based on the idealized values from Figure 13. The slight decrease in channel thickness will lead to higher flow velocities and a slightly different pressure distribution than the numeric model at the same flow rate.

Once all initial measurements were completed, the test section and flow loop was prepared for flow testing. LabView was used to control the flow rate and collect data on the flow rate, pressure, and plate deflection. To complete the flow test, the flow rate was started at the lowest possible value, and gradually increased to the maximum value

that the pump is capable of. Once at the maximum value, that flow rate was held constant for several minutes while measurements were taken at 18 different pressure taps along the length of both channels. Once these pressure measurements were completed, the flow rate was gradually returned to the minimum value, and the test completed. The results from this test are outlined in Chapter 6, along with the corresponding analytic and numeric results. It should be noted that in the case of the numeric results, the idealized geometry was used, and therefore it varies slightly from the actual, measured geometry of the test section.

Chapter 6: Flat Plate Results and Discussion

Experimental Results

Using the assembly outlined in Figure 13, flow tests were completed to determine the deflection at the leading edge of the plate. In the initial phase of the test, the flow rate is gradually increased with LabView recording the channel gap and flow rate. The change in the channel thickness at the midpoint is shown in Figure 19, with the flow rate profile shown in Figure 20. Since the flow rate is based on an incremental closing of a valve in a circular pipe, a function based on the sum of two sine curves works well to define the flow rate as a function of the experiment time. This equation is necessary so that the data collected from the lasers and the pressure transducer can be plotted against the flow rate data. Because the flow rate data is based on a frequency

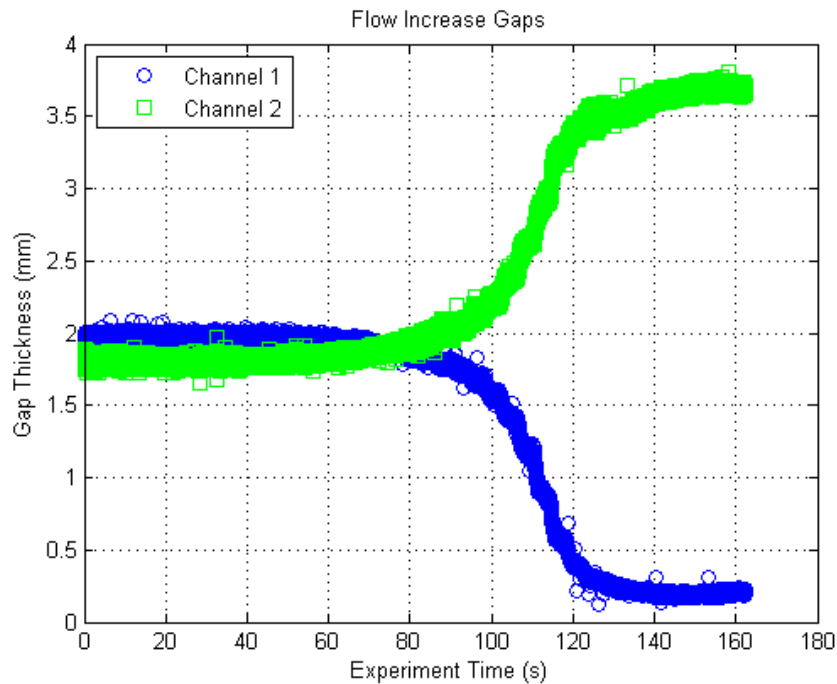


FIGURE 19. CHANNEL GAP AT MIDPOINT DURING INTIAL TEST PHASE.

measurement that is dependent upon the flow rate of the water, the data collected from the flow meter is independent of that collected from the lasers or the pressure transducer. Essentially, although the data collection rate for the lasers and the pressure transducer is synchronized, the flow data is not. Equation 24 was fit to the flow rate data in Figure 20. Using the flow rate data along with the average values of channel thickness from the initial profile in Figure 18, the average velocity of the fluid over the plates was plotted as Figure 21.

$$\dot{m}(t) = a_1 \sin(b_1 t + c_1) + a_2 \sin(b_2 t + c_2) \quad (25)$$

where:

- $a_1 = 20.44$
- $b_1 = 0.01934$
- $c_1 = -0.3285$
- $a_2 = 18.67$
- $b_2 = 0.0211$
- $c_2 = 2.729$

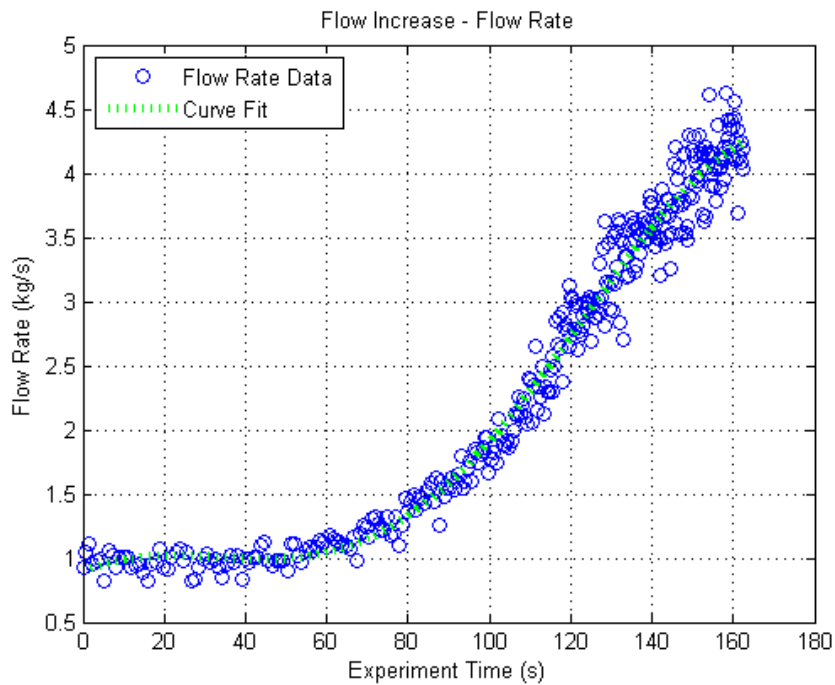


FIGURE 20. FLOW RATE DURING THE INITIAL TEST PHASE.

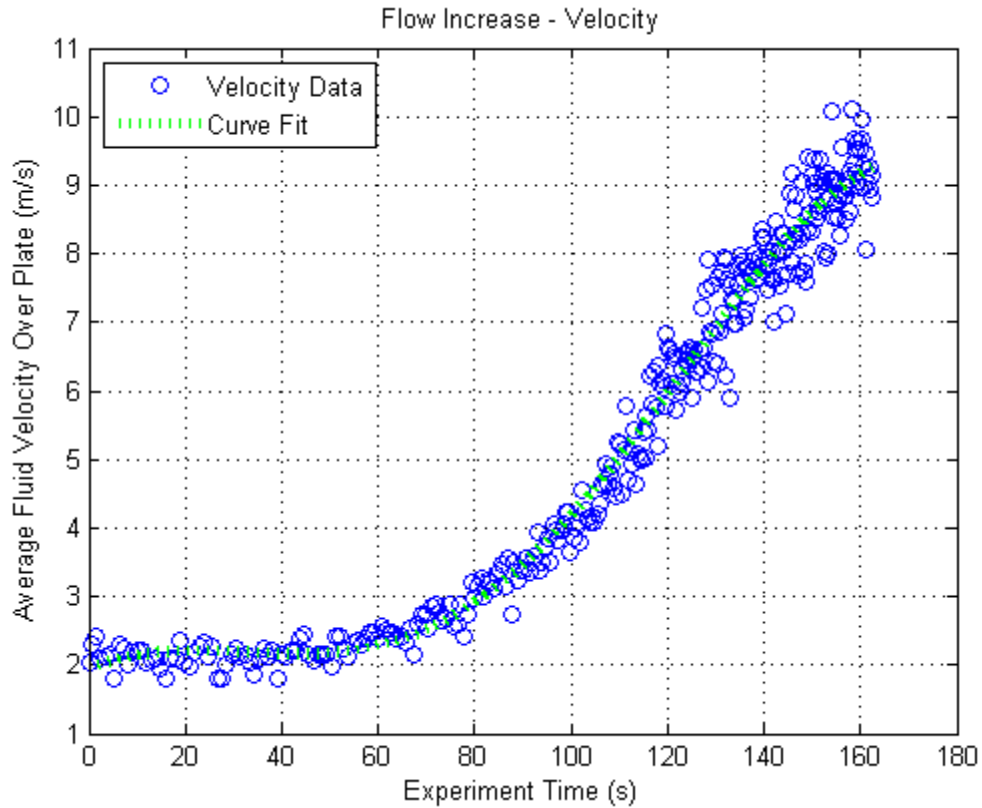


FIGURE 21. FLOW CHANNEL VELOCITY DURING INITIAL TESTING PHASE.

Using the flow velocity from Figure 21 with the channel gap data of Figure 19, we can now determine the deflection of the plate as a function of fluid velocity. This form of the deflection profile is convenient since most existing literature on flow induced plate deflection uses fluid velocity as the driving force in determining plate deflection.

$$V(t) = a_1 \sin(b_1 t + c_1) + a_2 \sin(b_2 t + c_2)$$

where:

$$\begin{aligned}
 a_1 &= 40.7 \\
 b_1 &= 0.01925 \\
 c_1 &= -0.3242 \\
 a_2 &= 36.82 \\
 b_2 &= 0.02119 \\
 c_2 &= 2.725
 \end{aligned}
 \tag{26}$$

Figure 22 shows the deflection data from channel 1 as a function of the fluid velocity.

Note that the plate deflection is into the larger channel.

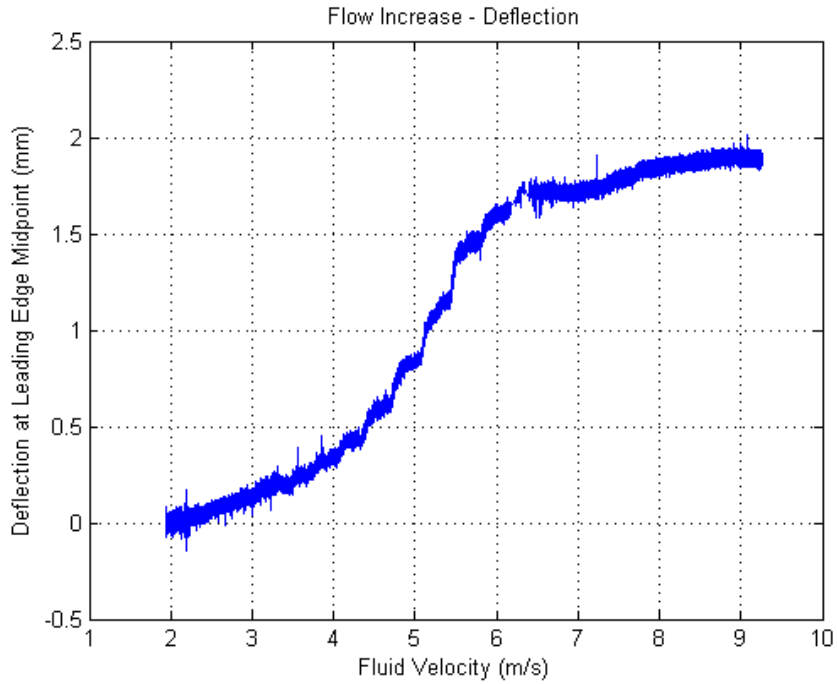


FIGURE 22. MAXIMUM PLATE DEFLECTION VS. FLOW VELOCITY.

To determine the pressure distribution in both channels, the test was repeated with the flow rate held steady at its maximum while pressure data was recorded in both flow channels. The pressure for the two channels shown in Figure 23 was collected at 18 total pressure taps (9 in each channel). The tap positions are noted in the figure. Using a linear trendline, the pressure values at the leading and trailing edges of the plate (i.e. the first and last pressure values for each channel) were extrapolated and included in the figure. It is interesting to note that the pressures appear to equalize closer to the leading edge of the plate rather than the trailing edge. This deviation from the simple analytic model is the result of flow redistribution due to plate deflection, which the analytic model neglects. Additionally, the higher pressure was recorded in the smaller channel, which corresponds to the data showing the plate deflecting into the larger channel. Using the data from Figure 23, the profile of the pressure

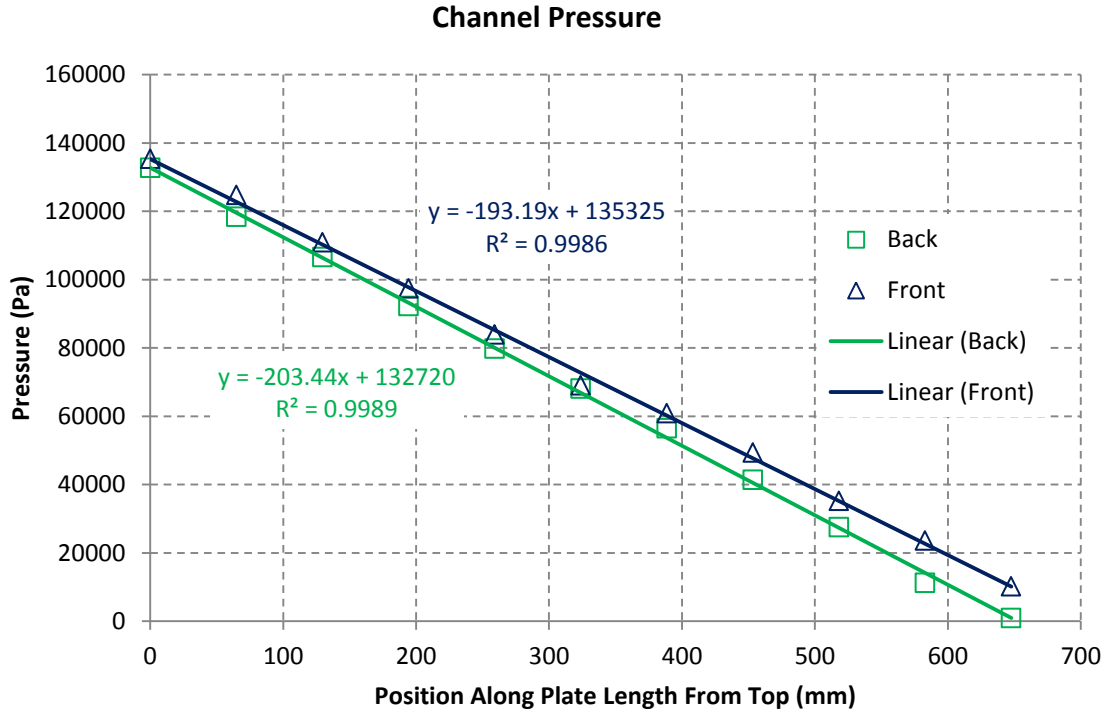


FIGURE 23. CHANNEL PRESSURE PROFILES AT MAX FLOW RATE.

differential along the channel can be determined, and is shown as Figure 24. Appendix 2 contains the raw data from this portion of the test.

For rectangular channels without considering flow redistribution, the plot of Figure 24 would be expected to be linear. However, since the plate has deflected significantly and the flow has redistributed, the definition of the pressure differential through the thickness of the plate becomes significantly more complex. These results are similar to results found by others in that the pressure profile loses a linear distribution as the plate deflects (Scavuzzo, 1965).

Finally, the third phase of the test called for gradually reducing the flow rate back to its minimum value. Like the first phase, data was recorded on the channel gaps

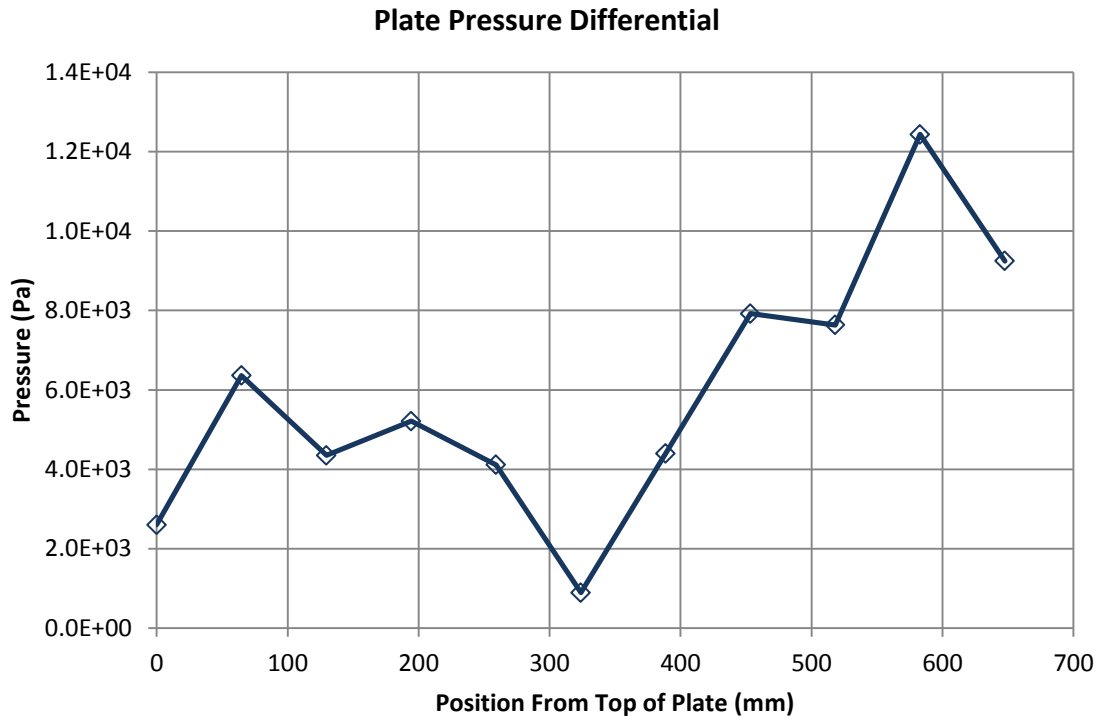


FIGURE 24. PLATE PRESSURE DIFFERENTIAL.

and flow rate. These results are similar to those shown in Figs. 18 & 19, and are presented in Appendix 2.

Computational Results

The FSI co-simulation technique allows for using CFD and FEM codes to solve for their respective domains, passing information between the codes at the interface between the solid and fluid domains. The solvers used by both codes are transient based solely for the purposed of providing a method for exchanging data between the programs at set intervals. Since the codes currently lack the capability to provide transient fidelity for this analysis, the goal is to find the steady state solution of plate deflection, utilizing ‘time’ solely as a parameter for data exchange. While these two particular codes provide built in functionality for explicit coupling of the fluid and solid domains, it is difficult to maintain simulation stability for applications containing a constrained fluid domain and high aspect ratio geometry. Therefore, work has focused

on finding a method for stabilizing the simulations to provide accurate solutions for the geometries present in reactor fuel assemblies.

Initial studies revealed that simulation stability can be achieved at the expense of computational time (efficiency). By utilizing very high density fluid domain meshes, instabilities in the fluid pressure field are controlled. However, this method involves fluid meshes in the tens of millions of cells, and can take up to a month to complete. Therefore, multiple options were explored to allow for the use of lower density fluid meshes without losing simulation stability. Since instabilities in the coupled simulations arise from sudden acceleration of the coupled fluid-solid interface, these methods are targeted at controlling the velocity and limiting the acceleration of the interface. These methods include scaling the fluid mesh anisotropically, damping the motion of the solid region, and ramping the fluid velocity and pressure values from lower levels up to the desired values. Velocity and pressure ramping has proven especially useful in preventing a shock to the solid model that causes instabilities to propagate during iterations of the simulation.

In order to evaluate the effectiveness of each of these techniques, a simplified model similar to that shown in Figure 13 was created. These models used a uniform geometry with properties shown in Table 3. Additionally, an inlet region above the leading edge of the plate has been incorporated to allow for prototypic flow.

TABLE 3. FSI MODEL PROPERTIES

Parameter	Value
Plate Thickness (a)	0.9652 mm = 0.038 in
Plate Length (L)	647.7 mm = 25.5 in
Plate Width (b)	110.3 mm = 4.342 in
Young's Modulus (E)	70 GPa = 10×10^6 psi
Poisson's Ratio (ν)	0.33
Water Density (ρ)	$997 \text{ kg/m}^3 = 1.93 \text{ slugs/ft}^3$
Water Viscosity (μ)	$8.8871 \times 10^{-4} \text{ Pa}\cdot\text{s} = 1.85 \times 10^{-5} \text{ lb}\cdot\text{s/ft}^2$
Front Channel Gap (h_1)	2.4 mm = 0.0955 in
Back Channel Gap (h_2)	2.2 mm = 0.0875 in
CFD Model 1 Mesh	6,174,614 Cells
CFD Model 2 Mesh	22, 385, 474 Cells

One method considered to improve the stability of the simulation is to ramp the fluid velocity from a low level to the desired level over the course of the simulation. In both models 1 and 2, the inlet velocity was ramped from 3 m/s to 8 m/s. Model 1 used a constant acceleration model, and Model 2 used a more gradual acceleration, as shown in Figure 25.

As shown by Equation 7, the velocity of the flow through a channel has a direct effect on the pressure in that channel. Given that the instabilities seen in earlier FSI models were the result of sudden changes in pressure on the interface surface, the ramped velocity method shown in Figure 25 was developed in order to indirectly ramp the pressure on the interface surface. Another method of directly ramping the interface pressure is provided by the CFD code. Later models have explored the option of directly ramping the exported pressure on the fluid-structure interface without the need to ramp the fluid velocity. This method provides the advantage of maintaining a

Simulation Velocity Stepping Scheme

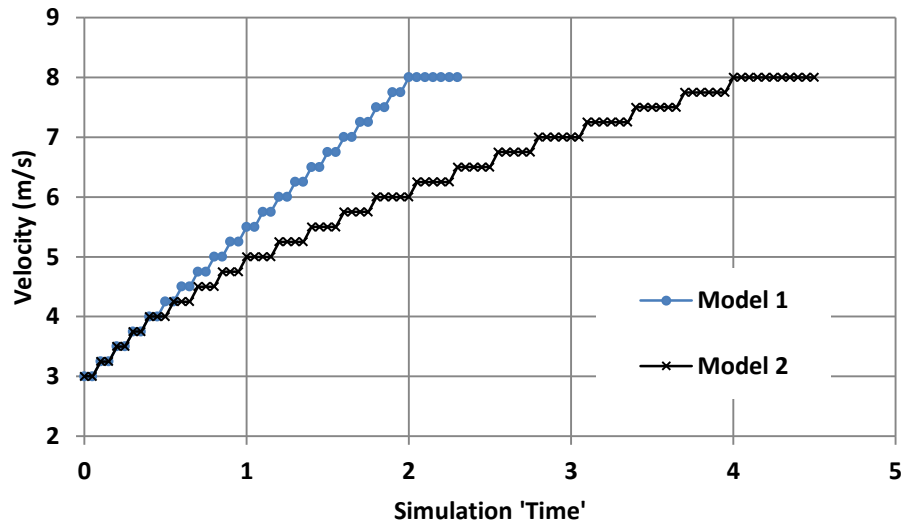


FIGURE 25. FSI MODEL VELOCITY RAMPING SCHEMES.

converged fluid field solution while simultaneously controlling the pressure exported to the FEM model.

A plot of the plate deflection results for Model 1 is shown in Figure 26. As can be seen, this simulation diverged, producing an unrealistic deflection. After analysis of the results from both the CFD and FEM models, the initial instability in the simulation was traced back to the pressure field of the CFD solution. As the simulation reached higher velocities in later time steps, the pressure field did not reach a converged solution prior to exporting pressure data to the FEM solver. While this initially started as a small perturbation of the solution, it quickly propagated and resulted in unrealistic pressure distributions in the channels on both sides of the plate.

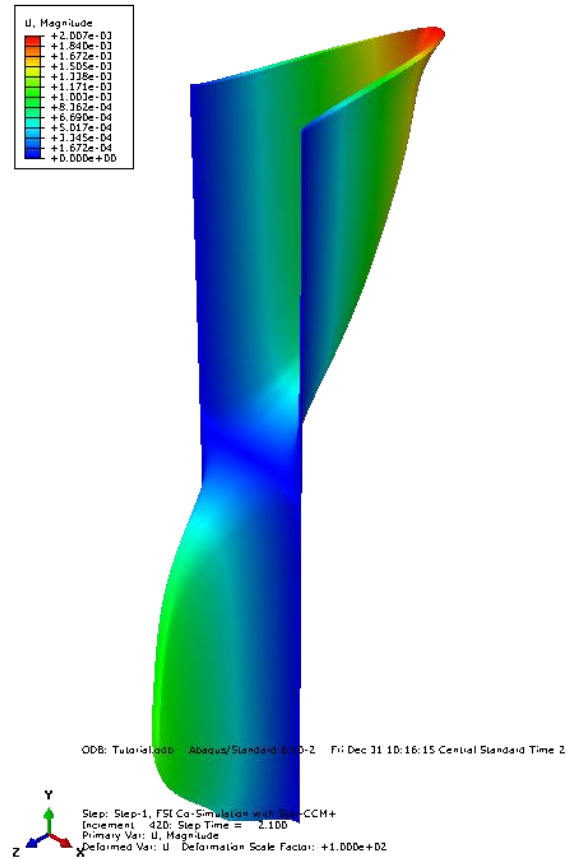


FIGURE 26. DEFLECTION PROFILE CAUSED BY NUMERIC INSTABILITY IN MODEL 1.

In order to address the issues presented by the poor fluid solution, the simulation was run again with two significant changes. The changes to Model 2 included a large increase in the mesh density of the fluid model, and a more gradual ramping of the inlet fluid velocity. A comparison of the fluid field mesh through a portion of the flow cross-section is shown in Figure 27 to illustrate to changes between the simulations. These two modifications increased the resolution of the fluid pressure field and decreased the changes in the fluid field between iterations. Together, these

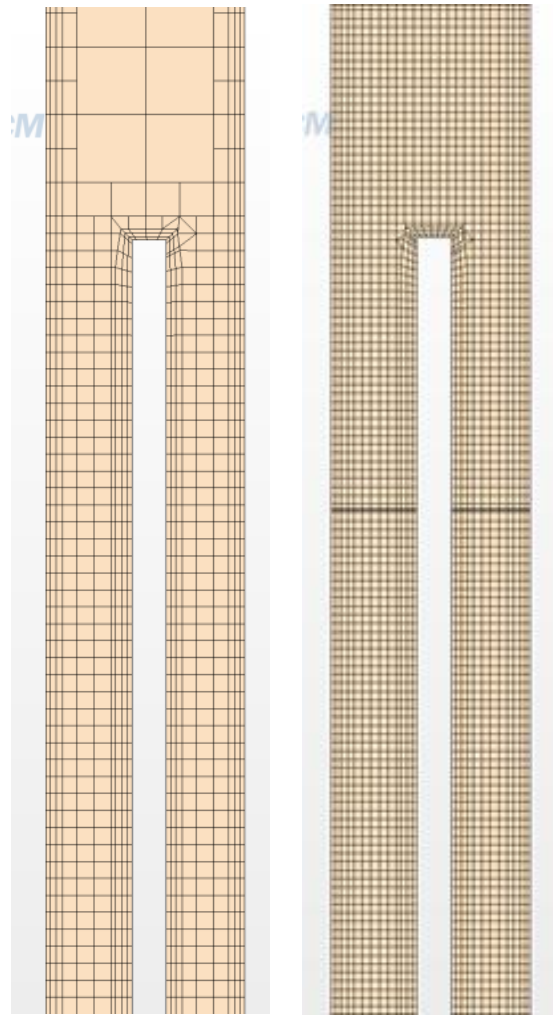


FIGURE 27. COMPARISON OF THE MESH FROM MODEL 1 (LEFT) AND MODEL 2 (RIGHT).

modifications worked to dampen out instabilities in the fluid field as the simulation progressed, thereby preventing the instabilities from propagating through the simulation.

As a result of these changes, a stable solution was achieved. The plate deflection results from Model 2 shown in Figure 28 present a more realistic deflection profile. As is shown through the analytic model, the pressure differential through the thickness of the plate is expected to be at its maximum at the leading edge. The results from Model 2 reinforce this conclusion by showing a maximum deflection at the leading edge that tapers off along the length of the plate.

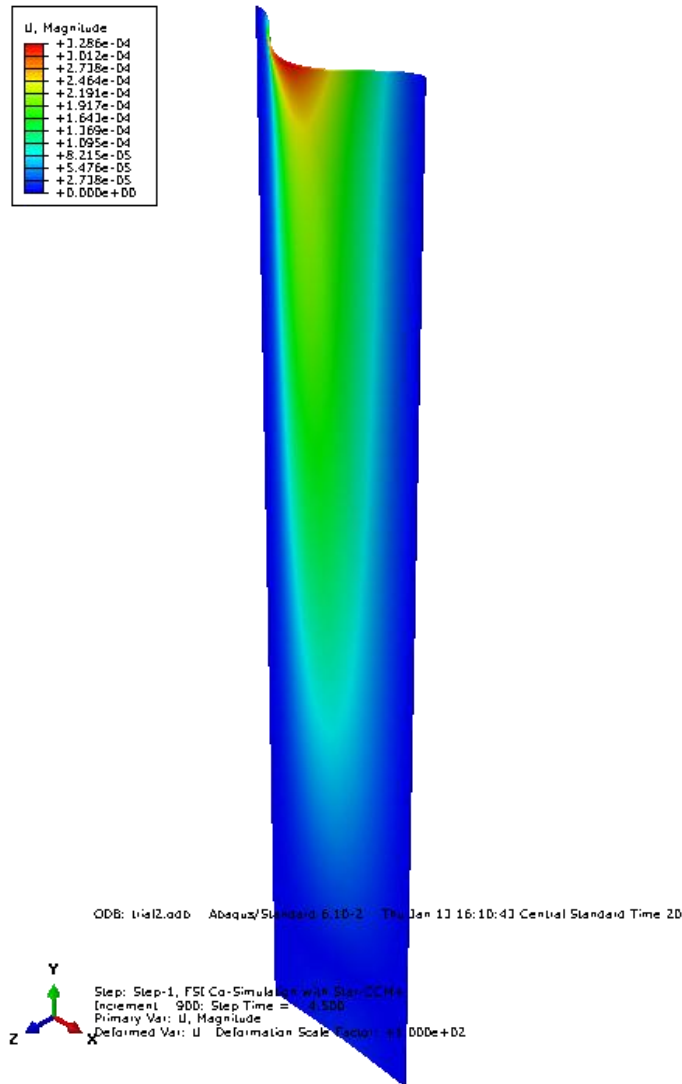


FIGURE 28. DEFLECTION PROFILE CAUSED BY NUMERIC INSTABILITY IN MODEL 1.

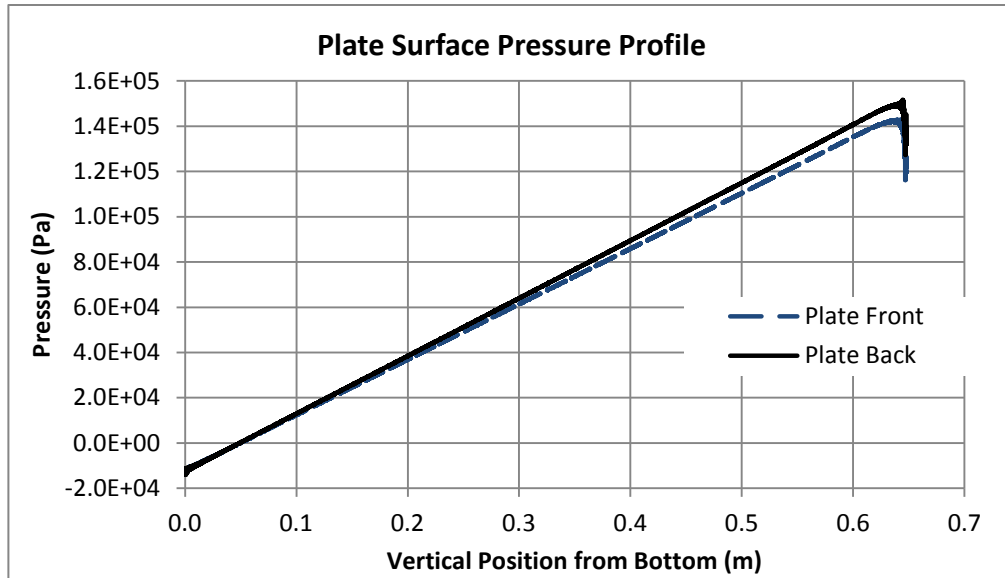


FIGURE 30. MODEL 2 STATIC PRESSURE DISTRIBUTIONS

After Model 2 completed, the static pressure profile on either side of the plate was plotted along the length of the plate. These pressure curves, shown in Figure 30, show a linear pressure drop along both surfaces of the plate. The maximum pressure differential, at the leading edge of the plate, is approximately 7000 Pa, as shown in Figure 29.

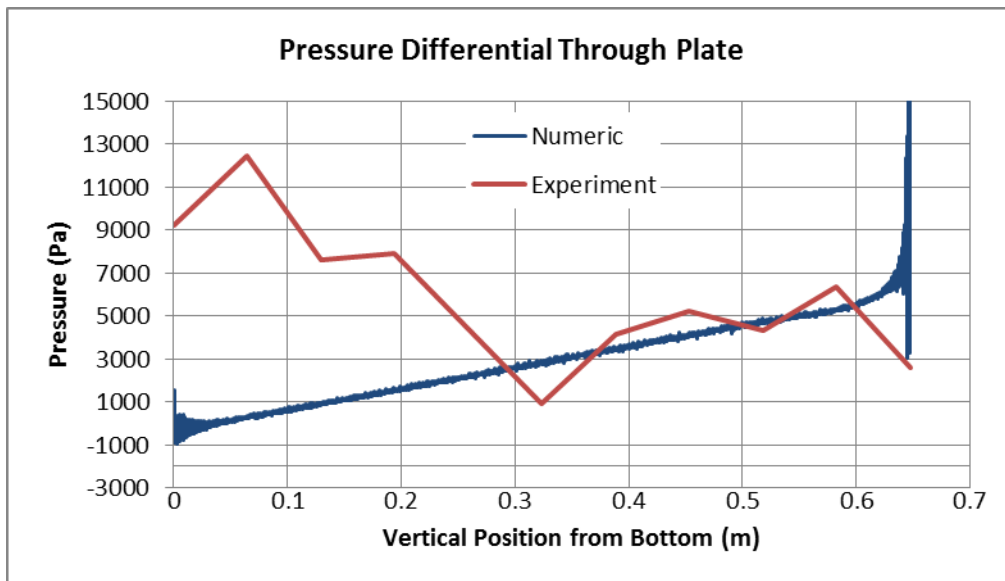


FIGURE 29. PRESSURE DIFFERENTIAL THROUGH PLATE

As seen in Figure 29, when compared to the experimental data, the qualitative profile of the pressure differential found in the numeric results is significantly different. However, the comparative magnitude of the pressure values is quite similar. This supports the conclusion that while more work is necessary to refine the models to improve accuracy, the numeric models are capable of supporting the experimental data. Additionally, while Model 2 did produce a significantly more stable solution than Model 1, the major drawback was the computational time required to find the solution. Running in parallel across 12 processors, Model 2 still took 25 days to complete. The expectation is that a single simulation takes no more than four days to complete. Therefore, additional investigation is necessary in order to produce fluid meshes with the magnitude of Model 1, while still maintaining the stability of Model 2.

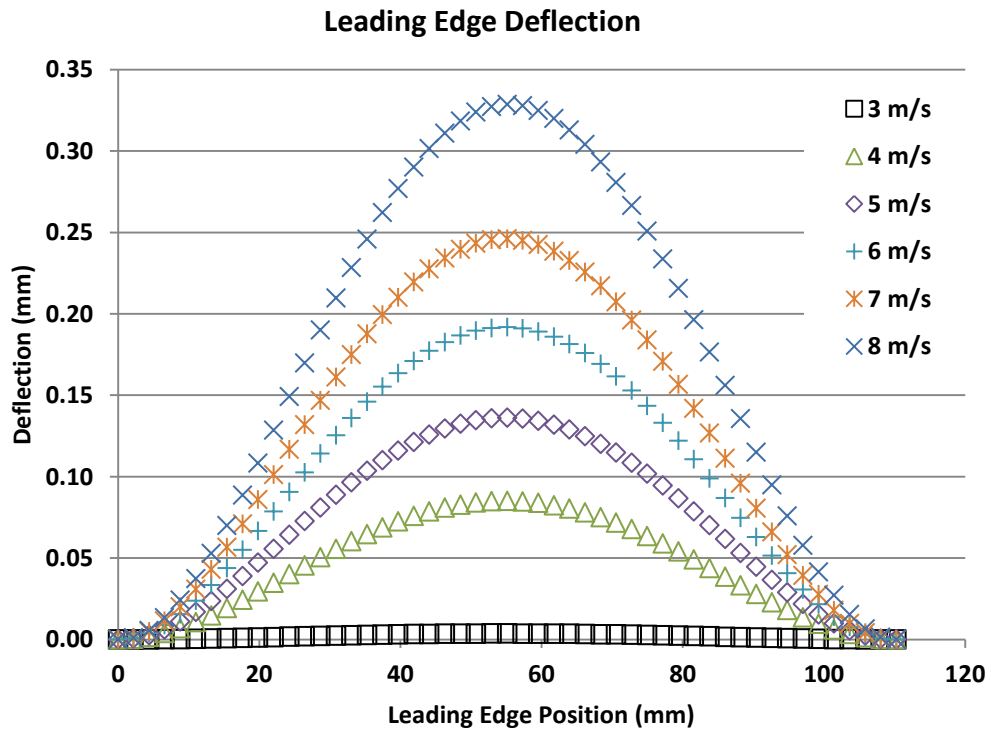


FIGURE 31. LEADING EDGE DEFLECTION PROFILE AT VARIOUS VELOCITIES.

Since the maximum deflection occurs at the leading edge of the plate, Figure 31 was created to show the leading edge deflection. Also, since the simulation was run through a range of velocities, the data was extracted and plotted at various inlet velocity conditions to illustrate the increase in leading edge deflection as the velocity increased.

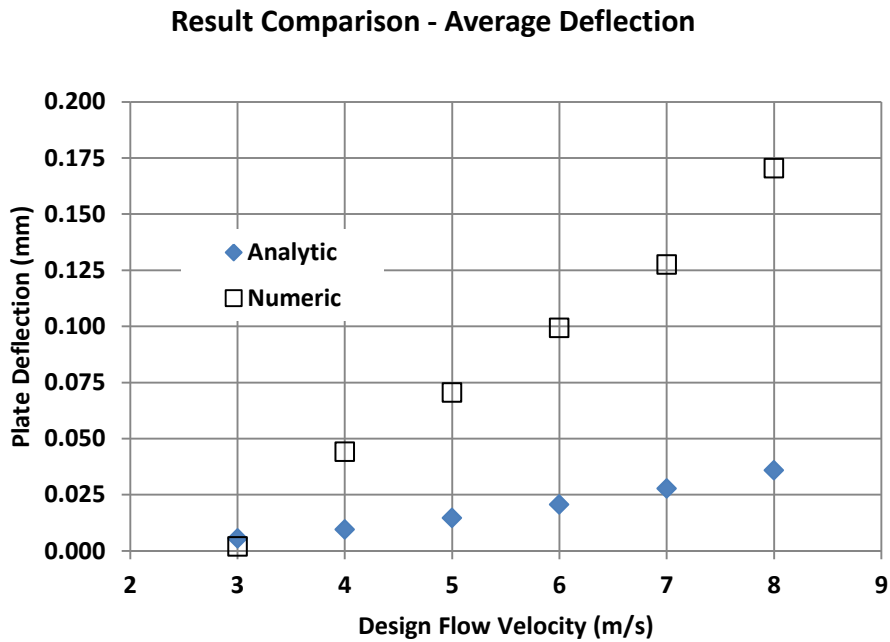


FIGURE 32. AVERAGE DEFLECTION COMPARISON BETWEEN NUMERIC AND ANALYTIC MODELS

Plotting a curve fit to the data sets shown in Figure 31 shows that the profile of the deflection is a fourth order polynomial. This qualitatively matches the profile predicted analytically by Eq. 21. However, when quantitatively compared to the analytic model in Figure 32, there is significant deviation. This deviation is likely due to the analytic model being based off of wide beam deflection equations. These models tend to lose accuracy with large deflections. Given that the magnitude of deflection of the plate is on the

order of the thickness of the plate, the analytic models from current literature are likely insufficient to predict deflection.

Chapter 7: Conclusion and Future Work

The primary focus of this research was to set up stable, explicitly coupled fluid structure interaction models utilizing Abaqus and Star-CCM+. This work has been successful in providing a means for completing these FSI models. Significant difficulty was found in producing CFD meshes which are dense enough to produce a stable solution, but not so dense that the simulation run times are excessive. A potential solution to this problem involves using Abaqus to mesh both the CFD and FEM models, producing CFD meshes which are an order of magnitude smaller than those produced in Star-CCM+. The Star-CCM+ mesher works well for larger, open objects with reasonable aspect ratios. However, in this application, the high aspect ratio of the channels forces the mesher to create overly dense meshes, and to produce low quality cells at the surface of the plate.

Building the solid model was significantly simpler than the fluid model. The solver for the FEM model allows for damping coefficients to be included in the material properties, thereby damping out excessive motion of the plate caused by inertia. This allowed for easy control of plate motion to help arrive at a steady state solution. Additionally, ramping the pressure output from the CFD model to the FEM model as the simulation iterates provides additional control to the stability of the model.

The techniques presented here detail the work in developing stable, efficient FSI models. The focus of this work was to develop techniques for FSI coupling and meshing of models. Additionally, parameters to control the stability of the simulations were also investigated. With this work now complete, future attention will turn to ensuring the

accuracy of the solutions from the FSI models. At present, there is inadequate experimental and analytic data available to directly verify the FSI results.

As the experimental studies on flow induced plate deflection continue, further FSI models will be run to check their accuracy, and to make adjustments where necessary. At present, experiments are planned for flat and curved plate assemblies of one or more plates. These should yield good data for comparison to FSI models. Once validated against experiments, new analytic models of plate deflection will also be developed. Much of this work has already begun, and it is apparent that a closed form solution for large deflection of a plate with two clamped and two free edges will be difficult, if not impossible. The experimental and numeric work to come will be used to inform an approximate solution to this problem.

The work to develop fluid structure interaction technology is just beginning. Given the continued advances in computational power, this field of study will only see increasing growth in the years to come. Coupling of codes for flow induced deformation analysis is only the beginning, with work now expanding to include coupling for thermal and even neutronics analysis. This is merely the first step toward developing technologies to fully model complete, complex engineering systems.

APPENDIX 1: Numeric Procedure (Tutorial)

Introduction

This tutorial presents the basic procedure for setting up and running a coupled Fluid-Structure Interaction (FSI) simulation using Star-CCM+ and Abaqus. This tutorial focuses on mechanical deformation analysis of a rectangular flat plate in a high velocity flow. The procedure can be easily adapted for more complex mechanical systems and also for thermal analysis.

The following processes are covered in this tutorial:

- Installing Star-CCM+ and Abaqus
- Setting up system environment variables
- Preparing the Abaqus solid model
- Modifying the Abaqus input file
- Preparing the Star-CCM+ fluid model
- Setting up the coupled simulation
- Executing the coupled simulation
- Viewing the results

Preparing for Coupled Simulations

Required Software

Ensure the following programs are installed for coupled FSI simulations:

- Star-CCM+ 5.06.007 or newer

- Change the installation directory from the default of “C:\Program Files\CD-Adapco” to “C:\CD-Adapco”
- Abaqus 6.10-2 or newer
- *Recommended:* Notepad++ (<http://notepad-plus-plus.org/>)

System Configuration

Add the following system environment variables:

- Variable: SIMULIA_CSE_LIBS
Value: C:\SIMULIA\Abaqus\6.10-2\exec\lbr
- Add the following to the system PATH environment variables
 - %SIMULIA_CSE_LIBS%\exec\lbr
 - %SIMULIA_CSE_LIBS%\External

Create the following directory structure on the computer being used for the analysis. If this analysis is being run on one of the workstations in the lab, this directory should reside within the “C:\SimTemp” folder. This will allow the simulation to run from the high speed solid-state drive on the workstation. Note that due to the limited size of the solid-state drive, all completed simulations should be moved either temporarily to the D: drive on the workstation, or permanently to the high capacity drive on the network controller.

- *SimulationFolder*
 - Abaqus
 - Star-CCM+

After making these changes, reboot the computer.

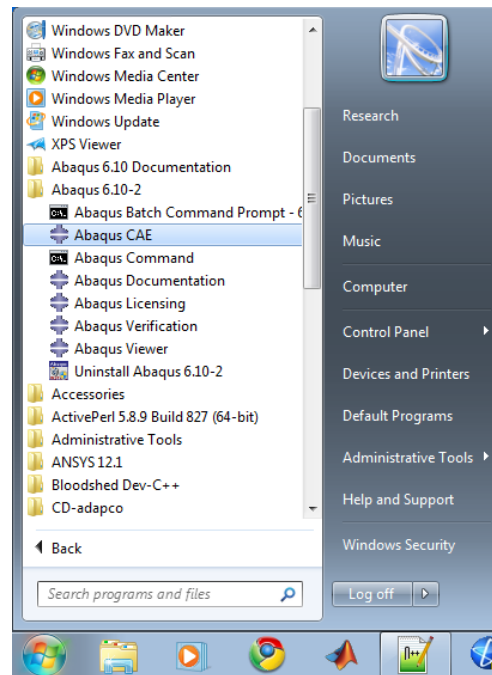
Preparing the Abaqus Solid Model

Building the Model in Abaqus CAE

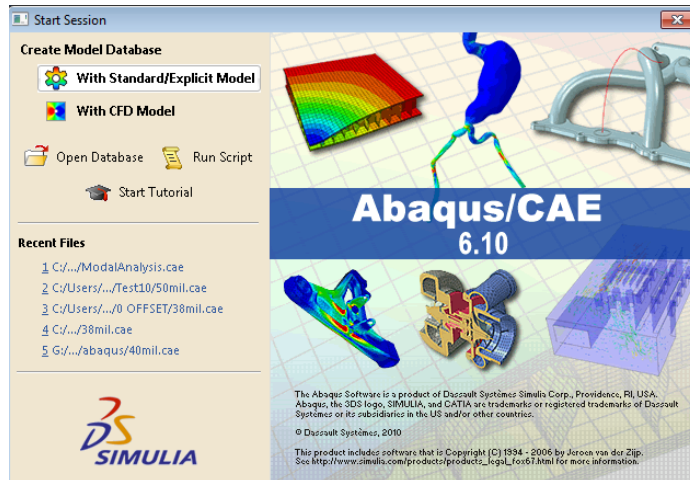
This section outlines the creation of the Abaqus input file using the Abaqus CAE GUI.

The input file contains all the information necessary to run an Abaqus simulation including node and element definitions, material definitions, and the analysis and output definitions.

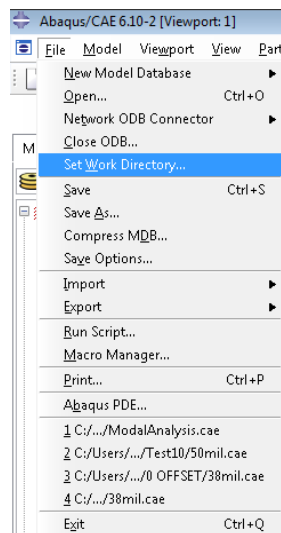
1. Launch Abaqus CAE: Start -> All Programs -> Abaqus 6.10-2 -> Abaqus CAE



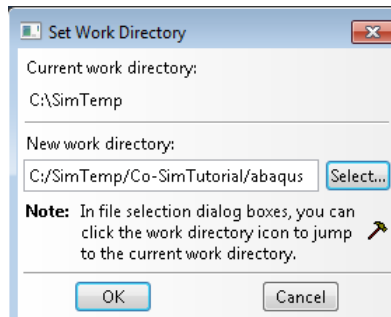
2. In the 'Start Session' dialog, select 'Create Model Database With Standard\Explicit Model'



3. Set the working directory to the Abaqus directory created earlier: File -> Set Work Directory

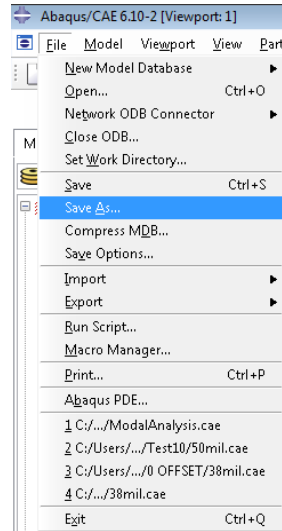


Then change the work directory (For this tutorial, C:/SimTemp/Co-SimTutorial/abaqus)

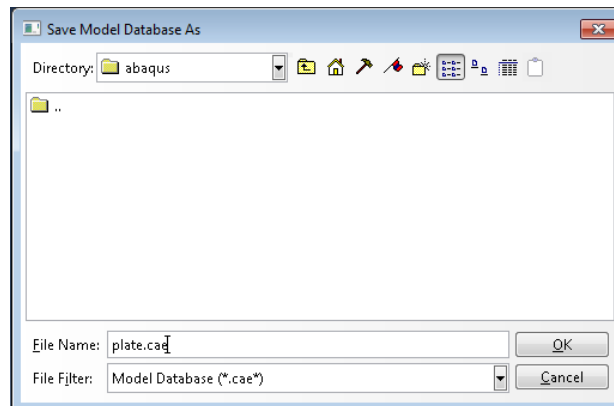


Select 'OK'

4. Save the CAE file: File -> Save As

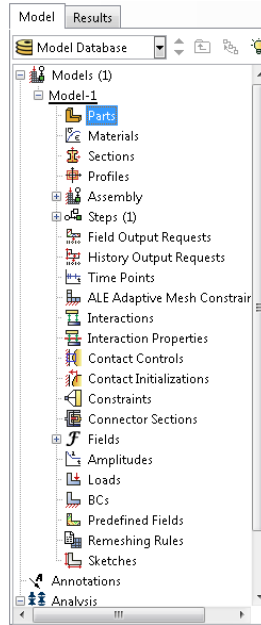


Save the file as 'plate.cae' in the work directory

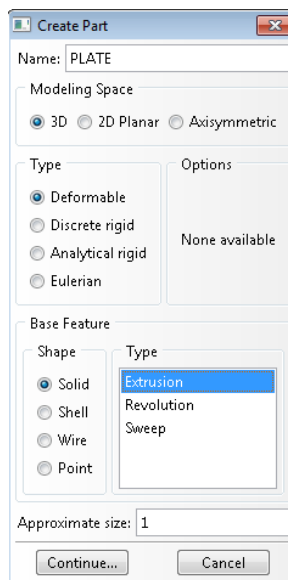


Select 'OK'

5. Next, begin building the model by working through each of the modules in the Model tree on the left side of the screen. Start by double-clicking on the 'Part' module:

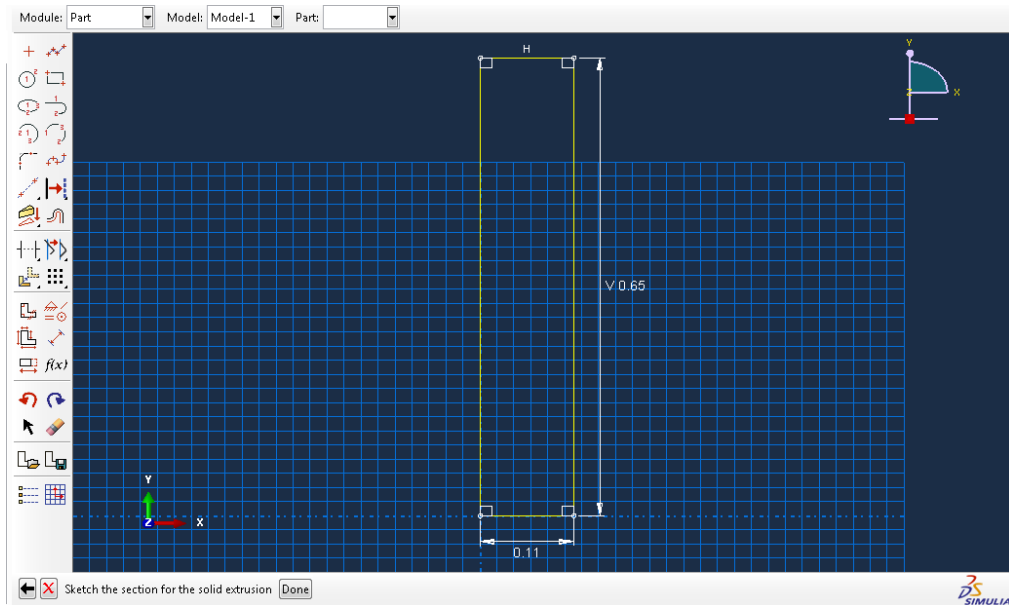


The 'Create Part' dialog is displayed.



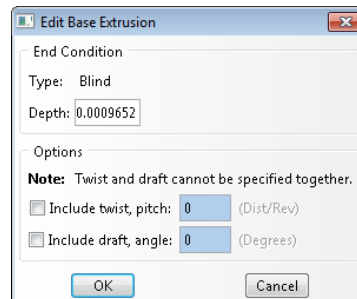
Name the part 'PLATE'. Make it a 3D, Deformable, Solid, Extrusion with an approximate size of 1. Select Continue.

The sketching plane is displayed. Create a rectangle with a width of 0.1102868 m (4.342 inches) and a length of 0.6477 m (25.5 inches). Ensure that the bottom left corner of the rectangle is at the origin.



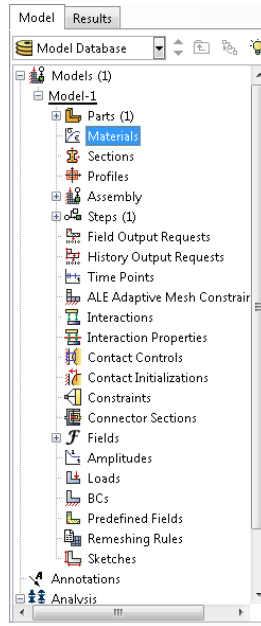
Select 'Done' at the bottom of the sketch window.

Enter an extrusion depth of 0.0009652 m (0.038 inches).



Select 'OK'

- Next, define a material by double-clicking on the 'Materials' module in the Model tree:

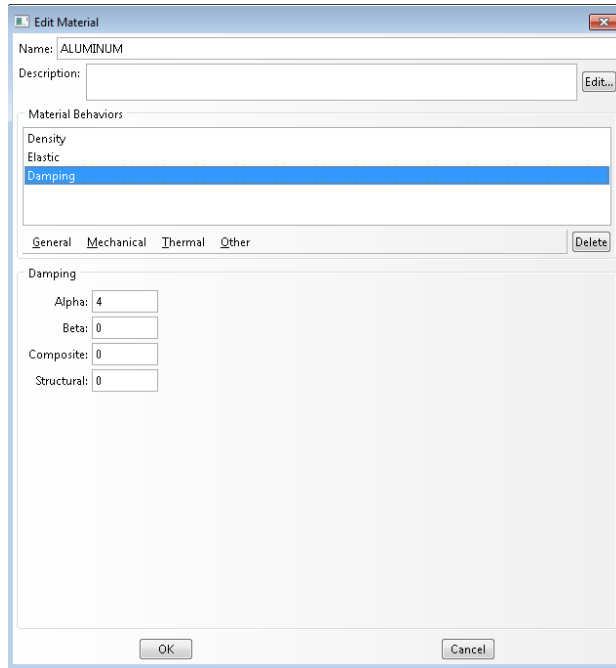


The 'Edit Material' dialog is displayed.

Name the material 'ALUMINUM'

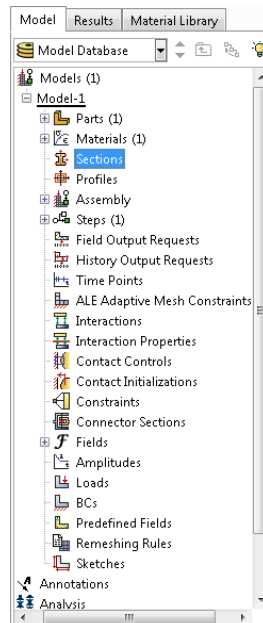
Select the following properties:

- General -> Density
 - Mass Density: 2700
- Mechanical -> Elasticity -> Elastic
 - Young's Modulus: 70000000
 - Poisson's Ratio: 0.33
- Mechanical -> Damping
 - Alpha: 4

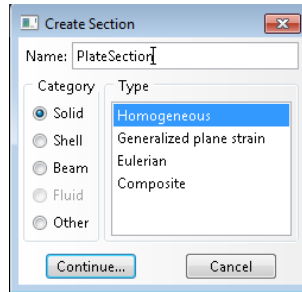


Select 'OK'

- Next create a section for the material by double-clicking 'Sections' in the Model tree.

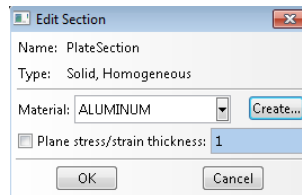


The 'Create Section' dialog is displayed.

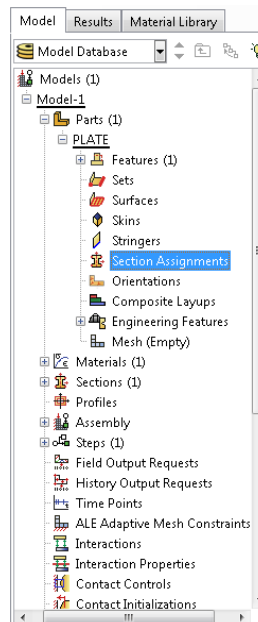


Name the section 'PlateSection', and select the 'Solid' and 'Homogenous' options. Click 'Continue...'

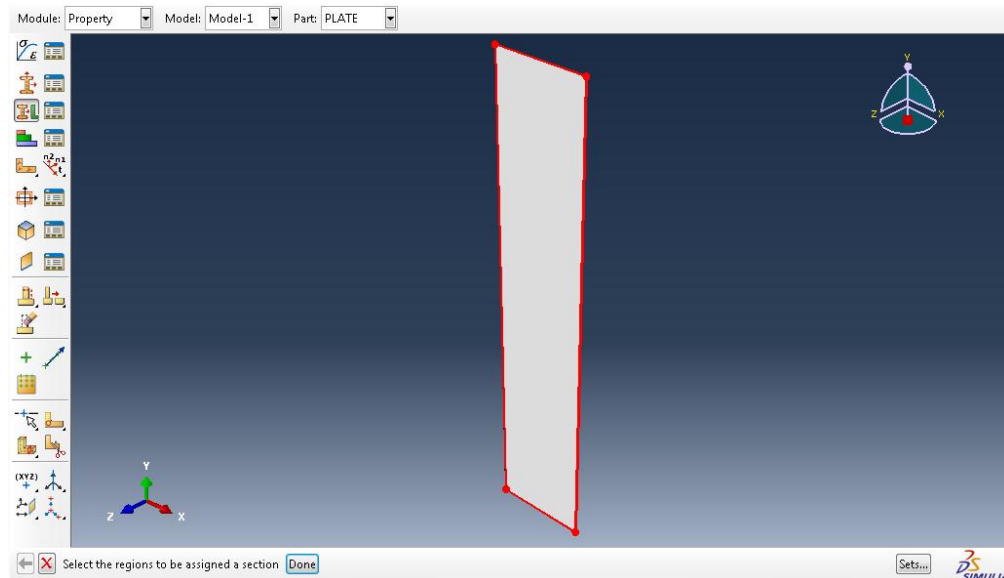
In the Edit Section dialog, accept the default settings and select 'OK'



- Next, create a section assignment for the Part 'Plate' by double-clicking the 'Section Assignments' node in the Plate part tree:

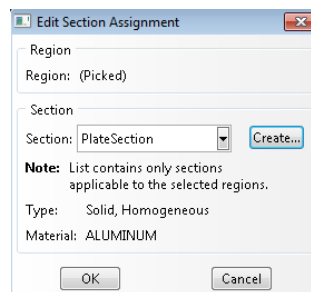


The message below the viewport window will prompt you to, “Select the regions to be assigned a section.” Click on the plate in the window to select it.

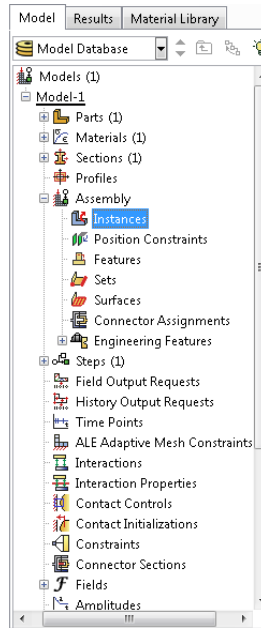


The plate will be outlined in red. Select ‘Done’ below the viewport window.

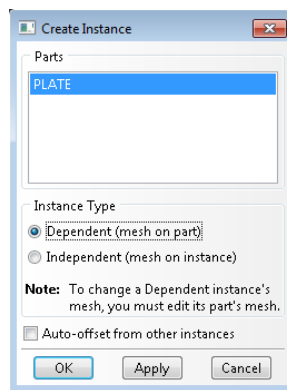
In the Edit Section Assignment dialog, accept the default settings and select ‘OK’



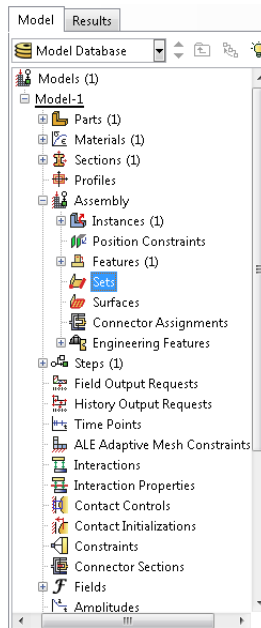
9. Next, create the assembly. Double-click the ‘Instances’ Node under the ‘Assembly’ module in the Model tree:



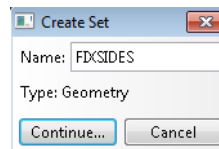
Accept the default settings in the 'Create Instance' dialog and select 'OK'



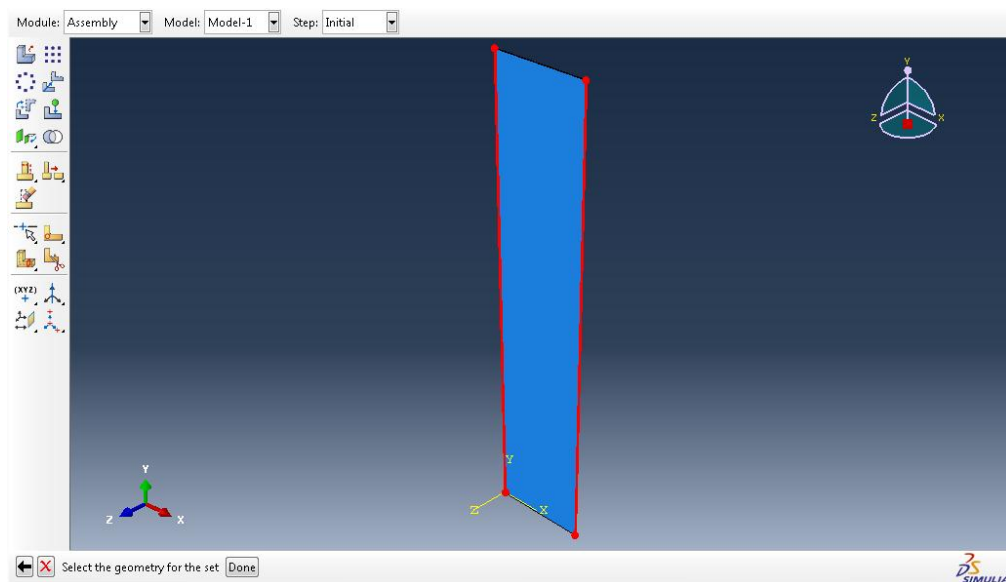
10. Create a set for the sides of the plate. This set will later be used to assign a boundary condition for the side edges of the plate. Double-click the 'Sets' node under the 'Assembly' module in the Model tree:



Name the set 'FIXSIDES' and click continue



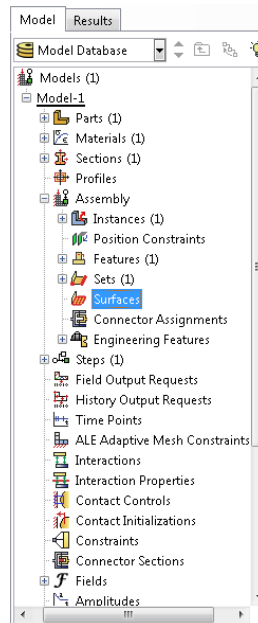
Select the two long edge surfaces of the plate



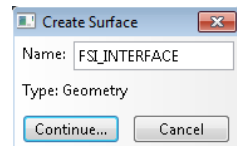
Select 'Done' below the viewport window.

11. Create a surface indicating where the fluid comes into contact with the plate.

Double click the 'Surfaces' node under the 'Assembly' module in the model tree:

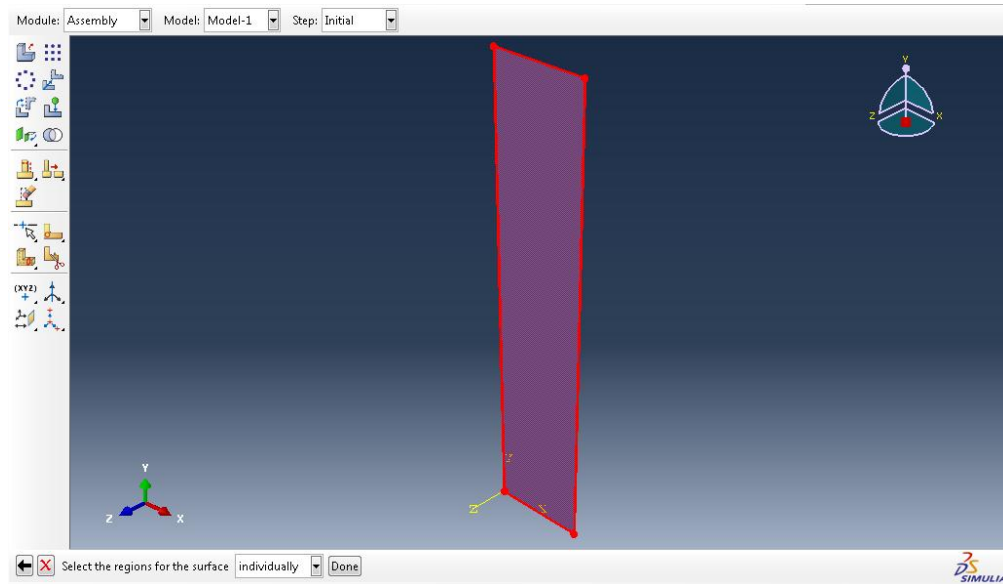


The 'Create Surface' dialog is displayed.



Name the surface 'FSI_INTERFACE' and click 'Continue...'

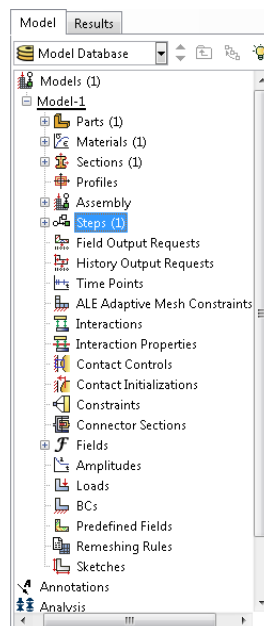
Select the four surfaces in contact with the fluid (Front, Back, Top and Bottom)



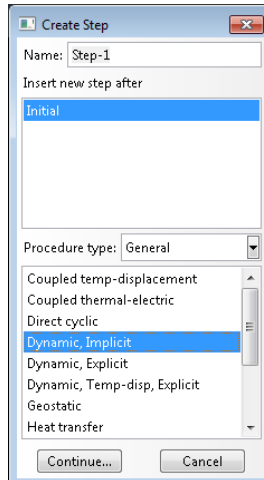
Click 'Done' below the viewport window to complete the surface definition.

12. Next, define the analysis step. Double-click the 'Steps' module in the Model

tree:

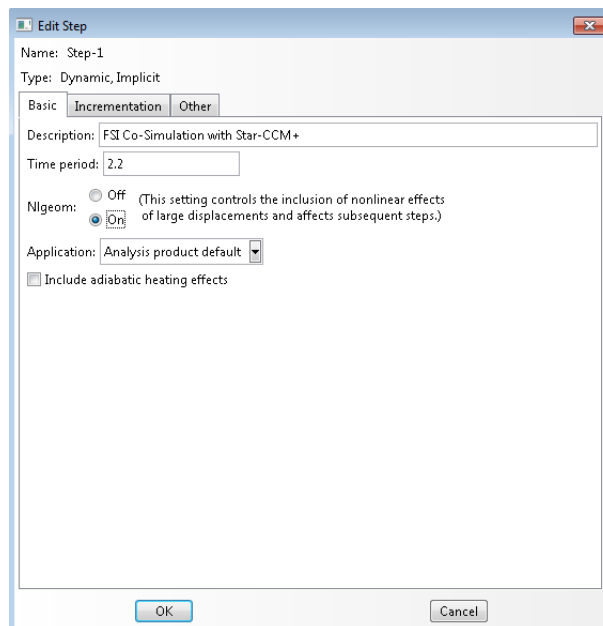


The 'Create Step' dialog is displayed



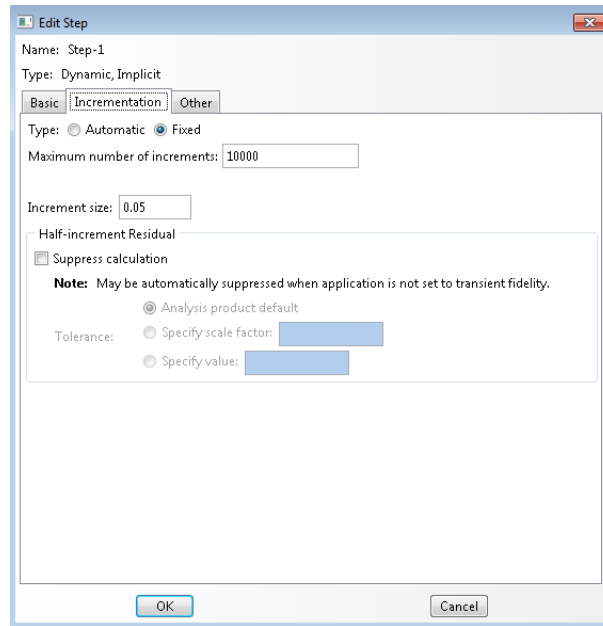
Leave the step name as 'Step-1'. Change the type to General -> Dynamic, Implicit. Select 'Continue...'

The 'Edit Step' dialog is displayed:



Set the following parameters on the 'Basic' tab:

- Description: FSI Co-Simulation with Star-CCM+
- Time Period: 2.2
- Nlgeom: On

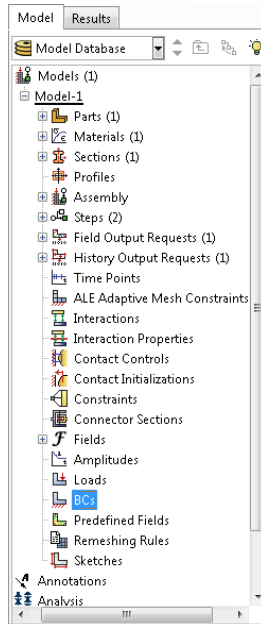


Set the following parameters on the 'Incrementation' tab:

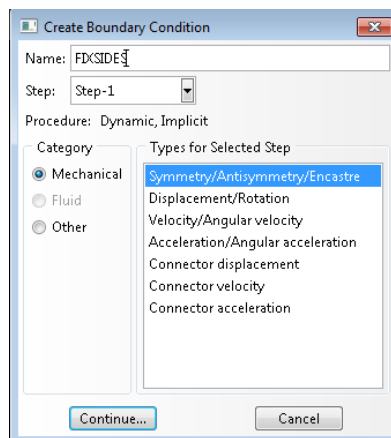
- Type: Fixed
- Maximum number of increments: 10000
- Increment size: 0.05

Click 'OK'

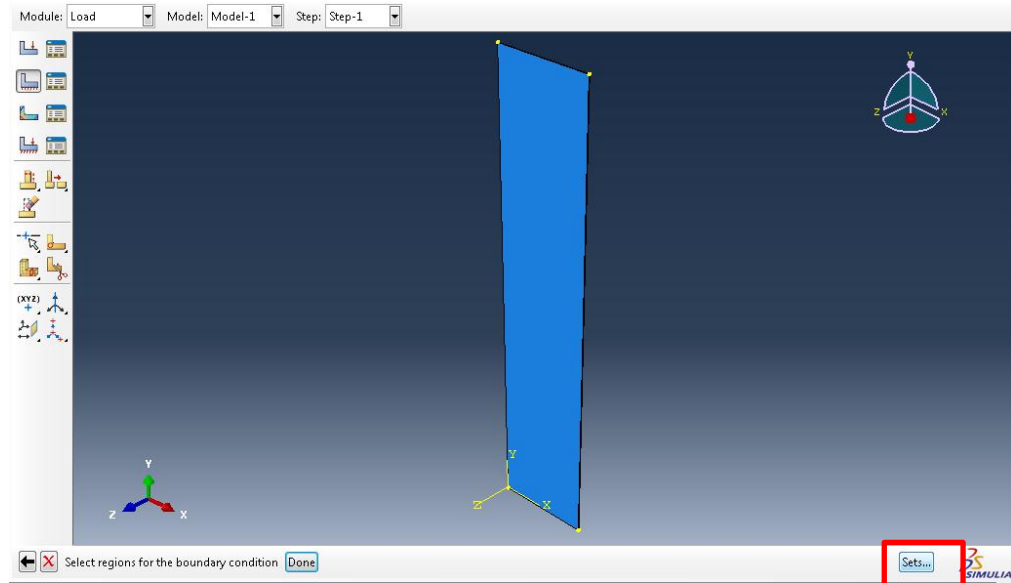
13. Define the Boundary Conditions. Double-click on the 'BCs' module in the Model tree:



The 'Create Boundary Condition' dialog is displayed

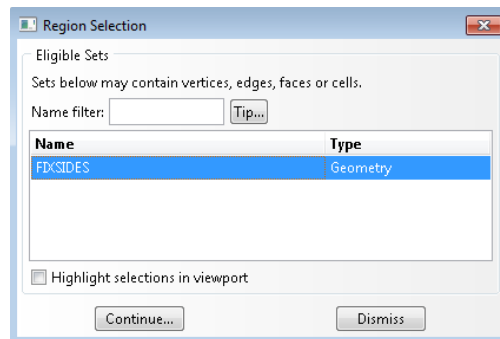


Name the Boundary Condition 'FIXSIDES'. Select a Mechanical, Symmetry/Antisymmetry/Encastre type. Select 'Continue...'



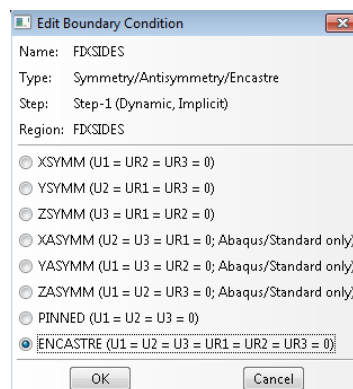
Click 'Sets' below the lower-right corner of the viewport window

The 'Region Selection' dialog is displayed



Select the 'FIXSIDES' set, and click 'Continue...'

The Edit Boundary Condition dialog is displayed

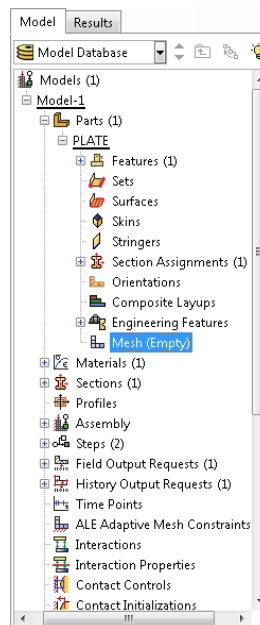


Select 'ENCASTRE (U1 = U2 = U3 = UR1 = UR2 = UR3 = 0)' and click 'OK'

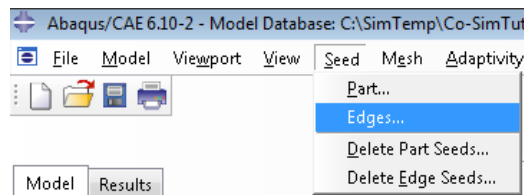
14. Seed the Model. The seed values used here produce a relatively fine mesh.

They can be adjusted to change the overall mesh density.

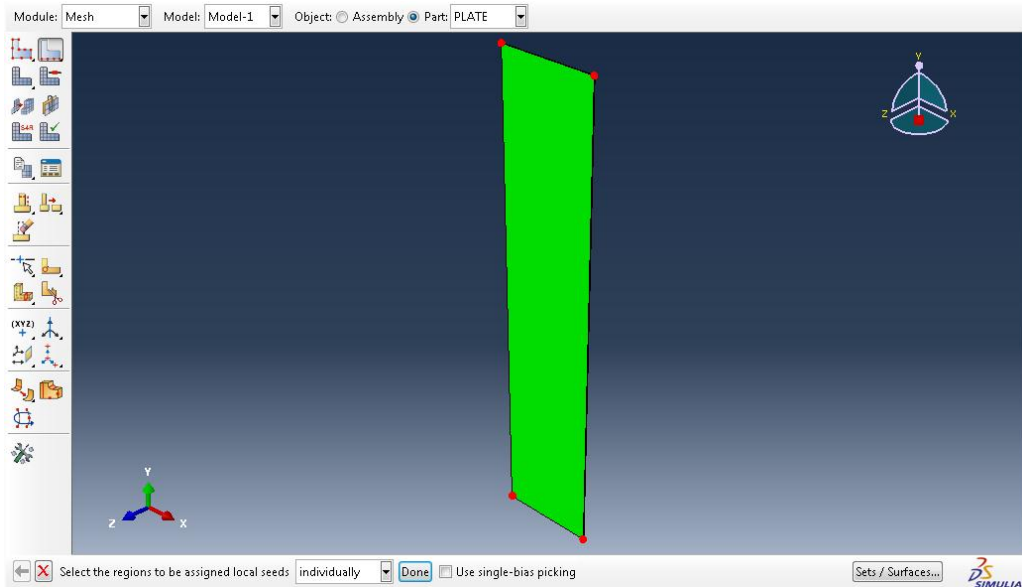
Double-click the 'Mesh' node under the Plate Part Module:



On the top menu bar, select Seed -> Edges

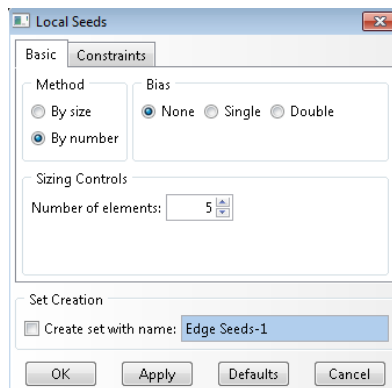


The prompt below the viewport states to 'Select the regions to be assigned local seeds'. To specify a custom seed through the thickness of the plate, select the four short corner edges of the plate.



Click 'Done' below the viewport window.

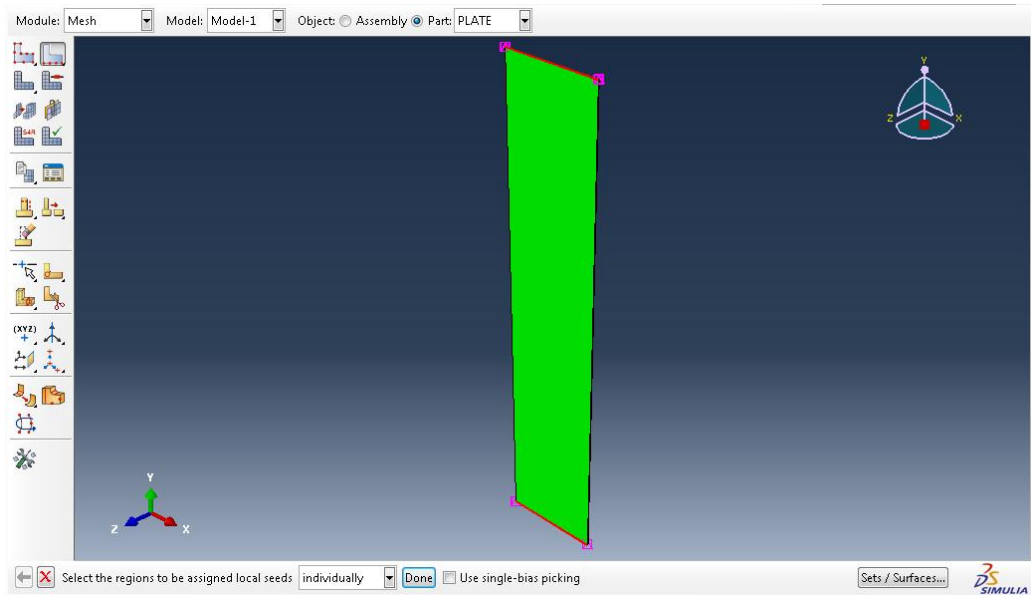
The Local Seeds dialog is displayed.



Set the 'Method' to 'By Number', and the 'Number of Elements' to 5.

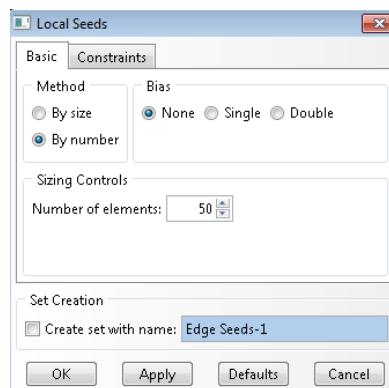
Click 'OK'

Repeat this procedure to select the four edges through the width of the plate



Click 'Done' below the viewport window.

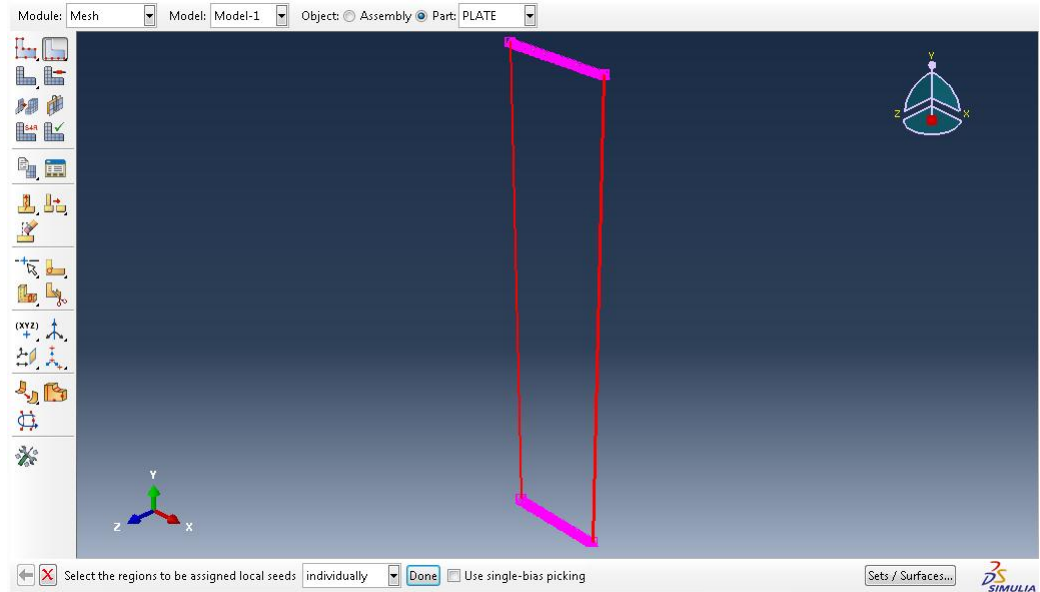
The Local Seeds dialog is displayed



Set the 'Method' to 'By Number', and the 'Number of Elements' to 50.

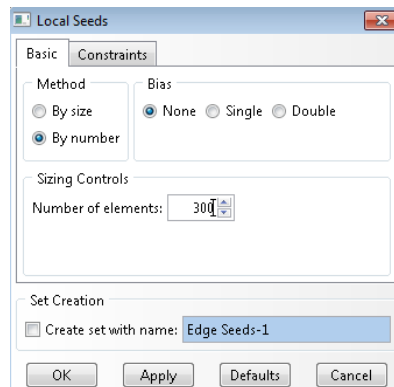
Click 'OK'

Finally, select the four remaining edges through the length of the plate



Click 'Done' below the viewport window.

The Local Seeds dialog is displayed

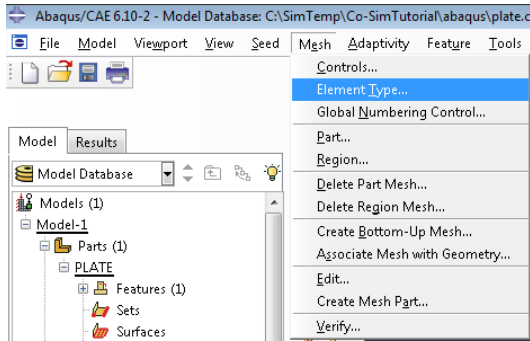


Set the 'Method' to 'By Number', and the 'Number of Elements' to 300.

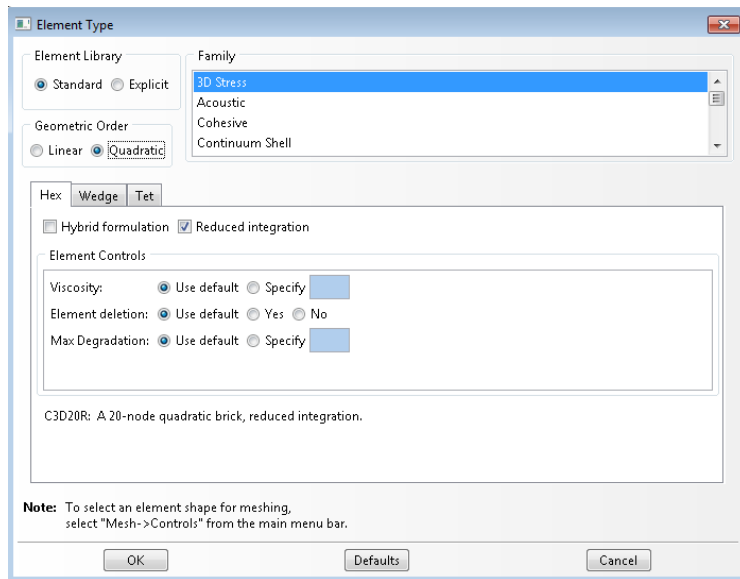
Click 'OK'

Click 'Done' below the viewport window.

15. Meshing the Model. From the top menu bar, select Mesh -> Element Type



The Element Type dialog is displayed

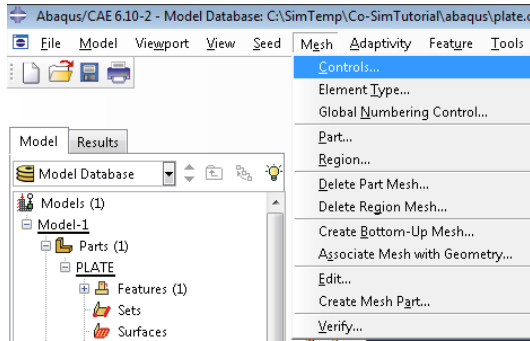


Set the following properties for the element type:

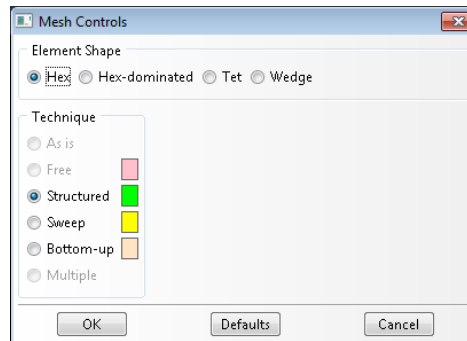
- Element Library: Standard
- Family: 3D Stress
- Geometric Order: Quadratic

Select 'OK'

From the top menu bar, select Mesh -> Controls

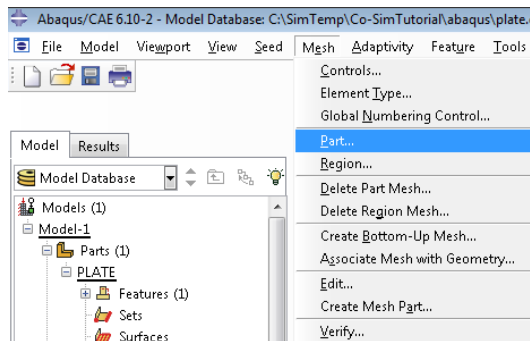


The Mesh Controls dialog is displayed



Ensure that a Hex, Structured mesh is selected and click 'OK'

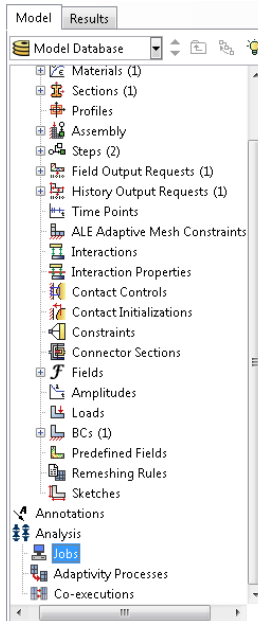
Finally, from the top menu bar, select Mesh -> Part



In the prompt below the viewport, click 'Yes' to mesh the part.

16. Writing the input file. Now that the model is meshed, the input file can be written.

First, create a job. Double-click the 'Jobs' module under the Analysis tree:



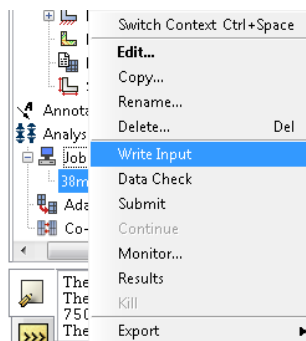
The Create Job dialog is displayed.



Name the job '38milPlate' and click 'Continue...'

The Edit Job dialog is displayed. Click 'OK'.

Now Right-Click on the newly created job and select 'Write Input'.



Abaqus will write the input file to the working directory.

Editing the Abaqus INput File

Open the Abaqus input file, 38milPlate.inp, in Notepad++. Scroll all the way to the bottom and add the missing lines to the Output History section. The end of the file should appear as follows:

```
*Output, field, variable=PRESELECT, frequency=1
**
** HISTORY OUTPUT: H-Output-1
**
*Output, history, variable=PRESELECT, frequency=1
**
*CO-SIMULATION, NAME=FSI_Mech, PROGRAM=MULTIPHYSICS, CONTROLS=Control-1
*CO-SIMULATION REGION, TYPE=SURFACE, EXPORT
ASSEMBLY_FSI_INTERFACE, U
ASSEMBLY_FSI_INTERFACE, VEL
*CO-SIMULATION REGION, TYPE=SURFACE, IMPORT
ASSEMBLY_FSI_INTERFACE, CF
*CO-SIMULATION CONTROLS, NAME=Control-1, COUPLING SCHEME=GAUSS-SEIDEL, SCHEME
MODIFIER=LAG,
STEP SIZE=0.05, TIME INCREMENTATION=SUBCYCLE, TIME MARKS=YES
**
*End Step
```

Bolded items need to be added to the file for the co-simulation and output settings.

The following is an overview of what each of these commands does:

```
*Output, field, variable=PRESELECT, frequency=1
**
** HISTORY OUTPUT: H-Output-1
**
*Output, history, variable=PRESELECT, frequency=1
**
```

These write field and history output to the output database file (*.odb) during the simulation. Data is written at every time step by setting the frequency to 1.

```
*CO-SIMULATION, NAME=FSI_Mech, PROGRAM=MULTIPHYSICS, CONTROLS=Control-1
```

This line begins the co-simulation definition. The Name is arbitrary, and the control set for the co-simulation is defined on a later line.

```
*CO-SIMULATION REGION, TYPE=SURFACE, EXPORT
ASSEMBLY_FSI_INTERFACE, U
ASSEMBLY_FSI_INTERFACE, VEL
```

These 3 lines specify what values should be exported from Abaqus to Star-CCM+. The surface is defined by *ASSEMBLY_SURFACE_NAME*, where *SURFACE_NAME* is the name given to the FSI surface when building the model. The variable 'U' is used to export nodal displacement, and 'VEL' is used to export nodal velocity.

```
*CO-SIMULATION REGION, TYPE=SURFACE, IMPORT
ASSEMBLY_FSI_INTERFACE, CF
```

These 2 lines specify what values should be imported to Abaqus from Star-CCM+. The surface for the import is defined the same as for the export step. The value 'CF' is used to import wall shear stress and static pressure on the surface of the plate.

```
*CO-SIMULATION CONTROLS, NAME=Control-1, COUPLING SCHEME=GAUSS-SEIDEL, SCHEME
MODIFIER=LAG,
STEP SIZE=0.05, TIME INCREMENTATION=SUBCYCLE, TIME MARKS=YES
```

These 2 lines specify the co-simulation controls referenced in the initial co-simulation definition line. The NAME must match the controls name in the initial co-simulation line.

The coupling scheme is set to Gauss-Seidel. This scheme has only Abaqus or Star-CCM+ running at a given time (i.e. serial coupling). Data is updated at intervals specified by the step size parameter.

Setting the Scheme Modifier to Lag means that Abaqus will run second in the co-simulation.

Setting the Time Incrementation to Subcycle allows Abaqus to reduce the increment size if necessary. If this happens, Abaqus will run multiple increments until reaching the required step size before exchanging data with Star-CCM+.

Time Marks set to Yes requires Abaqus to reach the specified step size in an exact manner, rather than going past it before exchanging data.

Something else to note is the Step definition in the input file. It appears just before the code shown above and should look like this:

```
** STEP: Step-1
**
*Step, name=Step-1, nlgeom=YES, inc=10000
FSI Co-Simulation with Star-CCM+
*Dynamic, direct
0.05, 2.2,
```

The two numbers in the final line dictate the step size for the Abaqus simulation and the total time of the simulation. The step size (0.05) can be equal to or less than that specified in the co-simulation definition. If it is less than what is in the co-simulation definition, then the co-simulation step size must be a multiple of the number in the step definition. For example, if you want Abaqus to iterate 10 times before exchanging data with Star-CCM+, then change the 0.05 in the step definition above to 0.005.

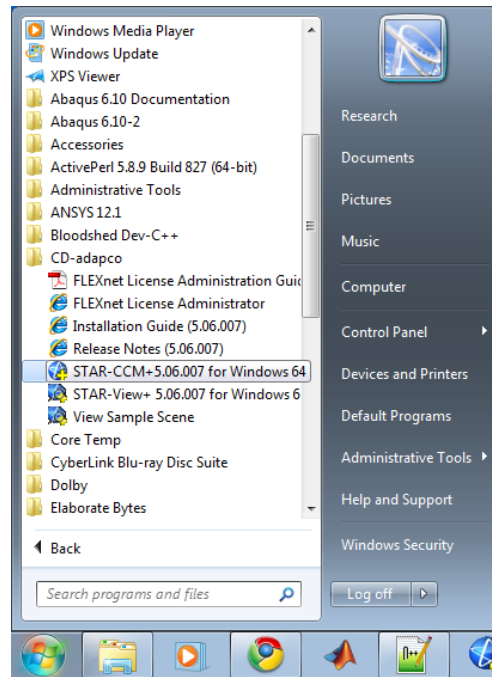
This completes preparation of the Abaqus model. Save the changes to the input file and CAE model and close Abaqus.

Preparing the Star-CCM+ Fluid Model

NOTE: Star-CCM+ tends to be a little glitchy and temperamental. Therefore, you should save early and save often to avoid losing any work!

Building the Fluid Model

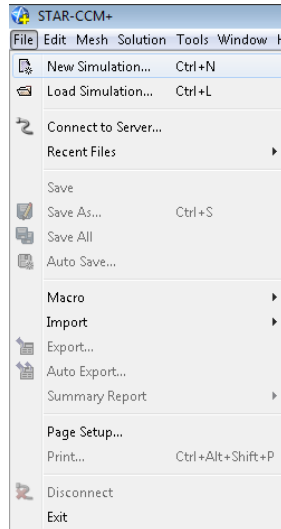
1. Open Star-CCM+ 5.06.007. From Windows, go to Start -> All Programs -> CD-Adapco -> Star-CCM+ 5.02.007 for Windows 64.



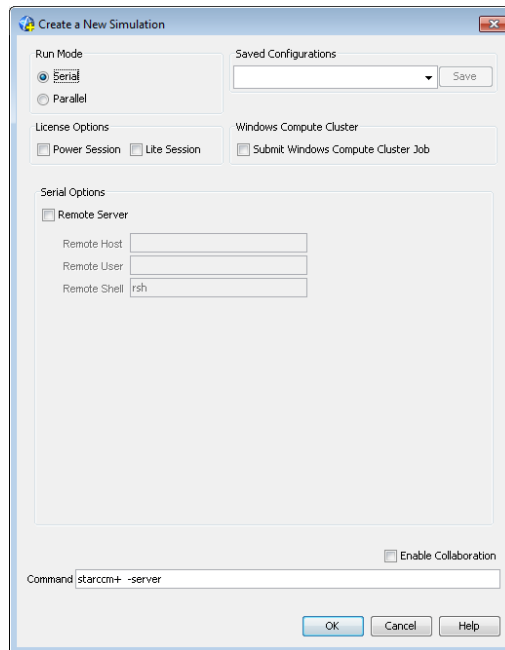
Click 'Yes' in the User Account Control Window

Star-CCM+ starts up.

2. Begin a new simulation. From the top menu bar, go to File -> New Simulation

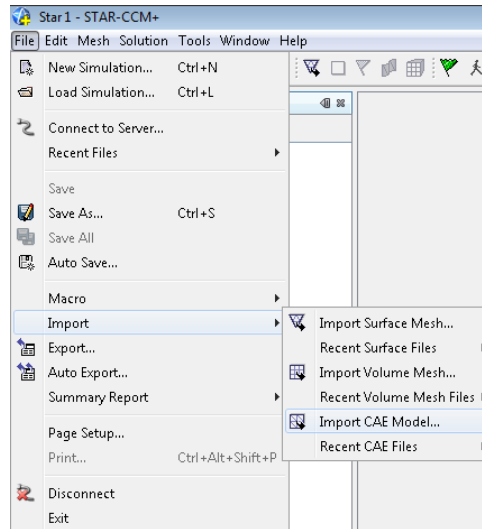


The Create a New Simulation dialog is displayed

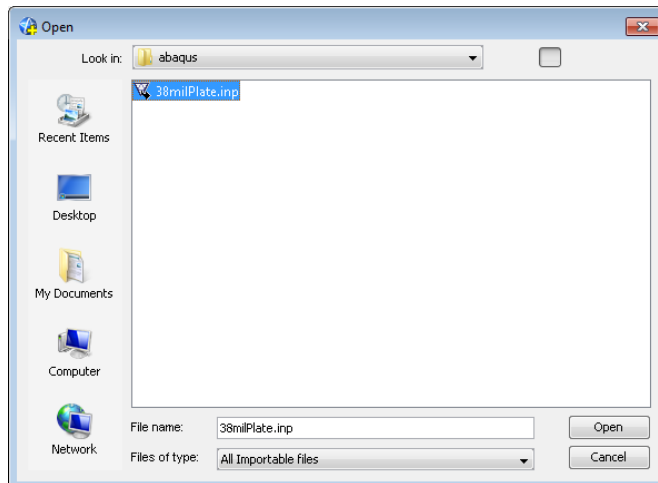


For building a model, only a single processor is needed. Therefore, the Run Mode of Serial will be used. Click 'OK'.

3. Define the FSI walls. Import the Abaqus model by going to File -> Import -> Import CAE Model

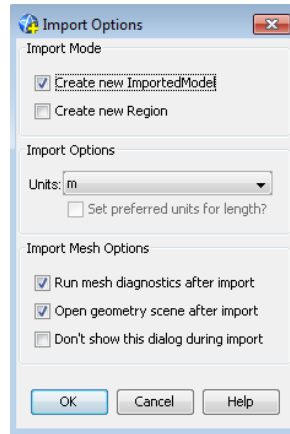


The Open dialog is displayed



Locate the Abaqus Input File created earlier, and select 'Open'.

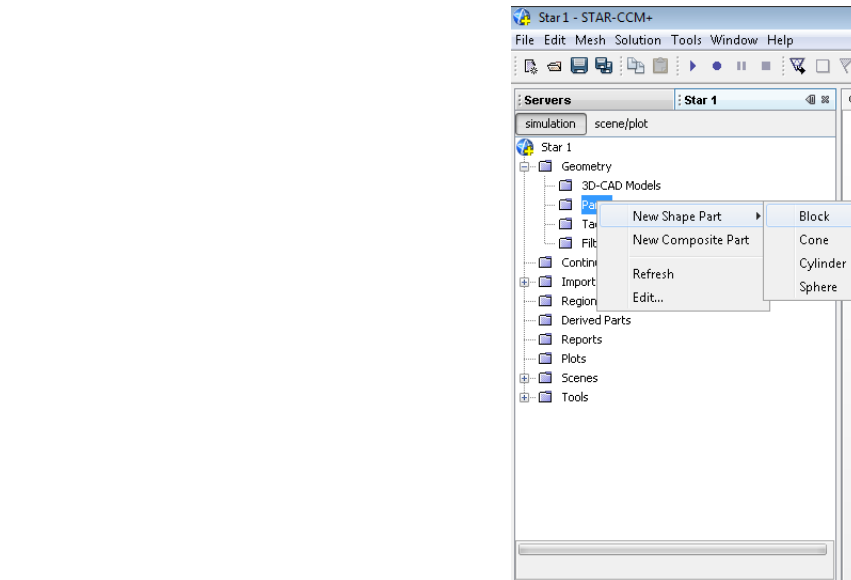
The Import Options dialog is displayed



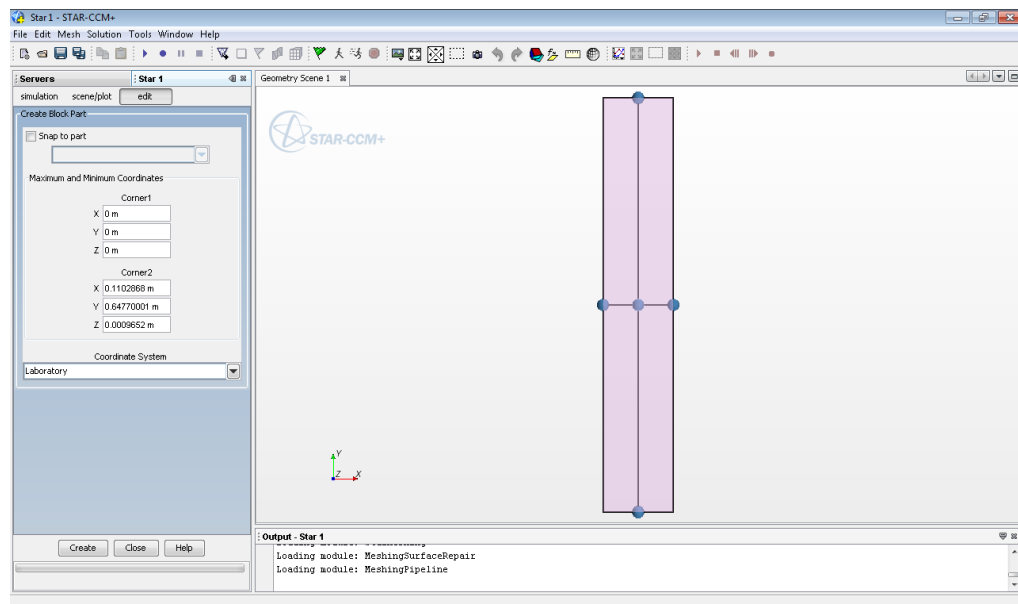
Ensure that 'Create new Imported Model,' 'Run mesh diagnostics after import,' and 'Open geometry scene after import' are selected, and 'Create new Region' is deselected. Click 'OK'

Once the model is imported, you now need to define a new part wraps the outer surface of the plate. Since the plate is nothing more than a rectangular block, this can be done relatively easily in Star-CCM+.

In the model tree on the left of the screen, expand the 'Geometry' node. Right-click on the 'Parts' container and select New Shape Part -> Block.



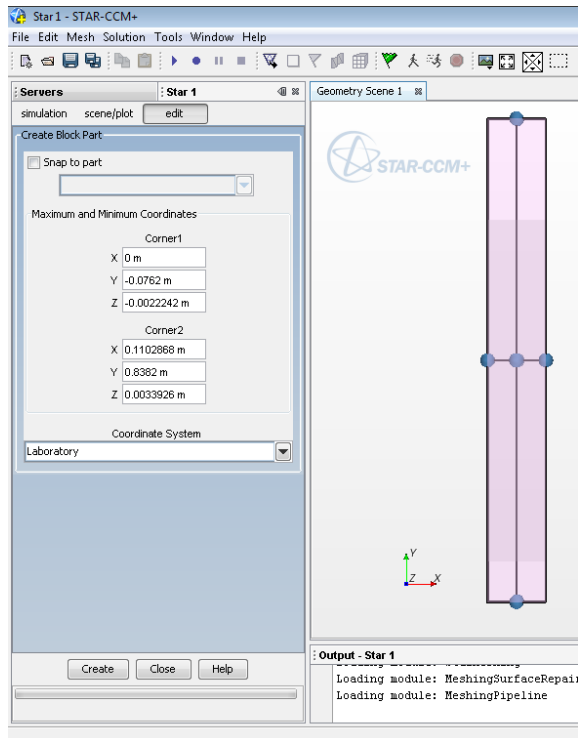
The left pane changes to show the part Edit controls. Also, a preview of the block is shown in the open Geometry Scene.



By default, Star-CCM+ has the new part enclose anything shown in the active scene. In this case, that is the imported plate geometry. Additionally, since the plate is a rectangular block aligned with the axes, the new block created by Star-CCM+ perfectly wraps the surface of the imported Abaqus model. This part will

be used to define the FSI Interface of the fluid model. Click 'Create' at the bottom of the Edit pane to create the block.

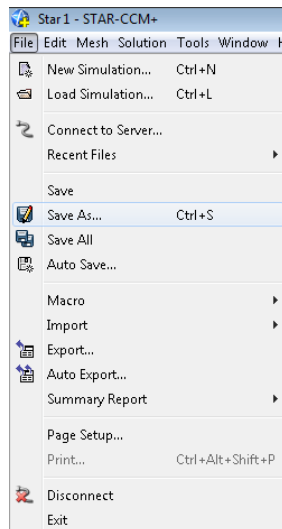
Although it can't be seen, the block has been created. Before closing the edit pane, we need to create another block to define the outer walls of the fluid channel. This channel will have the same width as the plate (the X dimensions will be identical). Along the length, it will extend 7.5 inches (0.1905 m) up to the inlet from the top of the plate ($Y2 = 0.64770001 + 0.1905 = 0.83820001$) and extend 3 inches (0.0762 m) down to the outlet from the bottom of the plate ($Y1 = 0 - 0.0762 = -0.0762$). This model is meant to simulate the plate being offset a distance of 4 mils (0.004 inches, 1.016×10^{-4} m) in a channel with a total thickness of 221.13 mils (.22113 inches, 5.6168×10^{-3} m). Therefore, Z1 is set to -0.0022242 and Z2 is set to 0.0033962.



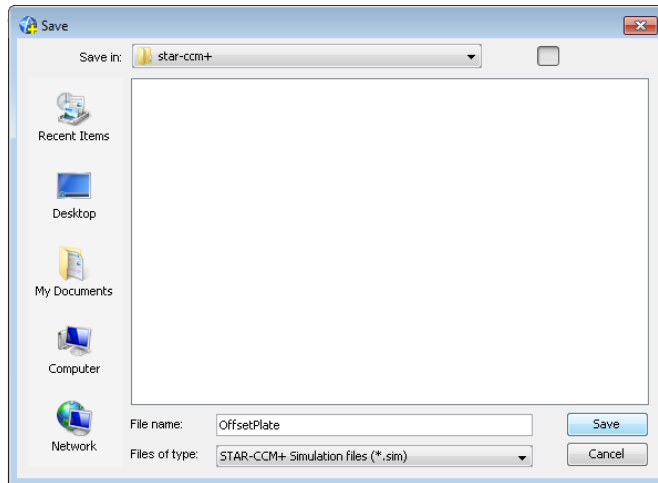
Click 'Create', then 'Close'.

If you expand the 'Parts' container, you will see the two parts that were just created.

At this point, save the simulation to the star-ccm+ directory created at the beginning of the tutorial. Go to File -> Save As

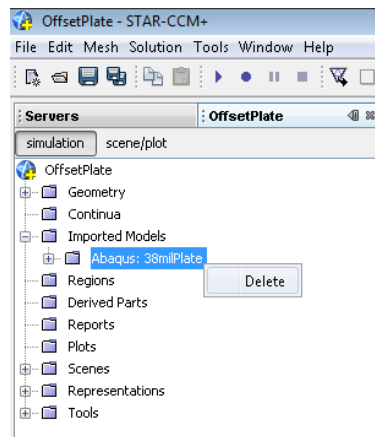


The Save dialog is displayed

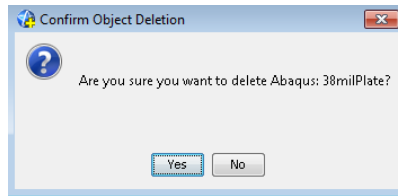


Name the file 'OffsetPlate.sim' and click 'Save'.

4. Now that the geometries necessary for defining the fluid region are in place, the Imported Abaqus Model can be removed. Expand the 'Imported Models' container, right-click on the imported model, and select 'Delete'.

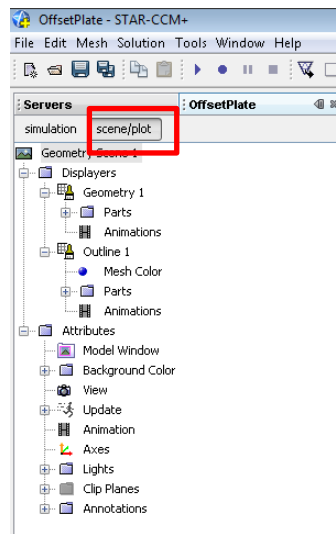


The Confirm Object Deletion dialog is displayed

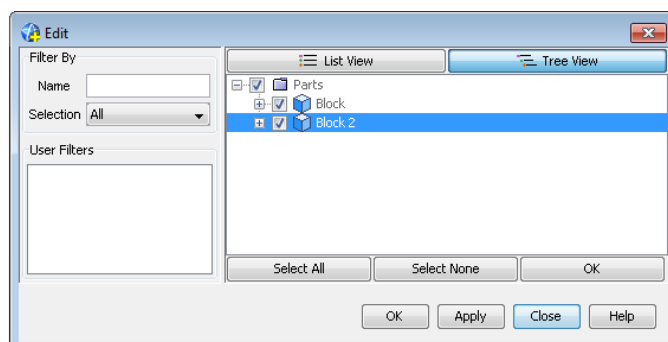


Click 'Yes'

You will now notice that the Geometry Scene is empty. To display the two blocks that were just created, click the 'scene/plot' button above the model tree.

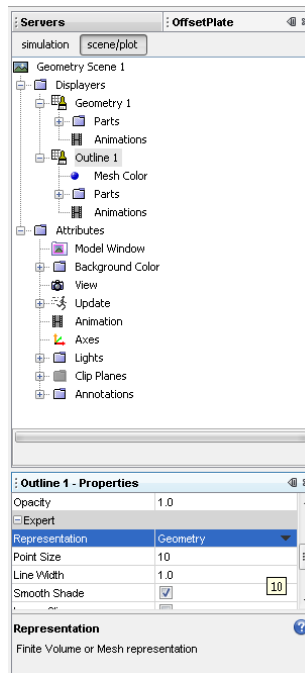


Double click on the Geometry Scene 1 -> Displayers -> Geometry 1 -> Parts Container to display the Edit dialog



Expand the Parts container, and select the check boxes next to the two parts shown in the list. Click 'OK'.

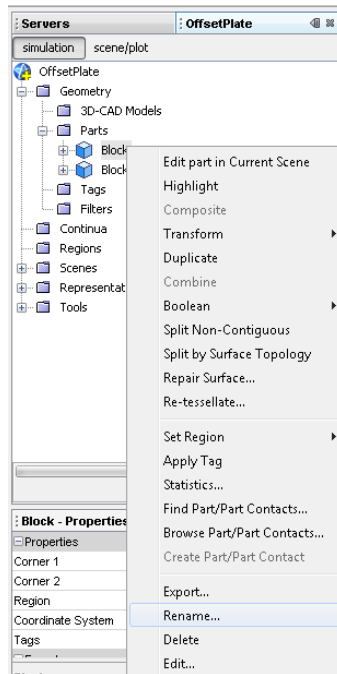
Now drag the Parts container from the Geometry 1 displayer down to the Parts container of the Outline 1 displayer. Finally, click on 'Geometry 1' in the Displayers container. In the properties pane at the lower left corner of the screen, scroll down to the 'Expert Options' and set the 'Representation' option to 'Geometry'. Repeat this for the 'Outline 1' displayer.



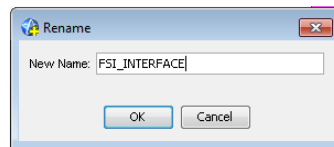
The two geometry parts should now be displayed in the scene.

5. Defining the boundaries. Return to the simulation controls by clicking 'simulation' above the model tree.

Expand the Geometry -> Parts container. Rename 'Block' to 'FSI_INTERFACE' by right-clicking on it, and selecting 'Rename'.

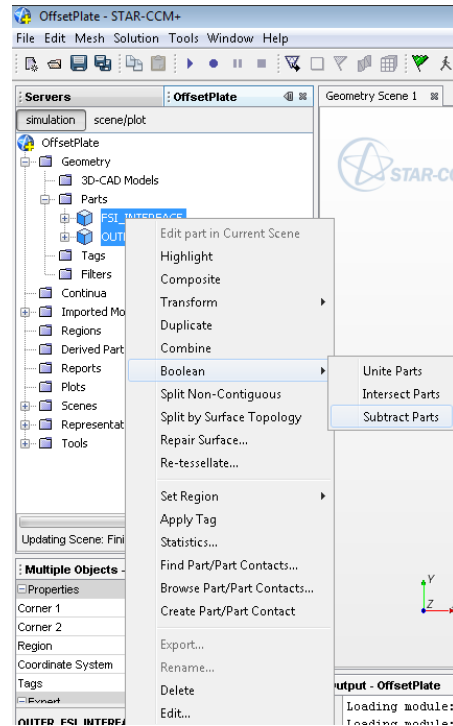


Enter the name FSI_INTERFACE in the Rename dialog and click 'OK'

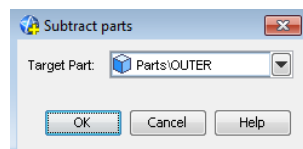


Rename Block 2 to OUTER

Use Ctrl+click to select both parts (FSI_INTERFACE and OUTER). Right-click on them and select Boolean -> Subtract Parts



In the Subtract Parts dialog, select the part you want to keep, in this case, OUTER.

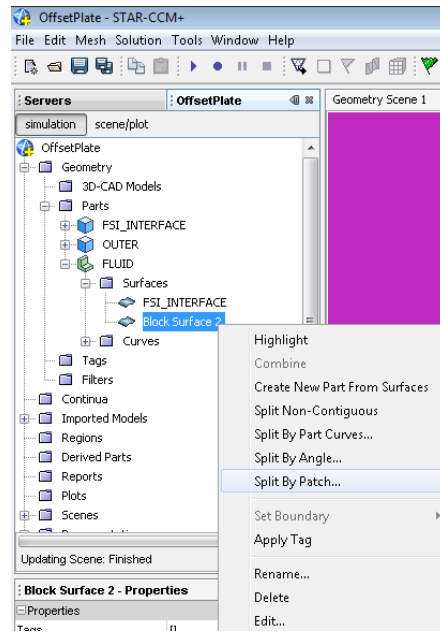


Click 'OK'

A new part named 'Subtract' has been created. Rename it FLUID.

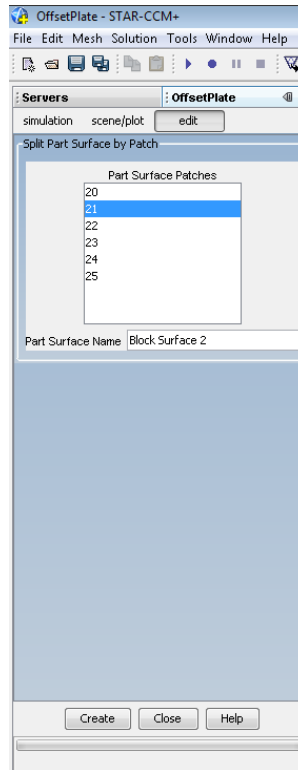
Update the Geometry Scene to show only the FLUID part.

Expand the FLUID -> Surface container. You will see two surfaces. One of these is the four walls of the FSI_INTERFACE. The other is the six walls of the outer channel. Rename the surface representing the FSI_INTERFACE as FSI_INTERFACE (clicking on the surface names in the model tree will highlight them in the geometry scene).



Now the Inlet and Outlet surfaces need to be split off from the remaining Block Surface. Right-click on the Block Surface representing the outer wall of the channel, and select Split By Patch...

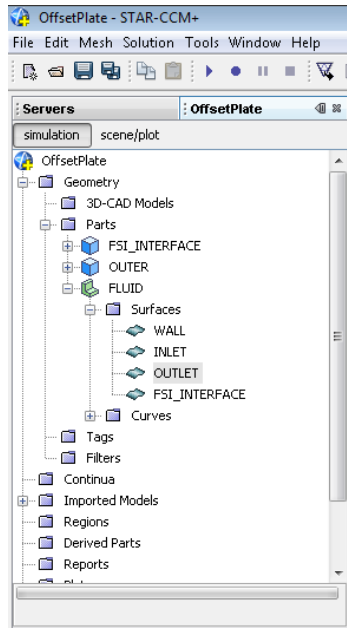
The Split Part Surface by Patch pane is displayed.



As you click each of the 6 Part Surface Patches in the list, that surface is highlighted in the scene. You may need to pan around to see them as they are highlighted. In the Split Part Surface by Patch pane, identify the two patches corresponding to the Inlet and Outlet. In this case, they should be numbers 21 and 23.

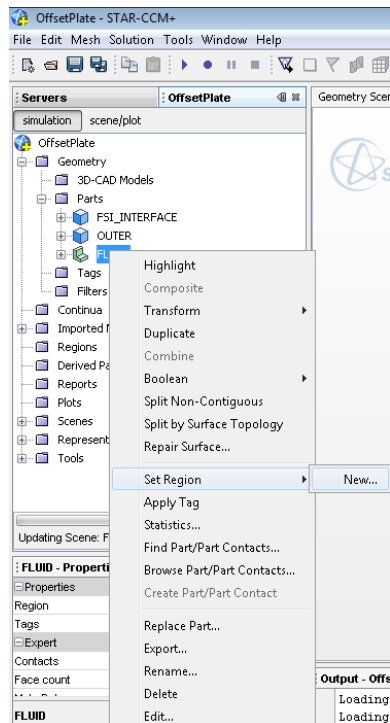
Select patch 21 and click 'Create'. Repeat for patch 23. Click 'Close'.

In the model tree, rename the Block Surfaces appropriately as INLET, OULET, and WALL.

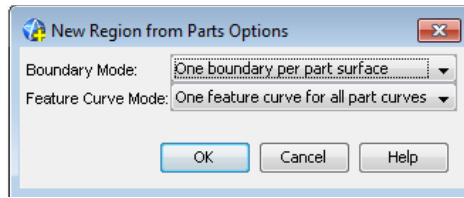


This would be a good time to save.

6. Creating the Region. Right-click on the FLUID part and select Set Region -> New.

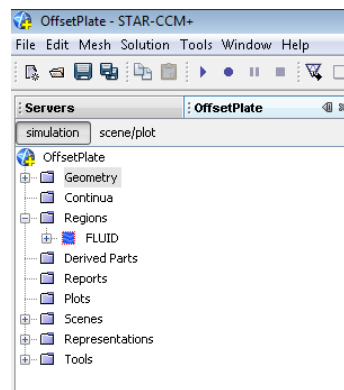


The New Regions from Parts Options dialog is displayed

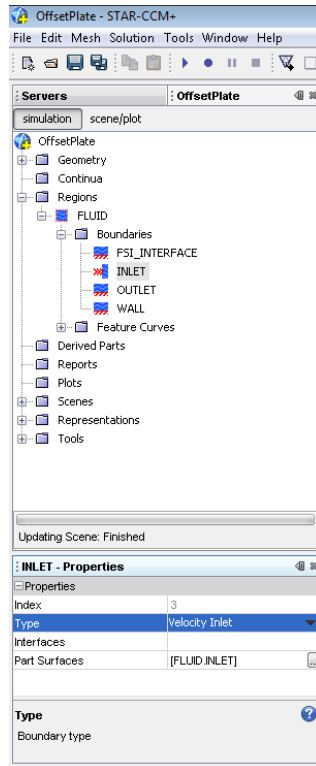


IMPORTANT!! Change the Boundary Mode option to 'One boundary per part surface'. DO NOT use the default of 'One boundary for all part surfaces'! Click 'OK'

You can now collapse the Parts folder and expand the Regions folder to see the new FLUID region.

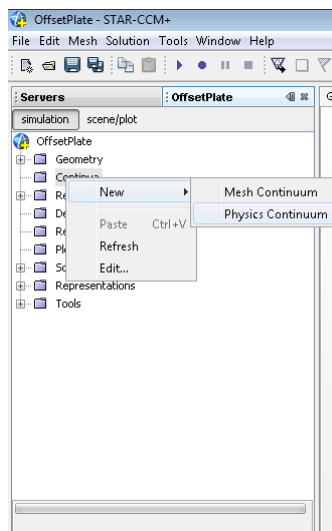


Expand the FLUID -> Boundaries container, click on INLET, and change its type to 'Velocity Inlet' in the properties pane.

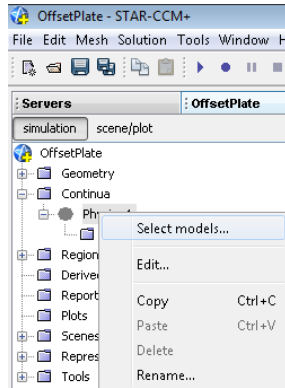


Repeat the procedure, changing the OUTLET boundary to a 'Pressure Outlet'.

7. Defining Physics Continuum. Collapse the 'Regions' folder. Right click on the 'Continua' folder and select 'Physics Continuum'.



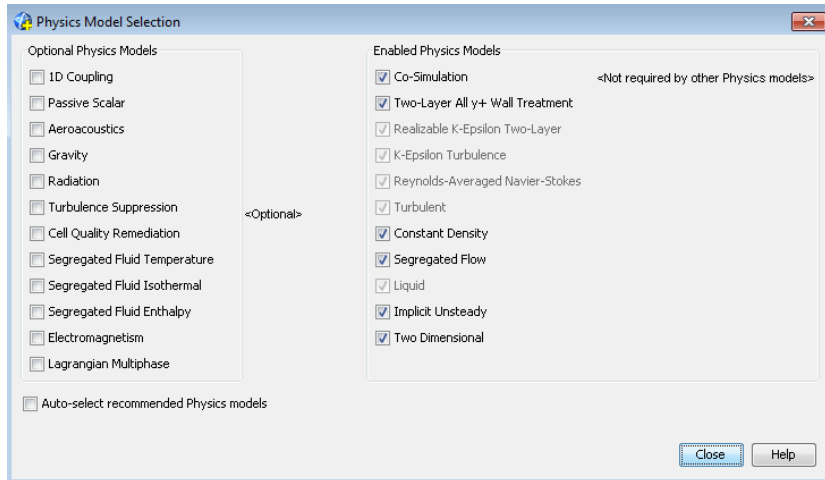
Right-click on Physics 1 and click 'Select models...'



Select the following models:

- Three Dimensional
- Implicit Unsteady
- Liquid
- Segregated Flow
- Constant Density
- Turbulent
- Reynolds-Averaged Navier-Stokes
- K-Epsilon Turbulence
- Realizable K-Epsilon Two-Layer
- Two-Layer All y^+ Wall Treatment

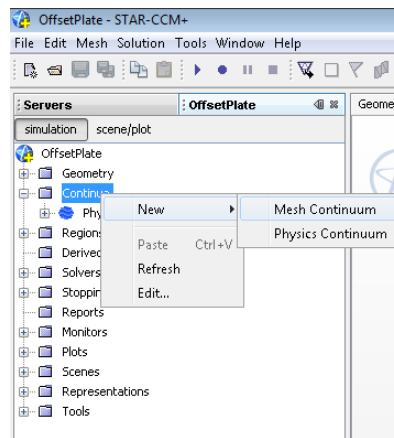
The Physics dialog should look like this when you are done (with the exception of the Co-Simulation Option – it should not be selected yet):



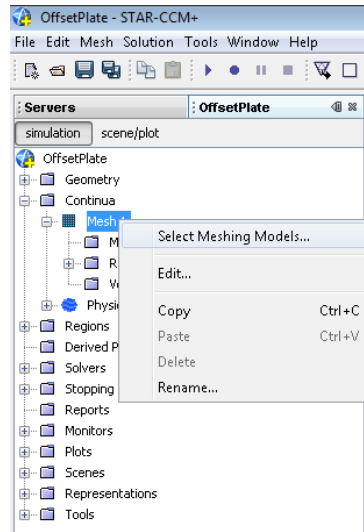
Click Close.

This would be a good time to save.

8. Define Mesh Continuum. Right-click on Continua. Select New -> Mesh Continuum



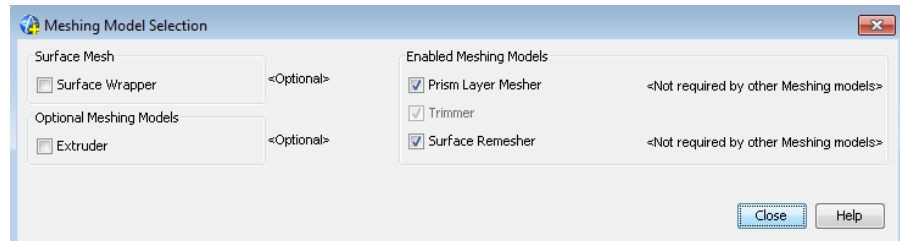
Right-Click on Mesh 1 and click 'Select Meshing Models'



Select the following models:

- Surface Remesher
- Trimmer
- Prism Layer Mesher

The Mesh dialog should look like this when you are done:



Click Close.

Expand the Mesh1 -> Reference Values folder. The settings in this folder affect the quality and density of the mesh, and therefore the quality and run time of the simulation. The following parameters are provided for an initial mesh, but can be changed to get a coarser or finer mesh. You can also use Volumetric Controls to control the mesh in specific areas. If desired, the surface can be

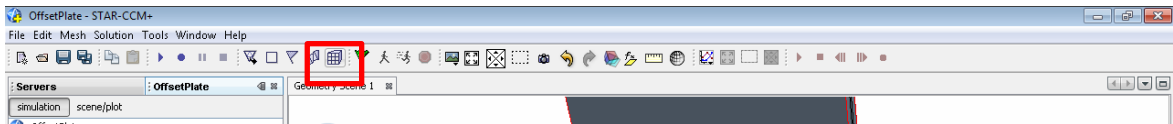
meshed first, and then the FLUID region scaled anisotropically. Then the model can be meshed and scaled back out to its original dimensions. This is useful for scaling the mesh along one or multiple axes.

Change the following parameters:

- Base Size: 9.652E-4
- Number of Prism Layers: 3
- Prism Layer Stretching: 1.2
- Prism Layer Thickness -> Absolute Size -> 4.6516 E-4

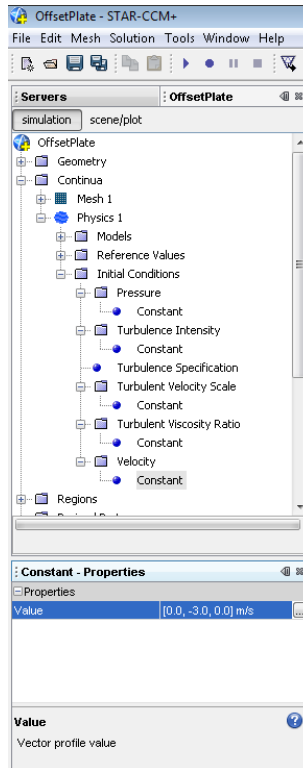
These parameters will produce a relatively fine mesh. The easiest way to adjust the mesh density is to modify the Base Size.

When you are ready to mesh, first save, then click the 'Generate Volume Mesh' button on the top toolbar.

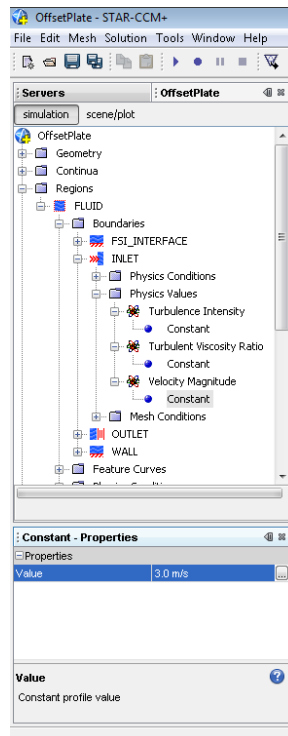


When complete, the mesh should be approximately 6,174,614 cells.

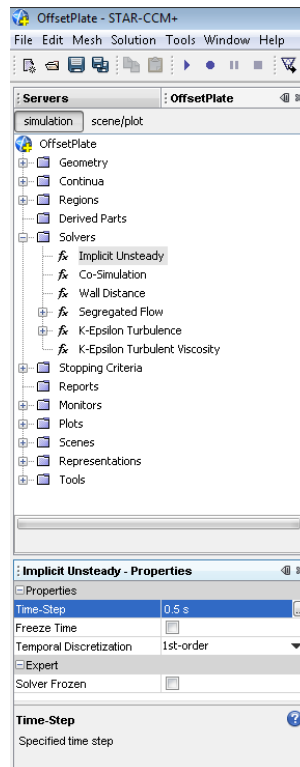
9. Preparing the Initial Simulation. Set the Continua -> Physics 1 -> Initial Conditions -> Velocity -> Constant Value to [0.0, -3.0, 0.0].



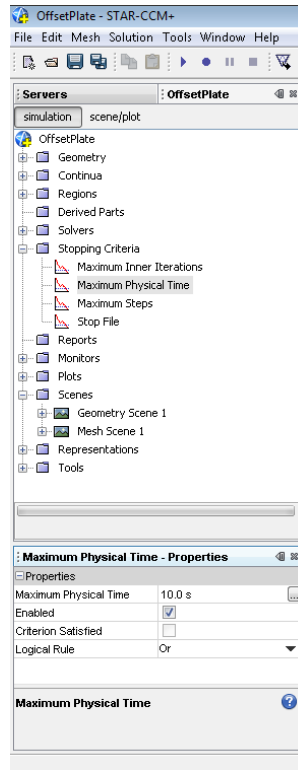
Set the Regions -> FLUID -> Boundaries -> INLET -> Velocity Magnitude ->
Constant Value to 3.0 m/s.



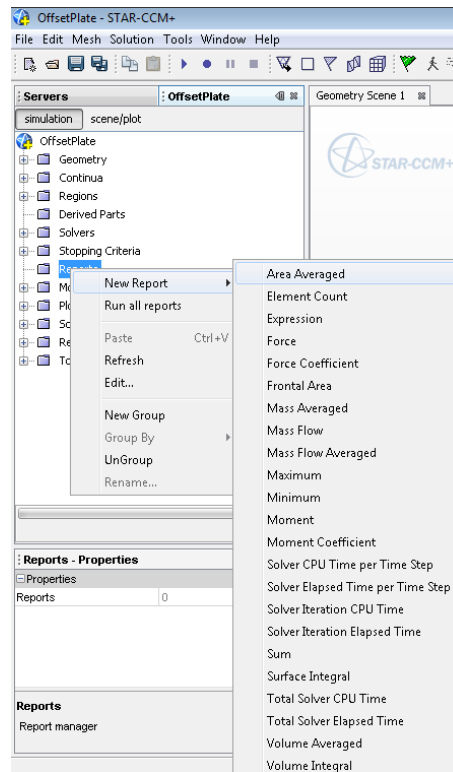
Set the Solvers -> Implicit Unsteady -> Time-Step Value to 0.5 s



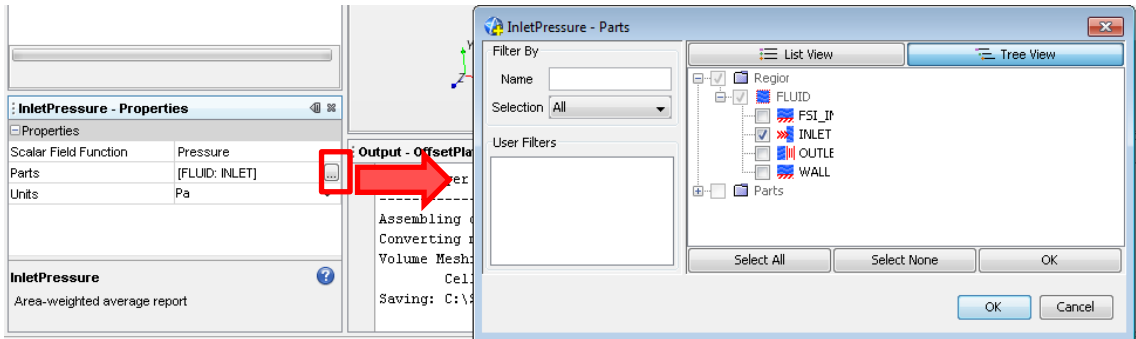
Set the Stopping Criteria -> Maximum Physical Time Value to 10.0 s



Right-click Reports. Select New Report -> Area Averaged



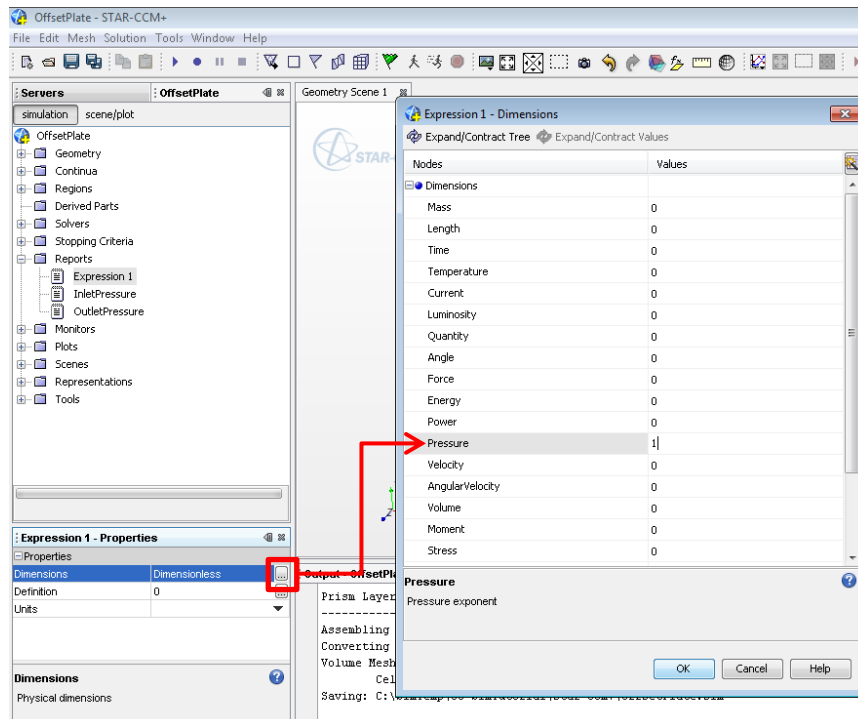
Rename the report as InletPressure. Set the Scalar Field Function to Pressure and the Parts to the FLUID: INLET boundary by clicking the ... in the parts box.



Repeat this for the Outlet Boundary, naming this report OutletPressure.

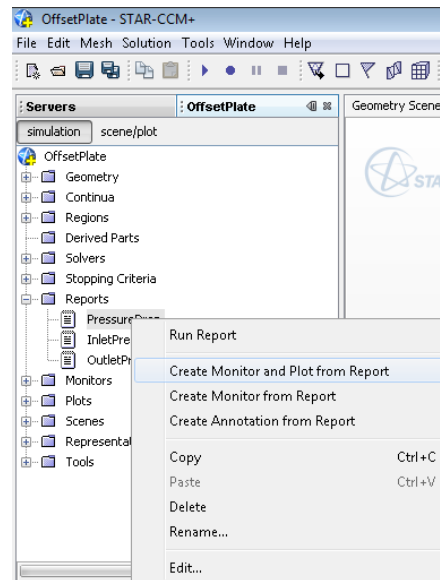
Create a new Expression Report by Right-clicking Reports and selecting New Report -> Expression.

Set the Dimensions to 'Pressure' by entering a 1 next to Pressure in the Dimensions dialog.

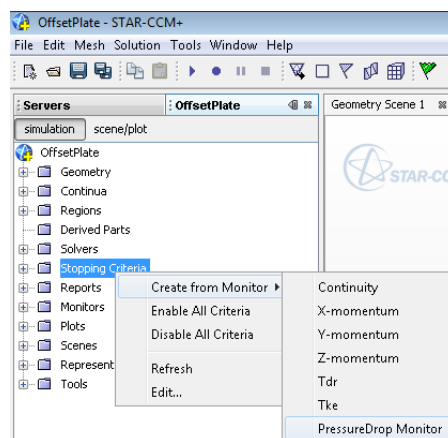


Set the definition to: \$InletPressureReport - \$OutletPressureReport

Rename the report as PressureDrop. Right-Click the PressureDrop report and select 'Create Monitor and Plot from Report'



Right-click Stopping Criteria and select Create from Monitor -> PressureDrop Monitor

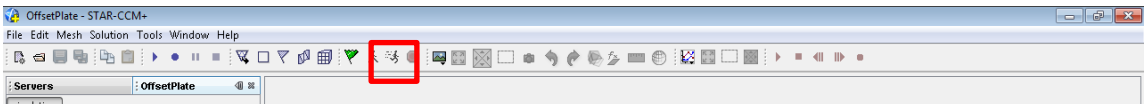


Change the Criterion Option from Minimum to Asymptotic. Click on 'Asymptotic Limit' and change the value for |Max-Min| to 0.5 Pa. Change the Number of Samples to 15.

Modify the Maximum Inner Iterations Stopping Criteria to 150.

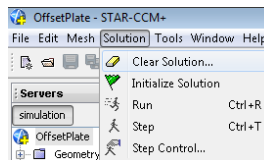
Save the simulation.

10. Run the initial simulation. Close the simulation and re-open it in parallel, using as many processors as the system allows. Once the simulation is loaded, click Run on the top toolbar.



When the simulation reaches a converged solution, save it.

Now go to Solution -> Clear Solution on the top menu bar



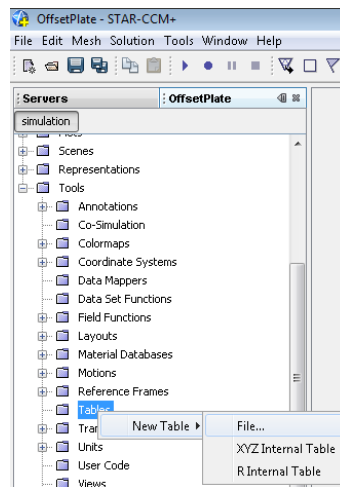
In the dialog box, clear the Fields box and click OK. This will keep the converged solution intact as the starting point for the next simulation.

Save the simulation. I would also recommend creating a copy of this file so that the converged initial solution is available should the file be saved again later on.

11. Setting up Variable Velocity. In Excel, create a table like the one below. Save it in the star-ccm+ directory as a Comma Separated Values (velocity.csv) file.

time	data
0	3
0.1	3.5
0.2	4
0.4	4.5
0.5	5
0.7	5.5
0.8	6
1	6.5
1.1	7
1.3	7.5
1.4	8
1.6	8.5
1.7	9
1.9	9.5
2	10

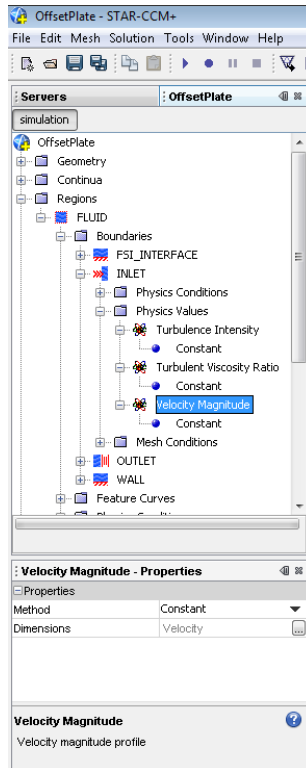
In Star-CCM+, under Tools, right-click on Tables and select New Table -> File



Locate the velocity.csv file and click 'Open'

Expand the Regions -> FLUID -> Boundaries -> INLET -> Physics Values -> Velocity

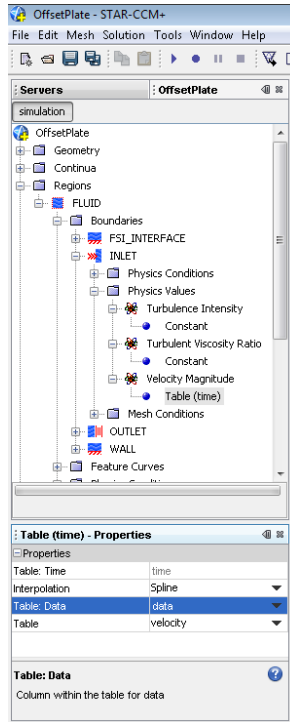
Magnitude option.



Change the Method from 'Constant' to 'Table (time)'

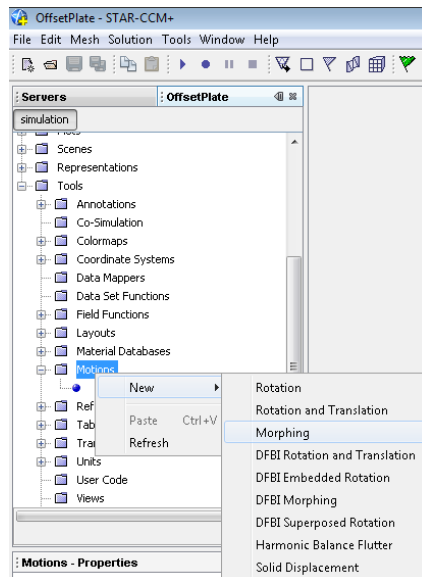
Click on 'Table (time)' in the Model tree and set the table to 'velocity'. Set Table:

Data to 'data'. Change Interpolation from 'Spline' to 'Step'



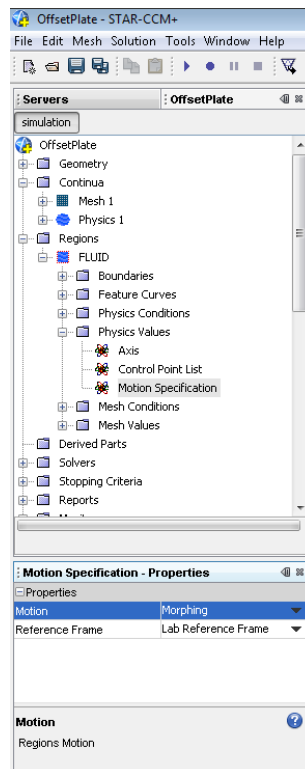
Save the simulation.

12. Set up the Co-Simulation. Under Tools, right click on Motions. Select New -> Morphing.

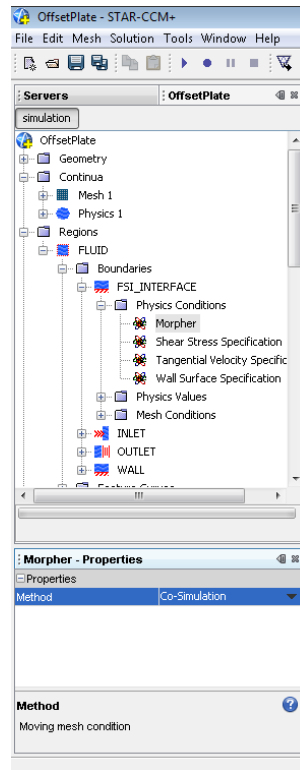


Add Co-Simulation to the Physics 1 continuum by right-clicking on Physics 1 and selecting 'Select Models...' Click the check box next to Co-Simulation and click Close.

Under Regions -> FLUID -> Physics Values -> Motion Specification, change the Motion property to 'Morphing'



Under Regions -> FLUID -> Boundaries -> FSI_INTERFACE -> Physics Conditions -> Morpher, change the Method to Co-Simulation.

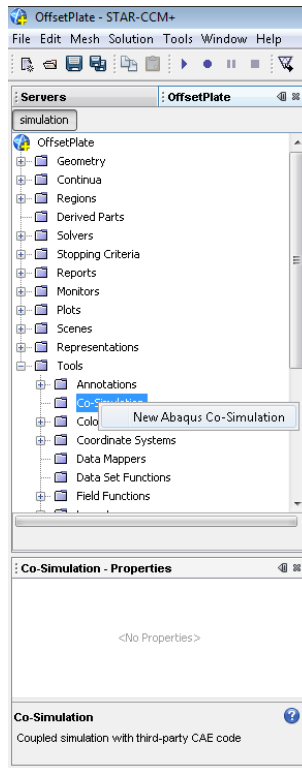


Save the simulation.

Make the following changes to the timing parameters of the simulation:

- Solver -> Implicit Unsteady -> Time Step: 0.05
- Stopping Criteria -> Maximum Physical Time: 2.2
- Stopping Criteria -> Maximum Steps -> ensure that the 'Enabled' box is not selected

Under Tools, right-click Co-Simulation and select 'New Abaqus Co-Simulation'

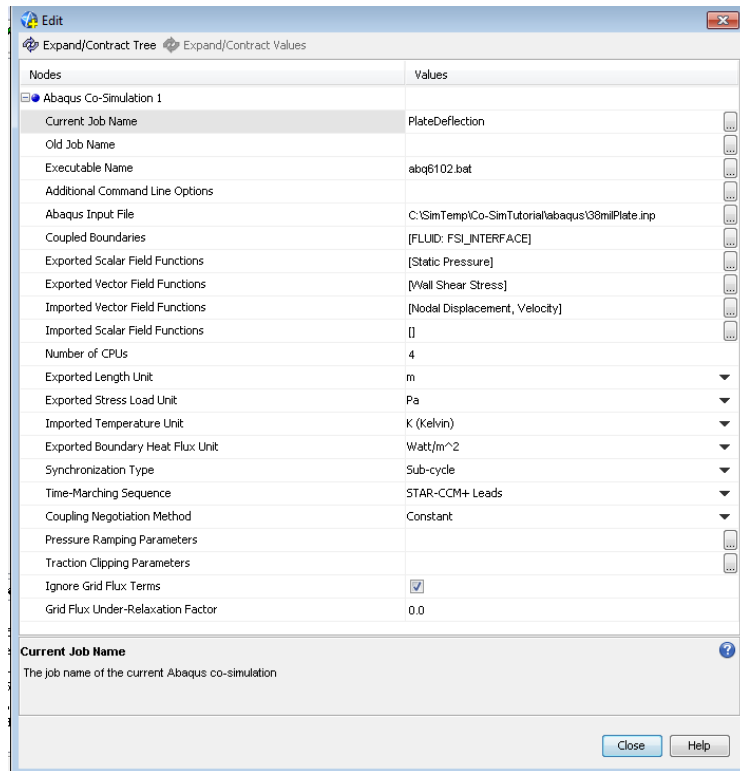


Set the following Co-Simulation properties:

- Current Job Name: PlateDeflection (this can be any arbitrary name)
- Executable Name: abq6102.bat
 - I would recommend copying the abq6102.bat file from the SIMULIA\Abaqus\Commands directory into the simulation abaqus directory. This helps to avoid issues with the system PATH in Windows
- Abaqus Input File: C:\SimTemp\Co-SimTutorial\abaqus\38milPlate.inp
- Coupled Boundaries: FLUID: FSI_INTERFACE
- Exported Scalar Field Functions: Static Pressure
- Exported Vector Field Functions: Wall Shear Stress
- Imported Vector Field Functions: Nodal Displacement, Velocity

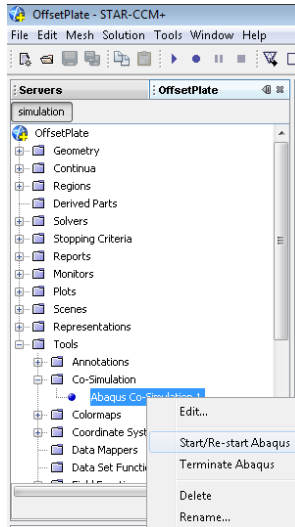
- Number of CPUs: 4-12 depending on the system and license availability
- Time-Marching Sequence: Star-CCM+ Leads
- Ignore Grid Flux Terms: Checked

The following is an overview of these settings in Star-CCM+



Save the simulation.

13. Run the Co-Simulation. Right-click on Abaqus Co-Simulation 1 and select Start/Restart Abaqus



Wait until the status bar between the model tree and the properties pane (where the moving green bar is) says, “Starting initial data transfer...: Finished.”

Now click the ‘Run’ button on the top menu toolbar.

14. Viewing results. While the simulation is running, the abaqus *.msg file can be viewed in Notepad++. It will provide several numbers, the most important of which is the maximum deflection for a given increment. If this deflection is greater than the thickness of the fluid channel, the simulation will crash since the plate as deflected outside of the channel. You can also open the abaqus *.odb file while the simulation is running to view the graphical results from Abaqus. This file should only be opened when Abaqus isn’t running (i.e. open it while Star-CCM+ is iterating)

APPENDIX 2: Experimental Data

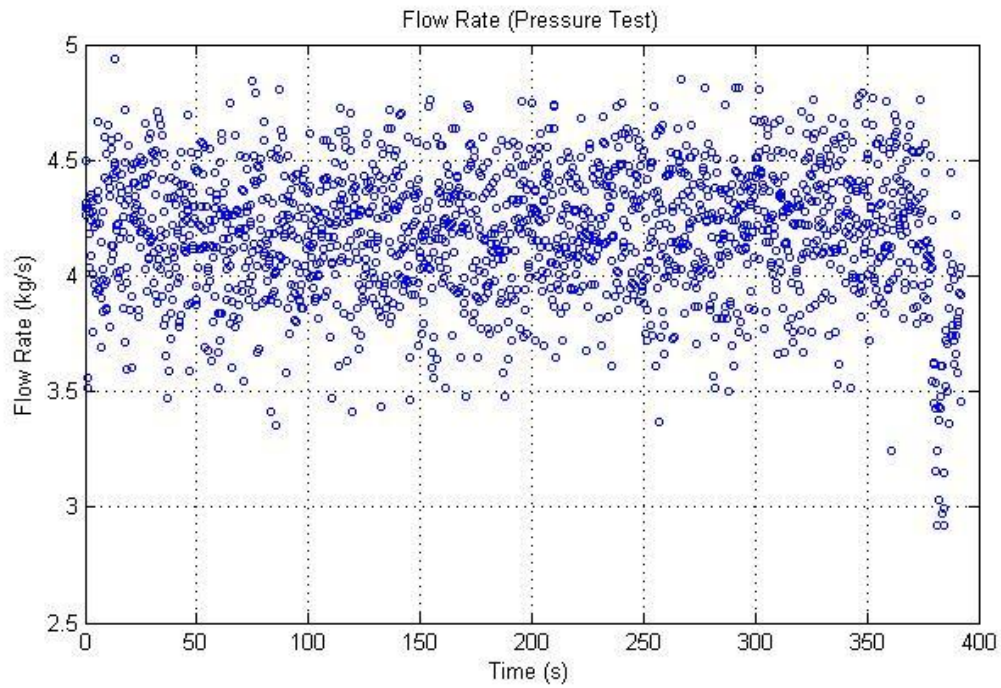


FIGURE A 1. FLOW RATE DATA FROM PHASE 2 OF FLOW TEST.

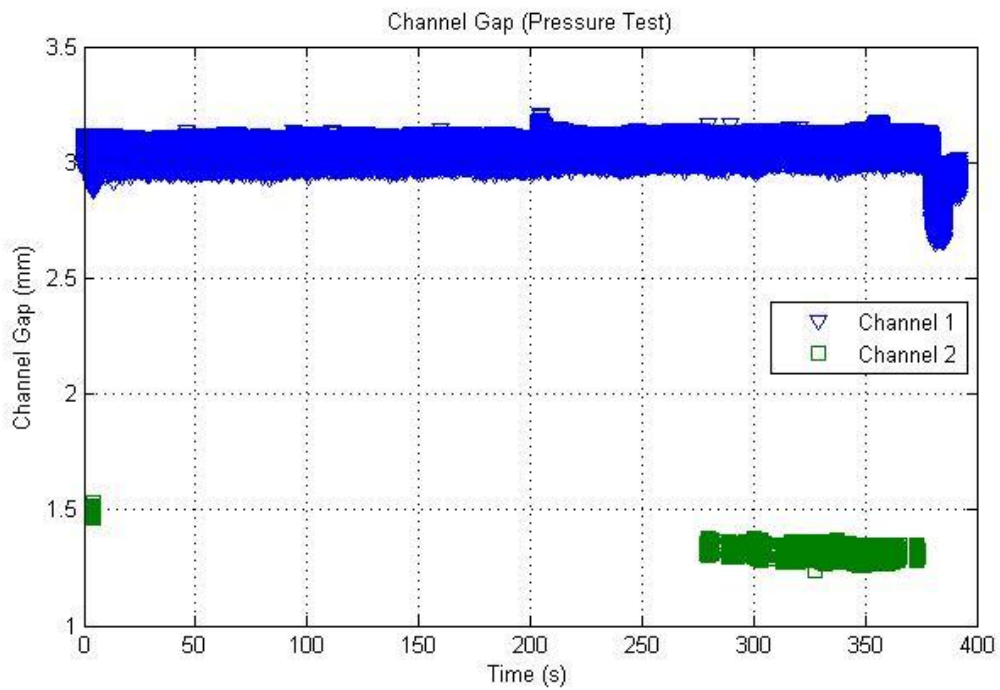


FIGURE A 2. CHANNEL GAP DATA FROM PHASE 2 OF FLOW TEST.

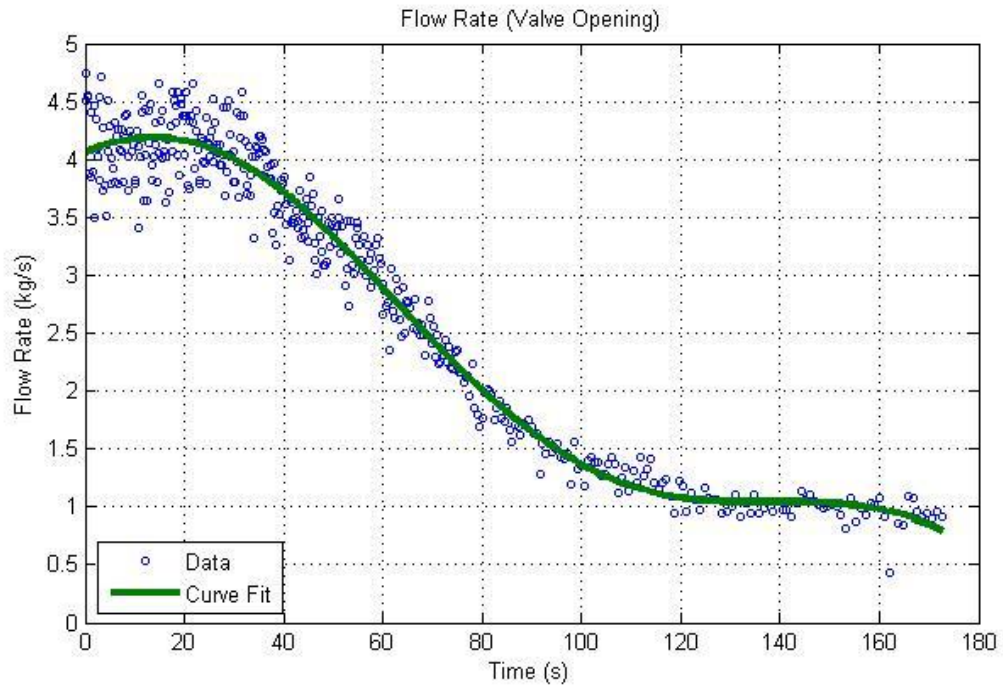


FIGURE A 3. FLOW RATE DATA FROM PHASE 3 OF FLOW TEST.

$$\dot{m}(t) = a_1 \sin(b_1 t + c_1) + a_2 \sin(b_2 t + c_2)$$

where:

$$a_1 = 3.397$$

$$b_1 = 0.009346$$

$$c_1 = 1.516$$

$$a_2 = 0.8027$$

$$b_2 = 0.03776$$

$$c_2 = 0.9763$$

(27)

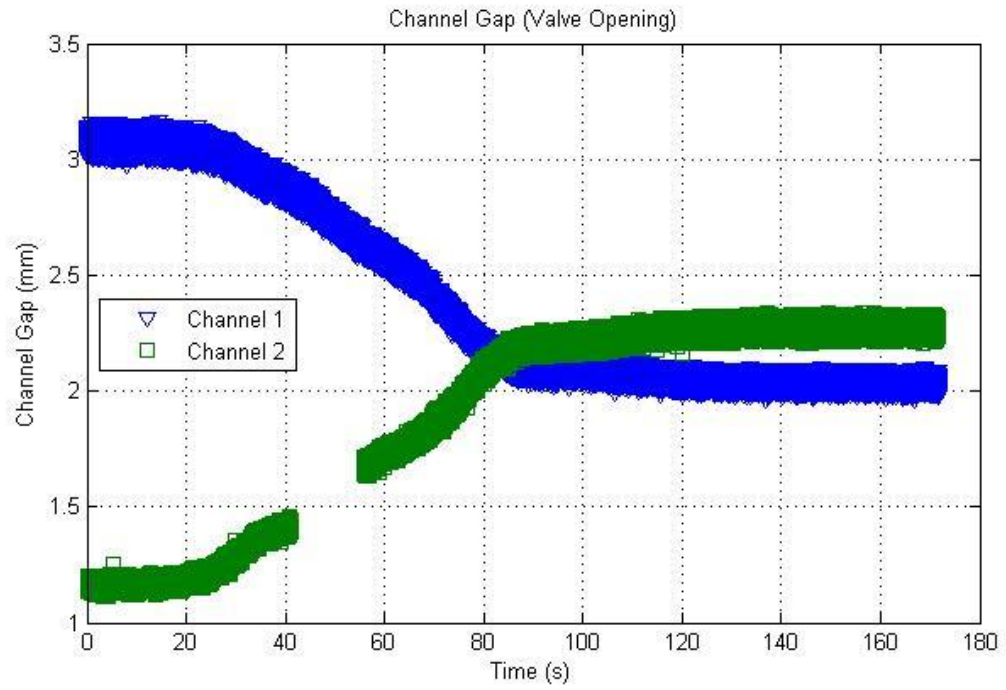
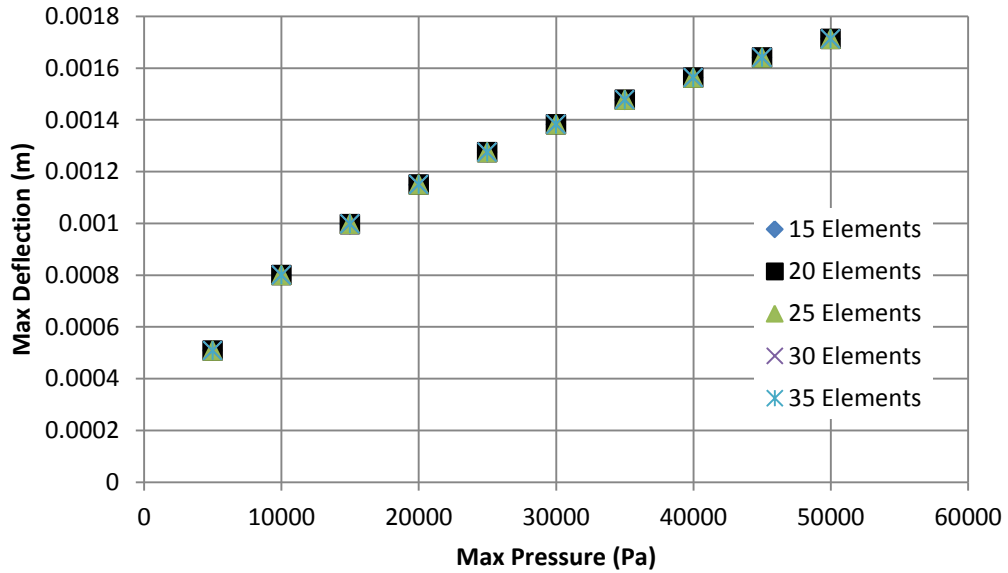


FIGURE A 4. CHANNEL GAPS DURING PHASE 3 OF FLOW TEST.

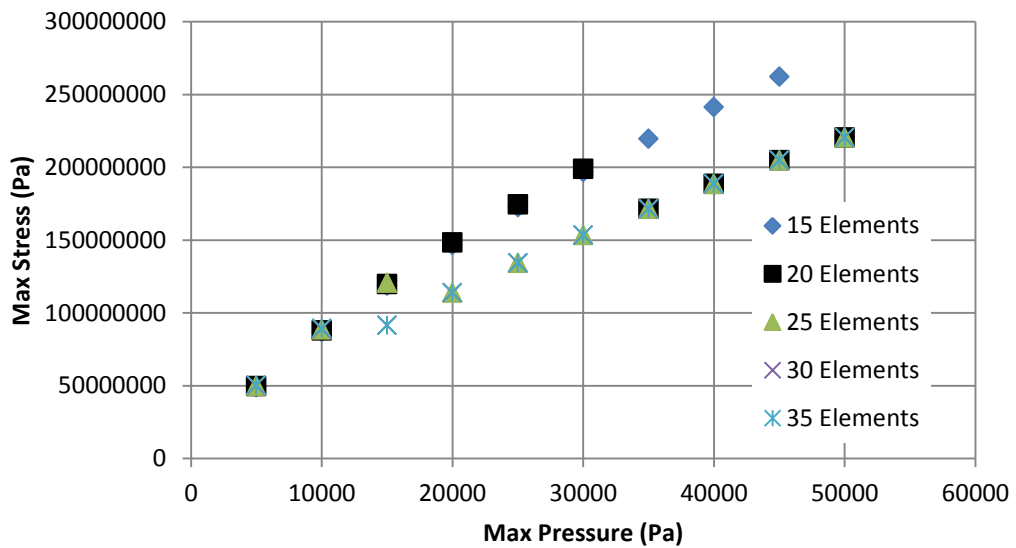
APPENDIX 3: Numeric Data

Abaqus Mesh Independence Study (varying number of elements through thickness)

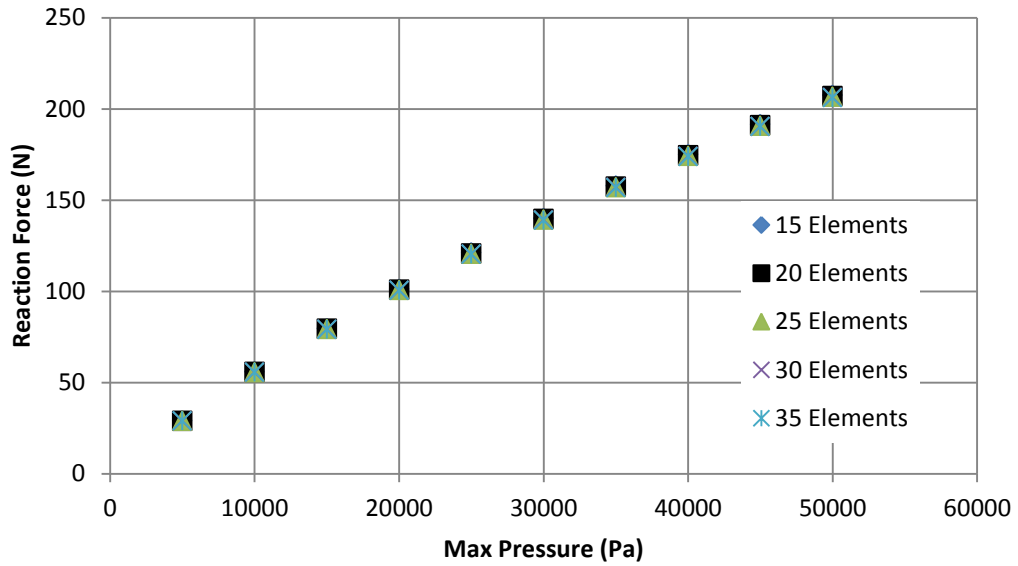
Leading Edge Max Deflection



Top Corner Max Stress

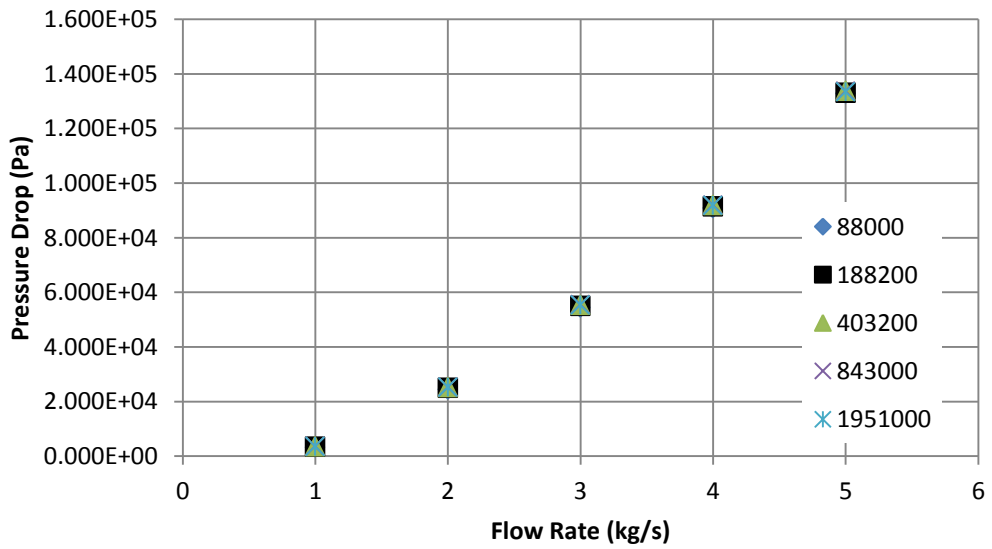


In-Plane Reaction Force at Leading Edge

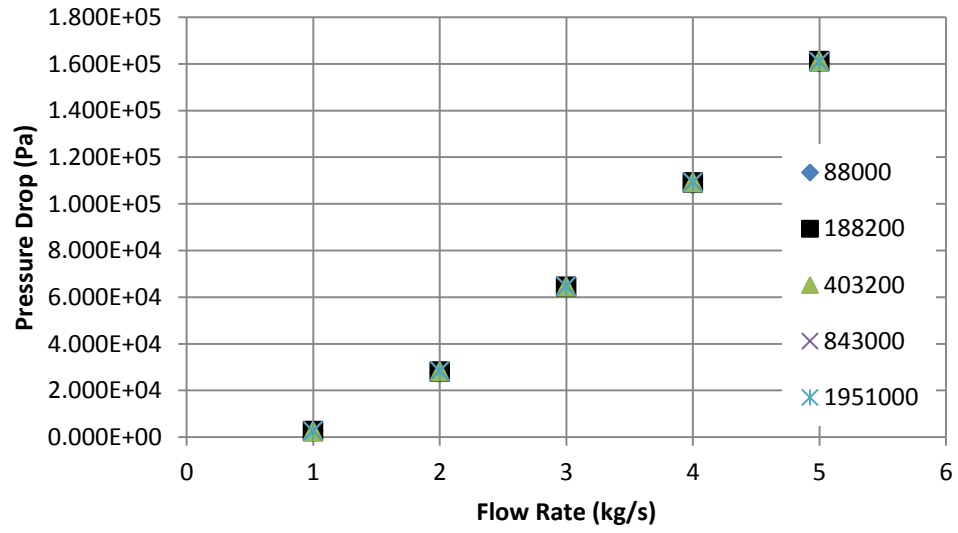


Star-CCM+ Mesh Independence Study (varying number of cells)

Plate Pressure Drop



Total Pressure Drop



REFERENCES

- ANL. (2010, May 19). *Reduced Enrichment for Research and Test Reactors (RERTR)*. Retrieved August 3, 2011, from Argonne National Laboratory:
<http://www.rertr.anl.gov/index.html>
- CD-Adapco. (2011). Star-CCM+ (Version 6.02.007).
- Donea, J., Huerta, A., Ponthot, J. -P., & Rodriguez-Ferran, A. (2004). Arbitrary Lagrangian-Eulerian Methods. In E. Stein, R. Borst, & T. J. Hughes (Eds.). John Wiley & Sons, Ltd.
- Dowell, E. H., & Hall, K. C. (2001). Modeling of Fluid-Structure Interaction. *Annual Review of Fluid Mechanics*, 445-490.
- Eisenhower, D. (1953, December 8). *Atoms for Peace*. Retrieved July 11, 2011, from Dwight Eisenhower Presidential Library and Museum:
<http://www.eisenhower.archives.gov/>
- Groninger, R. D., & Kane, J. J. (1963). Flow Induced Deflections of Parallel Flat Plates. *Nuclear Science and Engineering*(16), 218-226.
- Ho, M., Hong, G., & Mack, A. N. (2004). Experimental Investigation of Flow-Induced Vibration in a Parallel Plate Reactor Fuel Assembly. *15th Australasian Fluid Mechanics Conference*. The University of Sydney, Sydney, Australia.
- Miller, D. (1958). *Critical Flow Velocities for Collapse of Reactor Parallel-Plate Fuel Assemblies*. Schenectady, NY: U.S. Atomic Energy Commission.

- Moses, D. (2005). Lessons from the Atoms for Peace Research Reactor Fuels Program, 1955-1965. *International RERTR Meeting* (pp. S12-2). Boston: Oak Ridge National Laboratory.
- MURR. (2011). *Feasibility Analyses for HEU to LEU Fuel Conversion of the University of Missouri Research Reactor*. Columbia, MO: University of Missouri.
- MURR. (2011). *MU Research Reactor - History*. Retrieved August 2, 2011, from MU Research Reactor: <http://www.murr.missouri.edu/history.php>
- NNSA. (2011, June 8). *NNSA Administrator Highlights U.S.-Russian Cooperation on Reactor Conversion Program During Moscow Symposium (Press Release)*. Retrieved August 3, 2011, from NNSA Press Releases: <http://nnsa.energy.gov/mediaroom/pressreleases/reactorconvr1s6811>
- NNSA. (2011). *Office of Global Threat Reduction*. Retrieved June 25, 2011, from <http://nnsa.energy.gov/aboutus/ourprograms/nonproliferation/programoffices/officeglobalthreatreduction>
- Patankar, S. V. (1980). *Numerical Heat Transfer and Fluid Flow*. New York: Routledge.
- Razzaq, M., Turek, S., Hron, J., & Acker, J. F. (2010). Numerical Simulation and Benchmarking of Fluid-Structure Interaction with Application to Hemodynamics. In G. P. Galdi, & R. Rannacher, *Fundamental Trends in Fluid-Structure Interaction* (pp. 171-199). Singapore: World Scientific Publishing Co.
- Roe, B., Haselbacher, A., & Geubelle, P. H. (2007). Stability of fluid-structure thermal simulations on moving grids. *International Journal for Numerical Methods in Fluids*, 1097-1117.

Scavuzzo, R. J. (1965). Hydraulic Instability of Flat Parallel-Plate Assemblies. *Nuclear Science and Engineering*, 463-472.

Simulia. (2011). Abaqus (Version 6.10).

Smissaert, G. (1968). Static and Dynamic Hydroelastic Instabilities in MTR-Type Fuel Elements: Part I. Introduction and Experimental Investigation. *Nuclear Engineering and Design*, 7, 535-546.

Wachs, D. (2008). *Conceptual Process Description for the Manufacture of Low-Enriched Uranium-Molybdenum Fuel*. Idaho Falls, Idaho: Idaho National Laboratory.

White, F. M. (2003). *Fluid Mechanics: Fifth Edition*. New York: McGraw-Hill.